UMONS Université de Mons

POLYTECH MONS

2023

FLUCTUATION-AWARE WIND POWER SCHEDULING IN DAY-AHEAD ENERGY AND RESERVE MARKETS

SEYYED AHMAD HOSSEINI

Université de Mons

UMONS

Faculte Polytechnique de Mons

Fluctuation-Aware Wind Power Scheduling in Day-ahead Energy and Reserve Markets

By

Seyyed Ahmad Hosseini

A thesis presented for the degree of Doctor of Philosophy in Engineering Science pursued in the Electrical Power Engineering Unit of the University of Mons

Members of the Jury:

Prof. Fabian Lecron	(University of Mons, Chairman)
Prof. Souhaib Ben Taieb	(University of Mons, Internal member)
Prof. Lieven Vandevelde	(Ghent University, External member)
Prof. Paul Cuffe	(University College Dublin, External member)
Prof. François Vallée	(University of Mons, Supervisor)
Dr. Jean-François Toubeau	(KU Leuven, Co-supervisor)
Prof. Zacharie De Grève	(University of Mons, Secretary)

POLYTECH MONS

March 2023

Acknowledgments

This dissertation is a comprehensive summary of the research I conducted during my Ph.D. program at the Power Systems & Markets Research Group, University of Mons. The program was accomplished under expert guidance and with the invaluable support of several individuals.

First and foremost, I would like to thank my thesis supervisor, Prof. Francois Vallee, for his exceptional support and guidance throughout my Ph.D. journey. His expertise and insights into the research process helped me with the technical and theoretical aspects of my research.

I am also grateful to my co-supervisor, Dr. Jean Francois Toubeau, who had a great impact on my academic endeavors. He consistently made time for me and offered valuable advice whenever I needed to discuss my academic pursuits.

My next gratitude goes to Prof. Nima Amjady for his role in developing my research skills, during my M.Sc. and for inviting me to Federation University Australia as a visiting scholar, during my Ph.D., to further extend our collaboration.

I would like to express my sincere gratitude to the committee members for their invaluable support and guidance during my thesis. I would also like to express my gratitude in advance to the referees for their effort in evaluating this thesis.

I express my gratitude for the opportunity to complete my thesis under the BEOWIND project, supported by the FPS Economy, S.M.E.s, Self-employed, and Energy through the energy transition funds. I hope that the

findings of this thesis aid in the improved integration of wind power within power systems, ultimately contributing to the advancement of a sustainable future.

I would like to wholeheartedly thank all my fantastic colleagues in the lab who made my time memorable. I recall that Jérémie helped me set up my IKEA furniture during my first days in Belgium, showing his support and kindness. Behzad's presence in our office made my days more pleasant. I thank Arnaud and Martin for inviting me to participate in the students' initiation ceremony, a unique and culturally rich experience. Not to forget the cheerful games of table tennis after lunch, which have become an integral part of our daily work routine. Finally, I would like to thank all others - Manu, Thomas, Olivier, François, Jean-François, Zacharie, Bashir, Hooman, Jamal, Adriano, Pietro, Julien, Milahy, Louise, Thuy-Hai, Clélia, Aurélia. You guys made my time in the lab so much fun.

To close, I would like to express my warmest thanks to my family, friends, and all those who have been in my life. Your love, support, and presence are important to me and I am deeply grateful for that.

Ahmad Hosseini

Abstract

With the development of electricity market policies and advances in wind farm control technology, Wind Power Producers (WPPs) are, more than ever, motivated to take an active role in the electricity market. Accordingly, they have incentives not only to offer energy in the energy market but also to provide balancing services in the reserve market. This thesis aims to provide wind-only portfolios with the necessary resources and visions to effectively participate in the day-ahead energy and reserve markets. To achieve this, it is important to have a day-ahead awareness of wind fluctuations at a very short timescale, e.g., minutes (which is crucial for reserve scheduling), as well as short-term variations, e.g., on an hourly timescale (for energy scheduling). Furthermore, a dedicated decision model should be developed to leverage the obtained information on wind uncertainty at both time resolutions, thus optimally allocating the wind power share in the day-ahead energy and reserve markets. Also, the reliability of the offered reserve services, as a last resort of the system operator to balance supply and demand, should be considered in the decision framework.

In this thesis, we first present a motivational study to highlight the significant impact of wind fluctuations on WPPs' market contributions and the reliability of the submitted reserve bids. To alleviate the problem of the reliability of the offered reserve power, a new framework is proposed that contains a probabilistic constraint regarding the availability of the reserve power. When the fluctuations are low, this model provides WPP and system operators with more reliable and informed decisions.

However, since wind uncertainty is still modeled at an hourly resolution, this model is not very effective in the presence of large fluctuations.

Therefore, an original auxiliary classifier Wasserstein generative adversarial network is proposed to generate high-temporal-resolution (minute-wise) wind speed scenarios. Afterward, the obtained minute-wise wind scenarios are incorporated into data-driven multi-resolution probabilistic energy and reserve bidding framework. It is shown that compared to the outcomes of the single-resolution model that only uses wind uncertainty on hourly resolution, the profit loss and reserve reliability are significantly improved by the proposed model.

However, the proposed high-resolution scenario generation method does not consider time dependence between successive hourly periods as scenarios are generated independently for each period. To overcome the limitation of not accounting for time dependence between successive periods, we propose a compact day-ahead wind power forecasting model that not only captures intra-period wind fluctuations at a high resolution but also considers the time dependence between periods. Particularly, we formulate a day-ahead forecasting problem that provides second-wise information on intra-period wind variability by predicting the temporal distribution of wind power for day-ahead forecast horizons. Also, a differentiable loss, based on the Wasserstein distance is dedicatedly developed to compare distributions. Meanwhile, the developed multi-resolution bidding strategy is further modified to directly take the generated distributions as input to the decision-making framework, thus reducing the dimensionality of the problem. The effectiveness of the proposed fluctuation-aware data-driven method over its counterparts is verified regarding the minimization of the negative impact of wind fluctuations on WPPs' profit and real-time deviations of offered reserve bids using real-world market and weather data.

Contents

List of Acronyms (Alphabetical order)

Acronym	Definitions
ACWGAN	AUXILIARY CLASSIFIER WGAN
ARMA	AUTO-REGRESSIVE MOVING AVERAGE
BESS	BATTERY STORAGE SYSTEM
BM	BALANCING MARKETS
BRP	BALANCE RESPONSIBLE PARTY
BSP	BALANCING SERVICE PROVIDERS
BTCS	BI-OBJECTIVE TWO-STAGE CHANCE-CONSTRAINED STOCHASTIC
CE	CROSS-ENTROPY
CGAN	CONDITIONAL GAN
CLRA	CONFIDENCE LEVEL OF RESERVE POWER AVAILABILITY
CWGAN	CONDITIONAL WGAN
DAM	DAY-AHEAD MARKETS
DTW	DYNAMIC TIME-WARPING
DWPF	DAY-AHEAD WIND POWER FORECASTING
ERM	ENERGY AND RESERVE MARKETS
FCR	FREQUENCY CONTAINMENT RESERVES

FKL/RKL	FORWARD/REVERSE KULLBACK-LEIBLER DIVERGENCE
FRR	FREQUENCY RESTORATION RESERVES
GAN	GENERATIVE ADVERSARIAL NETWORK
GENCO	GENERATION COMPANY
IM	INTRA-DAY MARKETS
JSD	JENSEN-SHANNON DIVERGENCE
LCOE	LEVELIZED COST OF ENERGY
MCP	MARKET-CLEARING PRICE
MCV	MARKET CLEARING VOLUMES
MOP	MULTI-OBJECTIVE PROGRAMMING
NEMOS	NOMINATED ELECTRICITY MARKET OPERATORS
RES	RENEWABLE ENERGY SOURCES
RMSE	ROOT-MEAN-SQUARE ERROR
TIL	TURBULENCE INTENSITY LEVEL
TSO	TRANSMISSION SYSTEM OPERATOR
WGAN	WASSERSTEIN GAN
WPF	WIND POWER FORECASTING
WPP	WIND POWER PRODUCERS

List of Tables

List of Figures

Chapter 1. Introduction

1.1 Context

Harvesting energy from renewable energy sources (RES) continues its rapid growth throughout the world [1]. For perspective, the increasing trend of exploiting RES in the electricity sector is shown in Figure 1.1. In this figure, the vertical axis shows the total installed renewable capacity and the horizontal axis corresponds to the year. The contribution of each source of energy is indicated in the legend. Interestingly, it can be seen that in the last decade, the total worldwide installed capacity of RES is more than doubled, i.e., increased from 1.32 TW in 2010 to 2.80 TW in 2020 [2].

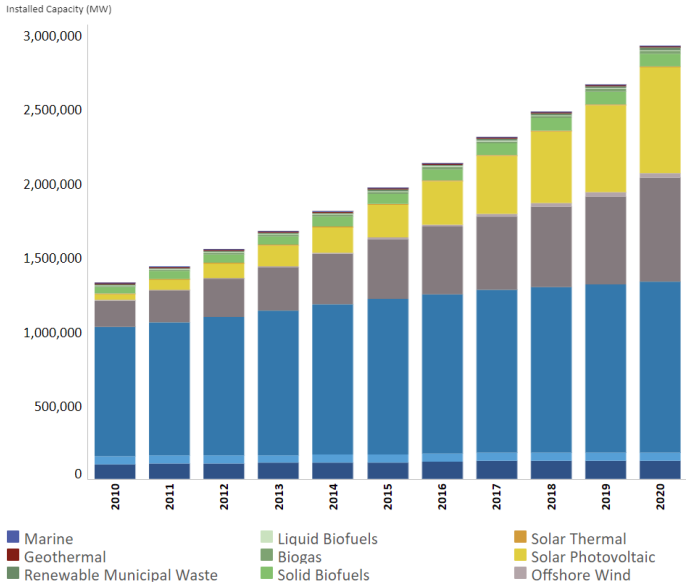

Figure 1.1) Cumulative global RES capacity installed between 2010 and 2020 [3].

Several factors contribute to such significant growth. Firstly, the environmental impact of RES is much less severe than the other fossil fuel-based conventional energy sources. This is in line with the current environmental aims, e.g., the Paris agreement which defines the corresponding guidelines and objectives, to deal with climate change and its adverse impacts. In particular, the amount of greenhouse gas emissions by RES is roughly 15 times less than the CO_2 generated by fossil fuel-based technologies [2]. Additionally, according to [3], RES is the primary substitute for nuclear energy in the optimal energy mix, which increases the need for flexibility in current energy systems. This flexibility is currently provided by gas-fired power plants at the production side.

The overall cost of energy production for fossil fuel-based plants was much cheaper than the RES a few decades ago. Thus, the government and policy-makers used to apply support schemes to incentivize RES to participate in the competitive electricity markets. Such support schemes include green certificates, subsidies, and feed-in tariffs [4]. Nevertheless, since technologies are nowadays more mature and cost-efficient, the cost of RES, e.g., construction, installation, and maintenance, is greatly reduced. Therefore, the support schemes for RES are being gradually removed as they are cost-competitive with respect to traditional sources. Particularly, the Levelized Cost of Energy (LCOE) from RES has been significantly reduced over the last decade [4]. LCOE measures the average net total cost of energy production for a generation source over its operational lifespan. As seen in Figure 1.2, the LCOE of RES, over the last decade, is significantly decreased.

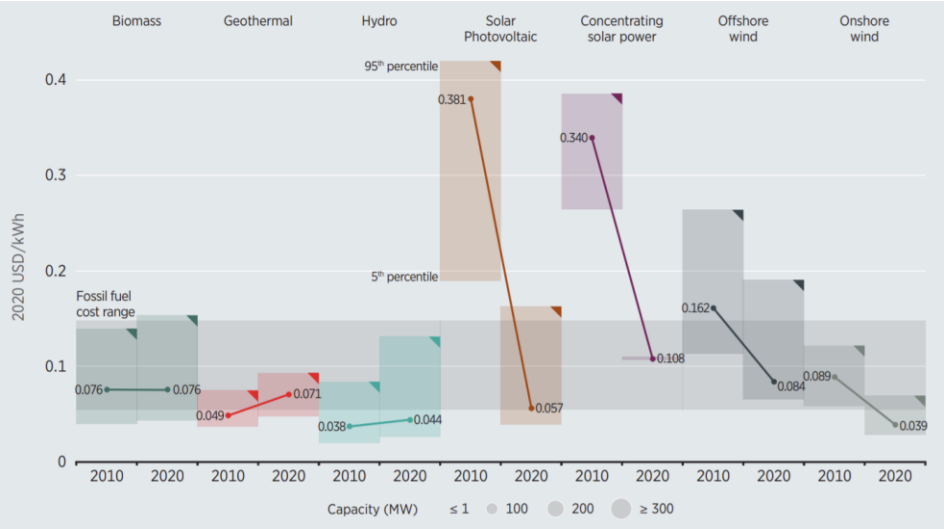

Figure 1.2) The LCOE of various newly commissioned RES from 2010-2020 [4].

1.1.1 Energy Security of Renewable Sources

For the economies to work appropriately, energy security should be ensured. The idea of energy security is generally connected with three themes [5]:

1) availability of sufficient supply to match with demand

2) affordability of the price

3) resiliency of energy systems.

While the theoretical targets of energy security have stayed unaltered, the methodologies to get these goals are nowadays changed. This revision is due to the expanding influence of politics, economics, and environmental matters as well as social and technical issues in the worldwide energy supply [5].

Specifically, all fossil derivatives are limited assets. By and large, this had never been a concerning issue for mankind in the past as the

consumption level of energy was far lower than the availability of such resources. Nevertheless, the current assessments regarding the availability of natural resources indicate that the current young generations may not witness the extraction of such resources at some point in their life. For instance, Japan estimates that recoverable reserves of oil will be exhausted in few decades [6]. This is mainly due to the increase in energy consumption, overpopulation, deforestation and the destruction of ecosystems, and the enormous extraction of natural resources over the last few decades. In contrast to non-renewable alternatives, renewable resources are characterized by a greater level of recovery, making them a more viable and sustainable option in the long term.

Regarding price affordability, traditional fossil-based technologies involve significant capital and operational costs. For perspective, the cost of coal-fired plants is estimated to be around 3500 $/kW [7]. On the contrary, the cost of energy production by RES is only associated with the project investment cost as their operational cost is around zero [4]. Moreover, the current advancements in technologies reduce their capital costs as well. Specifically, this decreasing trend can be seen in Figure 1.2.

Finally, renewable sources of energy improve energy resiliency. Particularly, RESs are localized, thus the adverse impacts regarding the loss of one or a cluster of RES units, e.g., wind turbines, is less treating to power systems than the loss of a centralized large fossil fuel-based unit.

1.1.2 Wind Energy

Wind is produced by the movement of air across lands or water masses. The kinetic energy of airflow, so-called wind energy, offers many benefits (which clarifies why it is one of the quickest developing energy sources on the planet).

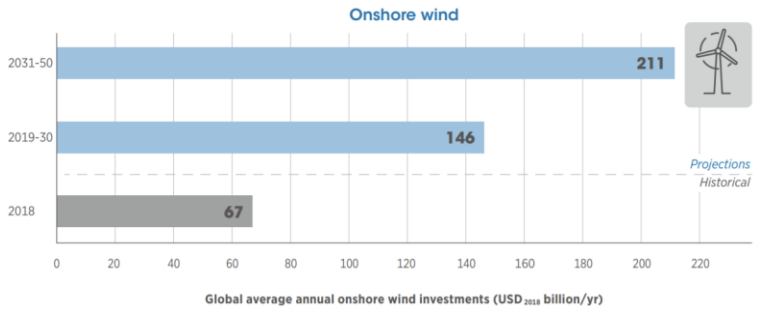

Figure 1.3) The current and future global expectations of onshore wind energy investment [8].

On-shore wind investment continuously increased from $ 63 billion to $ 80 billion from 2013 to 2016. In 2018, the investment was almost $ 67 billion. To reach a total installed onshore wind capacity of more than 5000 GW by 2050, an average annual investment of $ 146 billion per year until 2030, and $ 211 billion per year until 2050 would be required [8]. The current investment trend as well as its future expectation is shown in Figure 1.3.

Besides, the majority of the present yearly wind power investment goes toward the construction of new onshore wind generating capacity, with just a small portion needed to replace the retired ones. However, in the following decades, some investment will be required to replace current wind farms that are approaching the end of their lifetime. Accordingly, to replace present capacities with modern technologies by 2040, more than a third of the total annual onshore wind investment will be required [8].

Regarding the current capacities, wind energy is the second most renewable source of energy used in the world. For perspective, in 2019, the worldwide on-shore and off-shore wind energies, respectively, allocate 19.1% and 1.2% share of RES [9]. Meanwhile, in many European countries, e.g., Belgium and Germany, wind energy is the first RES for electricity generation. This could be due to the policies, environmental, geographical,

and climate characteristics of such countries. For example, on-shore and off-shore wind energy in Belgium are respectively, (by holding 26% and 23.8% of RES share) the first and second source of energy among other renewable technologies (as shown in Figure 1.4) [9]. Additionally, the assessments show that by 2050, in the world, on-shore and off-shore wind together would turn into the dominant source of energy by providing around 35% of global electricity demands.

Despite the capital-intensiveness of wind energy, its operation is not directly concerned with fuel cost. Additionally, with ongoing technical improvements and cost reductions, as well as the right policies in place, wind power generation can now compete in the competitive electricity markets. Remarkedly, it can be seen in Figure 1.2 that the LCOE of wind power is within a range range compatible with the cost of fossil fuels. New structures and rules are continuously emerging to accommodate wind generation in the liberalized competitive electricity markets.

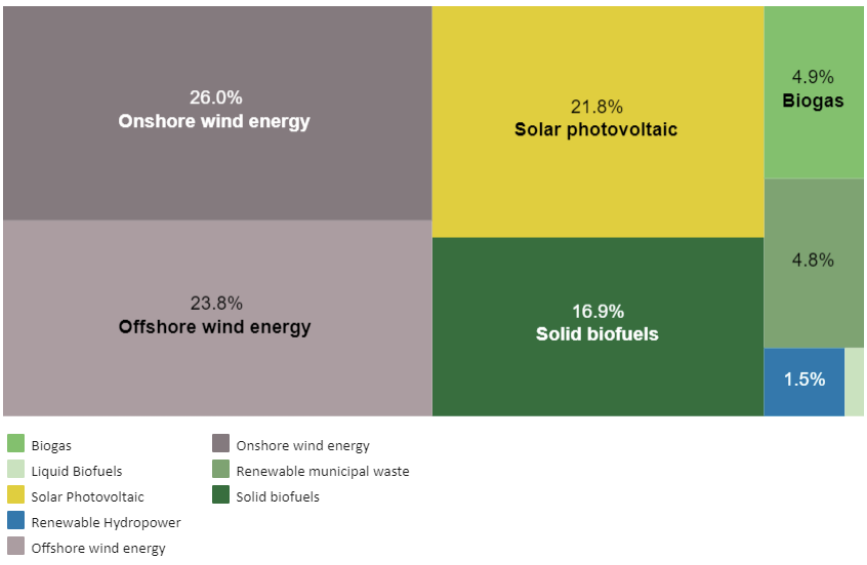

Figure 1.4) Share of different RES technologies for harvesting electricity in Belgium in 2019 [9].

Wind power producers (WPPs) in some markets, such as the Spanish, British, German, and Nordic power markets, have the choice of bidding in the reserve and electricity markets or selling all of their energy to the market operator [10]. Nevertheless, there are challenges regarding the integration of wind power in the electricity market, which are explained in the next subsection.

1.1.3 Challenges of Integrating Wind Energy into Electricity Markets

As mentioned, using wind energy has various advantages for power systems and wind power owners but it is also accompanied by some problems in restructured power systems. These problems are mainly rooted in wind stochasticity. In particular, wind prediction is already known to be a complex problem due to the high fluctuations of wind [11]. In the same way, modeling the stochasticity of wind speed, which is linked to prediction errors, is also burdensome. It should be emphasized that traditional long-term investment support schemes for wind power projects, based on the absorption of short-term market prices, do not provide sufficient incentives for wind power producers to actively participate in balancing the supply and demand mismatch of the power system. Therefore, the growing share of renewable energy resources (compared to conventional fuel-based power plants) rise great concerns for power system operators that have to continuously accommodate the resulting intermittent and uncertain power supply while ensuring system stability and security [12]. Therefore, electricity market policies are emerging for integrating such resources, which is mainly reflected by the advent of spot energy markets (in which the electrical energy is traded close to real-time delivery) and the development of efficient balancing mechanisms (by which system operators

can use the flexibility of market actors to maintain a stable system operation).

These market opportunities are further complemented with penalty mechanisms whereby deviations between scheduled bids and real-time delivery are charged with an imbalance fee, thus incentivizing market actors to effectively control the output power of their resources [13]. In this way, the real-time deviations of energy and reserve bids are financially penalized through energy imbalance settlement and balancing stage mechanisms [13].

Meanwhile, since uncertain generations become more significant in power systems, the need for a more responsive reserve power increases [14]. Consequently, there is an emerging opportunity for power producers (which have fast-ramping abilities) to achieve a greater economic advantage in the liberalized electricity market. In particular, WPPs could be incentivized to participate in the reserve market since wind turbines are nowadays equipped with fast control schemes that enable them to rapidly alter their output power [15], [16]. Different control techniques can be implemented, such as derating, as well as relative and absolute reserve procurement strategies. The derating method consists in restricting wind turbine maximum output power by a new specified upper bound, thereby creating a flexibility margin for upward regulation. The relative reserve power procurement strategy specifies a fixed percentage of the available wind power for curtailment. Finally, the absolute strategy restricts the wind turbine output power by a fixed quantity, given that sufficient power is available, to take part in the reserve market whereas the rest of the available power is allocated to the energy market [15]. The latter strategy thus prioritizes the provision of the contracted reserve power.

In some countries, like the US, the process of clearing these markets is done together, which means that the optimization of both energy and multiple reserve commodities happens at the same time. This leads to the characteristic of simultaneous co-optimization in these markets. In contrast, in European markets, the clearing process for the energy and reserve market floors is done sequentially. Despite this difference, WPP can still use a joint bidding strategy for energy and reserve power. This is due to the close proximity of the clearing processes, which creates a link of uncertainty, and the short time gap between the clearing of the two floors [17], [18].

Therefore, business bidding models should be developed for WPP so that they effectively participate in these day-ahead energy and reserve markets (ERM). Importantly, these models should appropriately consider wind uncertainty regarding financial compensation/ penalty that is paid due to the real-time deviations from their day-ahead offers in the energy-only and reserve markets. In this way, portfolios avoid ex-post disappointment due to discrepancies between expected profits and actual realizations (after the actual clearing of energy and reserve markets).

Meanwhile, it should be noted that a simple profit-based offering strategy of the WPP does not ensure a firm reliability level regarding the scheduled reserve power [19]. In other words, the WPP offers power quantities such that the income resulting from the positive incentives is greater than the negative incentives. Also, the transmission system operator (TSO) is not informed about the confidence level of the contracted bid which, in return, deteriorates the system security. Also, in a long run, it would discourage the TSO to rely on WPPs as reserve providers.

It should be noted that the real-time financial compensation for reserve occurs at a much shorter time interval than the financial compensation for

energy deviations in the imbalance settlement mechanism, e.g., minute-wise versus hour-wise (or quarter-hourly in some European markets) [19]. The shorter time scale in the balancing stage is because the reserve providers should guarantee that the power scheduled as a reserve is available at any time without failure. Therefore, an effective bidding model should be able to capture wind uncertainty regarding different temporal resolutions in order to account for the deviations of the submitted power in the energy and reserve markets. Such an effective model has not yet been developed in the literature due to the difficulty of modeling high-resolution forecasts and the complexity of rendering this high-dimensional information into a tractable decision framework.

Forecasting wind fluctuations at high temporal resolutions, such as minutes to seconds, is a major challenge in the field of renewable energy. The difficulty lies in the complex dynamics of wind, which makes it challenging to model wind uncertainty with high accuracy. This is a critical issue because accurate forecasting of wind patterns at high temporal resolutions is essential for feeding into a dedicated multi-resolution bidding model. Despite the importance of this issue, there is currently a lack of effective models in the literature that can capture wind fluctuations at such high temporal resolutions. This highlights the need for further research and development in this area to improve the accuracy and reliability of wind forecasting models.

This thesis is aimed at tackling the challenges of integrating wind power into the day-ahead energy and reserve markets. Specifically, it focuses on addressing the difficulties related to accurately forecasting wind fluctuations at high temporal resolutions as well as developing effective bidding

strategies for WPP. The next subsection will delve deeper into this issue and present the contributions proposed in this thesis to overcome these challenges and facilitate a smooth integration of wind power into the energy and reserve markets.

1.2 Objectives and Contributions

In light of the incentives for participation of WPP in day-ahead energy and reserve markets, the objective of this thesis is to develop efficient models to allow wind-only portfolios to participate in the energy and reserve markets (as explained in 1.1.3).

Notably, a great effort is devoted in the literature to hourly wind forecasting and scenario generation models [20]. In this regard, the available bidding models for WPP participation in the energy and reserve markets take hourly wind uncertainty as input. As a result, the actual wind capacity available in real-time, accounting for inherent fast wind speed fluctuations, is not considered in the literature. Such models thereby fail to capture penalties arising from the WPP's inability to deliver the capacity offered at the day-ahead stage, which potentially leads to ex-post disappointment regarding the actual profit.

Contribution 1. As the first contribution of this thesis, we aim to properly evaluate the impact of fast wind fluctuations on hourly wind power bidding (which is based on hourly wind uncertainty). To that end, we formulate a day-ahead problem for a WPP targeting to maximize its profit in the energy and reserve markets. Once the optimal bids are obtained by the bidding model, an empirical ex-post analysis, with high temporal granularity, is performed to assess the impact of actual wind speed fluctuations on the WPP's profit. This contrasts with the current literature

that performs ex-post analyses using the same time resolution as in the optimization, which hides the true impact of the underlying modeling assumption. Finally, we separately compare the revenue streams resulting from different market floors with their expected values, so as to determine the losses regarding the inability of both reserve capacity procurement and activation as well as deviations from the scheduled energy.

The scientific contribution regarding this part, i.e., evaluating the impact of fast wind fluctuations on WPP's profit in the energy and reserve market, is:

> S.A. Hosseini, J.-F. Toubeau, N. Singh, J. De Kooning, N. Kayedpour, G. Crevecoeur, Z. De Grève, F. Vallée, L. Vandevelde, "Impact of fast wind fluctuations on the profit of a wind power producer jointly trading in energy and reserve markets," The 9th Renewable Power Generation Conference (RPG Dublin Online 2021), Dublin, Ireland (Online), 2021, pp. 240–245. doi: 10.1049/icp.2021.1386

Reserve capacity requirement is conventionally considered as a deterministic metric, e.g. fraction of demand, the largest generator, or line contingency, in the market clearing process [21]. However, such practice can impose a great cost on the power systems operation as it disregards the compromise between the systems operating cost and the security of supply [21]. Moreover, such a criterion leaves out the stochastic nature and underlying reliability of the committed units and, thereby could result in a substantial loss-of-load in the power system [22]. Accordingly, several approaches in the course of the past decades have been presented to integrate a probabilistic reserve constraint in market-clearing algorithms [22].

Contribution 2. As the second contribution of this thesis, an advanced bidding strategy dedicated to optimal dispatch of the WPP in the energy and reserve market is proposed. The suggested strategy exploits a novel bi-objective two-stage chance-constrained stochastic model in which various revenue streams, stemming from both day-ahead and real-time stages, are fully accounted for. The first objective of the presented model is to allocate the optimal share of the power assigned to each market floor in the day-ahead stage so as to maximize the WPP's profit. Then, the formulation considers the confidence level of delivering the contracted reserve power in real-time through an additional competing objective. Meanwhile, the presented method allows us to also illustrate the effect of reserve availability as a probabilistic measure on WPP's profit. The obtained revenue streams regarding each market floor, as well as the total revenue of the WPP, are then evaluated in a Monte Carlo out-of-sample analysis. The scientific contribution regarding this part is as follows:

S. A. Hosseini, J.-F. Toubeau, Z. De Grève and F. Vallée, "An advanced day-ahead bidding strategy for wind power producers considering confidence level on the real-time reserve provision", Appl. Energy, vol. 280, p. 115973, 2020. doi: 10.1016/j.apenergy.2020.115973

Ensuring acceptable forecast performance is more difficult for wind forecasting with ultra-short-term intervals than for short-term (hourly) intervals [20]. The increased difficulty of wind forecasting with ultra-short-term granularity is due to the higher randomness and volatility as well as a large number of prediction steps [20]. Therefore, extracting a function or a model that relates the complex nonlinearity between the input features and the future wind speed is not suitable for ultra-short-term prediction [23]. Thus, due to the mentioned difficulty, the current wind power bidding models have merely employed hourly wind uncertainty for the remuneration

of real-time energy and reserve deviation.

Contribution 3. As the third contribution of this thesis, an advanced scenario generation model is presented to generate effective scenarios of wind deviations conditioned on wind fluctuation levels with high temporal resolution. For this purpose, the well-known generative adversarial network (GAN) is further improved by using a more effective loss function and enriching it with an auxiliary classifier so as to generate wind scenarios with high granularity. The architecture of each agent of this model is carefully designed to boost the performance of the proposed scenario generation while avoiding any pre-processing of the input data. The performance of the proposed scenario generation method is compared to the state of the art in terms of statistical and similarity metrics.

Contribution 4. Additionally, a novel multi-resolution probabilistic bidding framework is proposed to optimize the profit of WPPs in energy and reserve markets. Compared with existing works, the minute-level wind power variations are also embedded in the proposed WPP bidding strategy to precisely model the scheduled reserve bids at the balancing stage (cleared at minute-wise intervals). Besides, the model is enriched with a probabilistic constraint controlling the confidence level of the wind capacity offered to the reserve market. We show that the acquired optimal bids not only enhance the WPP profit in the market but also satisfy the required confidence level concerning reserve availability.

The scientific contribution regarding the proposed scenario generation model and multi-resolution bidding model is as follows:

S. A. Hosseini, J.-F. Toubeau, Z. De Grève, Y. Wang, N. Amjady and F. Vallée, "Data-Driven Multi-Resolution Probabilistic Energy and Reserve Bidding of Wind Power," *in IEEE Transactions on Power Systems,* vol. 38, no. 1, pp. 85-99, Jan. 2023, doi: 10.1109/TPWRS.2022.3155865.

While scenario generation methods offer insight into potential outcomes, they also show major limitations, including the representation of a wide range of uncertainty and inadequate reflection of true probability distributions, leading to potential over- or under-confidence in projections. Additionally, scenario generation techniques, such as GANs, struggle to capture time dependence between successive periods in generated scenarios, as they are typically trained on large amounts of data without considering inter-sample temporal relationships. On the other hand, conventional forecasting models, while capturing time dependency, are not capable of effectively predicting wind variability with high temporal resolution over the day-ahead horizon. This is attributed to the substantial difference between the forecast horizon (e.g., day-ahead) and the ultra-short timescale (e.g., seconds), resulting in higher forecasting errors due to the unavailability of future information and the accumulation of errors at each time step.

Contribution 5. As the fifth contribution, we go beyond the traditional approach and formulate a day-ahead wind power forecasting problem that renders information on intra-period wind variability with high resolution (second-wise), by predicting the intra-period temporal distribution of wind power for day-ahead forecast horizons. To this end, the forecaster's loss should be able to compare distributions, rather than individual elements, as in conventional time-series forecasts. First, a parametric and several entropy-based losses are tailored to this problem to acquire candidate

solutions using classical approaches. Then, a differentiable loss, based on the Wasserstein Distance (WD) is dedicatedly developed to overcome the inherent limitations of the tailored losses while conserving end-to-end gradient learning of the proposed forecasting model. The superiority of the proposed Wasserstein distance-based loss is verified by comparing its predictions with those of classical losses, using real-world datasets. Also, through a comprehensive analysis of real market data, a day-ahead wind power scheduling problem further demonstrates the added economic value and the motivation behind leveraging the proposed forecasting model.

The scientific contribution regarding the proposed distribution forecasting model and bidding model is as follows:

S.A. Hosseini, J.-F. Toubeau, N. Amjady, F. Vallée, " Day-Ahead Wind Power Temporal Distribution Forecasting With High Resolution " *IEEE Trans. Power Syst.*, (In Revision), 2023.

1.3 Outline

The organization of the presented thesis is explained in this subsection.

Chapter 2 provides a general overview of the current structure of electricity markets in Europe. To this end, after a brief introduction to different trading floors in the electricity market, the market floors of interest, in this thesis, for trading wind power are detailed. Additionally, the mechanisms for real-time compensations regarding day-ahead energy and reserve bids are illustrated. Finally, the state of the art on WPP bidding approaches is given.

Chapter 3 starts with an introduction to our motivation for assessing the impact of intra-hour wind speed variations on conventional WPP bidding and revenue streams. To do so, a bidding model for WPP trading in both day-ahead energy and reserve market floors is presented. Then, an empirical ex-post analysis, considering a high temporal resolution (to evaluate the impact of using hourly steps in the optimization), is performed. Afterward, the corresponding numerical results are detailed. Finally, the conclusion of this assessment is given at the end of the chapter.

Chapter 4 presents a bi-objective WPP bidding model in which a risk threshold regarding the confidence level of the offered reserve bid is integrated so as to maximize WPP's profit while respecting market policies. The effectiveness of the proposed approach (as compared to the ones excluding a risk-based index for reserve availability) is then illustrated. Then, the impact of market incentives on the proposed WPP bidding is shown. The acquired conclusion is given at the end of the chapter.

In Chapter 5, the proposed high temporal resolution wind speed scenario generation model, as well as the advanced probabilistic multi-resolution WPP bidding framework, is presented. First, the proposed formulation for a multi-resolution WPP bidding strategy that considers wind uncertainty at different time scales is presented. Then, the basic idea of vanilla GAN and its variants for scenario generation along with their limitations are discussed. Afterward, we present our contributions beyond the state of the art by incorporating an auxiliary classifier in the proposed Wasserstein-based GAN scenario generation model. The benefits of combining both devised scenario generation and bidding models in a unique trading framework are discussed in the numerical result section, and the Chapter is then concluded.

Chapter 6 proposes a forecasting model for the prediction of the intra-period temporal distribution of wind power for day-ahead horizons. In this chapter, the day-ahead wind power temporal distribution forecasting problem is, first, formulated. Then, it is explained how classical machine-learning losses can be tailored for the presented task. Afterward, an effective loss based on Wasserstein Distance, which overcomes the limitations of the classic losses, is presented. Finally, the numerical results are given and the chapter is concluded at the end.

In chapter 7, the main contributions and relevant findings of the thesis are reemphasized. Also, the perspective of future works regarding this thesis is given.

Chapter 2. Wind Energy in Electricity Markets

2.1 Introduction

Historically, the organization of the electric industry was established based on integrated structures and strict controls that allowed no opportunity from market forces. This vertically integrated organization of the electricity sector was supported by scale and scope economies [24]. However, a few decades ago, this idea was questioned as it adversely affected the price of electric power and quality service due to the lack of competitiveness and options for users to choose their suppliers [19]. Therefore, a new theory based on privatization came into play. In this structure, privatized companies, e.g., generation companies, are exposed to neoliberal and competitive market environments.

The physical characteristics of electrical energy make the electricity markets substantially different from other competitive markets. For example, electrical energy cannot be economically stored in large quantities. The volume of electrical energy transferred from one point to the other is constrained by the line capacities. Also, at every instant, the generation and demand must match to avoid the risk of a blackout.

These special characteristics of electricity explain the complex structure of current electricity markets which are comprised of several products and market floors before real-time delivery.

2.2 Electricity Market Framework

European electricity markets operate on various levels. Wholesale markets are organized differently than retail markets, which serve consumers. Markets may vary in geographical scope, ranging from local offers on the retail market to transnational wholesale markets. Based on their time scale, wholesale markets range from real-time physical markets to long-term financial contracts [25].

Forwards and futures are long-term financial markets, which run from years before up to the day before the delivery of electricity. They serve market participants as a hedge and speculating tool for reducing their exposure to price fluctuations in short-term physical markets. It is in the interest of electricity producers to contract future electricity sales using forward and future markets in order to hedge price risks, i.e., reducing their exposure to price decrease in the short-term markets [26].

It is also important to distinguish two ways in which electricity can be traded in different types of wholesale markets. The first way is bilateral trading, in which producers and customers directly negotiate and agree on the price of electricity. The second way is trading at power exchanges or organized trading platforms. Power exchanges are usually designed as continuous trading or discrete auctions. A discrete auction is a form of trading where market participants submit generation and demand bids that are used to obtain supply and demand curves. The market-clearing price for each trading period is based on the supply and demand curve intersection. Continuous trading implies trades between market participants when one accepts offers from another without the formation of a uniform market clearing price. The price is formed for each of the trades independently [26].

Day-Ahead Markets (DAM) are the basis of physical electricity trading, where electricity is traded one day before the delivery. Their high importance arises from the day-ahead supply and demand balance requirement of the entire bidding zone, i.e., in a bidding zone, the planned electricity generation must be equal to the forecasted demand plus the difference between imports from and exports to the other bidding zones. European day-ahead markets usually use discrete auctions as a form of trading.

In Intra-Day Markets (IM) the electricity is traded on the delivery day. These types of markets supplement the DAM and secure the balance between the supply and the demand caused by unexpected events that can occur between closing the DAM and the delivery time, e.g., due to unexpected power plant outage or inaccurate wind forecast. In other words, using the IM platform, market participants can minimize the gap between the day-ahead settlements and the actual produced/consumed volume of electricity.

European intra-day markets are still not harmonized and either designed as continuous trading or discrete auctions [27]. Importantly, modeling intra-day markets is more challenging than day-ahead markets (DAM) due to their shorter horizon, pay-as-bid and over-the-counter nature. Consequently, the complexity of the intra-day market may prompt the use of simplified assumptions in modeling. However, from a portfolio perspective, it is essential to recognize that relying on such simplifications can potentially have negative impacts on the effectiveness of decisions made in the intra-day market, and more critically, on day-ahead decisions when a co-optimization of both is sought. As such, an alternative approach, for the portfolio, could be to focus on DAM and adjust its day-ahead offers based on new information that becomes available within the delivery day.

The role of the TSO is to maintain a real-time balance by activating reserves at the system level. Balancing Markets (BM) are used by the TSO to procure reserves. Balancing markets can be divided into reserve procurement and financial settlement of imbalances. Reserve procurement is a reservation of spare firm capacity in advance. This capacity can, if needed, be used for generation demand balancing. Financial settlement, e.g., in a single price imbalance mechanism, can be defined as a penalization for market participants causing imbalance and financial awards for market participants used for imbalance mitigation (e.g., reserve providers) [19]. In a dual price imbalance mechanism, participants who are deviated from their scheduled bids are subject to a penalty regardless of their contribution to system balancing [19].

Electricity markets in Europe are organized by the Nominated Electricity Market Operators (NEMOs), while the TSOs are in charge of balancing markets. The various market floors in European electricity markets are shown in Figure 2.1. This thesis will focus on trading wind energy in the day-ahead market while WPPs are responsible for their real-time deviations. The market floors of interest in this thesis for WPP bidding are shown by blue blocks in Figure 2.1.

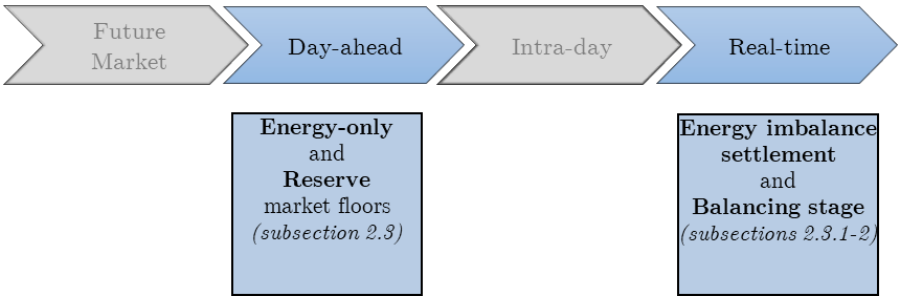

Figure 2.1) The market floors of interest in this thesis are shown by blue blocks

2.3 Day-Ahead Energy and Reserve Market

In the literature of the electricity market, day-ahead means trading energy for the following day considering available transmission capacity. Electricity may be traded for individual or all 24 hours of the next day, at any time on any day [26].

The day-ahead market is important because the market zone must be in balance at the end of the day-ahead market. In other words, the scheduled generation in the market zone equals demand in the market zone and the net exchange to other market zones. The day-ahead energy trading in the Belgian market zone is the EPEX day-ahead market. Market players can bid or offer their orders up until 12 pm.[28].

The Belgian market zone is indirectly linked with other market zones using EPEX DAM. Under implicit cross-border allocation, a buyer or seller of electricity automatically has the usage right of transmission capacity by submitting orders to the power trading platform. Energy and transmission capacity are thus traded together. Today, the Belgian day-ahead market is linked with several countries such as the Netherlands, Luxembourg, the United Kingdom, Germany, France, and Norway.

Each Balance Responsible Party (BRP) submits a balanced portfolio to the TSO, i.e., nominations, after the clearing of the day-ahead markets. These nominations indicate the scheduled generation or consumption for each asset of the BRP [26]. Notably, the nominations differ from the EPEX DAM market-clearing in three aspects: the nominations contain the total scheduled generation or consumption, the nominations are made at the power plant level, whereas on EPEX DAM electricity is traded at the BRP level, and the nominations have a quarter-hourly time resolution, whereas

EPEX DAM has an hourly time resolution. In Belgium, a BRP must submit its day-ahead portfolio to Elia by 2 pm.

Market players submit two kinds of orders in the auction to deal with the inherent non-convexities in the techno-economic characteristics of (both demand- and supply-sides) electrical technologies: 1) orders for each delivery period that reflect their desire to purchase or sell, for all price segments between the minimum and maximum range in the auction, in a given volume. 2) block orders that link multiple delivery periods. A demand curve is created based on the buy orders, and a supply curve is created based on the sell orders (called aggregated curves, both for each hour of the following day). The market-clearing price (MCP), which reveals supply and demand, is located at the intersection of the two curves. An auction has the advantage of gathering liquidity at a given point in time while providing full transparency on traded market clearing volumes (MCV)[26].

In order to ensure the sufficient provision of balancing services, the system operator may establish balancing market mechanisms. The balancing market is a centralized market platform managed by the TSO where balancing service providers (BSPs), such as generators, renewable energy sources, storage, and demand response, can submit bids for balancing. BSPs may be individual entities that provide reserves or an association of several such entities. Balancing bids can be divided into two types:

- Bids for balancing capacity: the availability of the amount of capacity bid must be ensured to the system operator for the trading period in question; it will be activated if needed.

- Bids for balancing energy: the BSP must either increase or decrease its generation capacity/demand, or use other technologies, for the quantity of energy offered for the trading period in question if the TSO requests it.

These bids can be made for various types of balancing services, they can either be symmetrical (BSPs offer a band in which they must change their production/demand in accordance to the TSOs choice), upwards (they undertake to increase their generation, or decrease demand), or downwards (they undertake to reduce their generation or increase demand). The main balancing services in the reserve market are discussed in the following.

Frequency containment reserves (FCR) are remotely regulated and locally activated reserves that are utilized to stabilize the frequency within seconds [19]. To rebalance the system from frequency distortion, frequency restoration reserves (FRR) are used. Frequency restoration reserves are operational for a period of seconds to 15 minutes. Notably, they are managed and activated centrally [29].

Importantly, the availability of the contracted balancing capacity is frequently far more important than their actual activation. That is because the System Operator must ensure that enough energy will be available to resolve all possible system imbalances [29].

Real-world European electricity markets, as applied in this thesis, are such that the reserve and energy market floors are cleared sequentially via independent day-ahead auctions [18]. Nevertheless, as a common fair approximation in the dedicated literature [19], ensuring an acceptable accuracy, we adopt a joint WPP bidding formulation. It is justified since there is a strong relationship between the contribution of WPP in the energy-only and reserve markets [18] due to the capacity constraint, hourly and minute-wise wind uncertainty coupling constraint, and the risk of real-

time reserve unavailability. Therefore, on account of this interdependency, and the short delay between the clearing of day-ahead energy and reserve markets [18], the proposed framework is formulated as a single decision-making problem to achieve the optimal trade-off between the energy and reserve shares based on the scenarios of wind uncertainty.

2.3.1 Real-Time Energy Imbalance Settlement

The transmission system operator is responsible for maintaining the equilibrium between supply and demand to support grid stability and reliability. In the design of the current market, TSO transfers part of this responsibility to balance responsible parties in terms of financial liability.

It should be mentioned that in many day-ahead electricity markets, e.g., the ones operated by EPEX-Spot and Nord Pool (which include several countries, such as Belgium), any producer providing a block bid size of 0.1 MWh is able to participate in the day-ahead energy market [10]. Additionally, any portfolio that merely meets the necessary financial solvency conditions and capital guarantees, regardless of its total power exchange, can conclude a BRP contract [29].

In this study, WPPs can play the role of BRP and are thus able to contribute to the day-ahead energy market. Therefore, WPPs could submit a power bid P^{Eo} regarding the energy market for each market period Δt of the following day. The deviations from the day-ahead scheduled bids are compensated by an imbalance settlement mechanism. Indeed**,** the quantity of energy fed in the system by a BRP may likely deviate from its nominated bid due to the inherent uncertainties in power generation. Therefore, the TSO applies an imbalance pricing mechanism to improve the real-time demand-supply balance at the system level. To do so, the deviating BRP is expected to purchase its generation deficit and sell its generation surplus at

the energy imbalance price. The imbalance pricing scheme varies between markets [19]. The most commonly used imbalance settlement mechanisms in real-world electricity markets include single and dual pricing [19]. Single pricing, e.g., used in Germany, refers to the settlement procedure in which the BRPs with energy deficit have to pay the same imbalance price as the BRPs with generation surplus [19]. In contrast, dual pricing, e.g., used in Denmark, penalizes net generation surpluses and deficits with different prices to create a better incentive for the BRPs to remain in balance.

In this thesis, we consider an imbalance settlement mechanism in which BRPs are discouraged to deviate from the contracted bids by means of dual pricing. The net revenue of the BRP regarding the day-ahead energy market and imbalance settlement, $\mathcal{R}^E$, versus the injected power to the network, P^E, in this scheme is graphically shown in Figure 2.2. As seen in this figure, the BRP receives a defined revenue with respect to the offered energy bid and day-ahead energy market price, λ^{Eo}. However, real-time over-generation is remunerated to the committed unit at a lower price, $\lambda^{B\uparrow}$, with respect to λ^{Eo}. Likewise, the BRP should purchase the deficit of generation at a higher price, $\lambda^{B\downarrow}$.

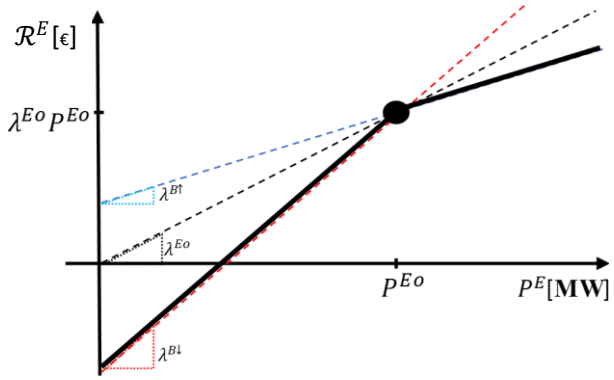

Figure 2.2) Revenue obtained at day-ahead energy and imbalance settlement vs delivered power.

Such a market structure strongly incentivizes market actors to stay in balance (irrespective of the global frequency conditions within the system).

2.3.2 Real-Time Balancing Stage

In the case of a real-time mismatch between supply and demand at the system level (arising from the aggregated imbalances of all BRPs), TSO relies on various capacity services that are purchased from balance service providers (BSPs) in the reserve market. The reserve market services are categorized by their response time and duration [30]. The BSPs should comply with balancing rules concerning the offered flexibility. This study focuses on frequency containment reserve (FCR), which has the fastest time response in the balancing market. The capacity test control requires the FCR providers to deploy the submitted capacity within a short time interval, e.g., 10 seconds to one minute [19]. The producers who offer FCR are remunerated based on the offered power in the day-ahead capacity reserve market. However, depending on market rules, they can also get additional energy-based revenue for real-time activation of FCR [31]. Meanwhile, as the obligation of means states, the TSO should have access to the FCR provider's measurements and control system states to verify the availability of the offered capacity within the very short-term intervals and to penalize the reserve providers which fail to provide the offered capacity [19]. Consequently, the BSP should satisfy the confidence level of the scheduled reserve bid. Deviations from the offered FCR are financially settled in the balancing stage.

The required real-time percentage of the FCR, θ, which is automatically activated by the TSO in a decentralized way, is a function of the system frequency deviation Δf. In this regard, when a deviation is within the dead-band, $|\Delta f| \leq 0.01$ Hz, the system is considered to operate normally and no

FCR service is activated. However, a specific percentage of FCR is activated for $0.01 \leq |\Delta f| \leq 0.2$ as a linear function of Δf. Then, the full power is activated for $|\Delta f| \geq 0.2$. This relationship between the FCR activation and the system frequency deviation is illustrated in Figure 2.3. It should be noted that positive frequency deviations indicate a surplus of generation and thus a down-regulation requirement, whereas negative Δf requires the activation of upward regulation. Two penalty prices can be considered in the energy and reserve markets, i.e., ERM, structure in order to meritoriously remunerate committed reserve providers.

Particularly, in the day-ahead stage, the FCR provider is paid for the offered quantity, P^{Ro} (MW) at the cleared reserve market price, λ^{Ro} (€/MW/h). However, at the balancing stage, the real-time deviations from P^{Ro}, are penalized by another rate λ^{Ro}. Moreover, when the reserve provider fails to provide the required FCR, the unit pays an additional penalty. This adaptive mechanism ensures that the FCR provider yields no advantage regarding the activated FCR in terms of energy when it fails in the availability check. The net revenue of WPP in the reserve market, $\mathcal{R}^R$, versus the available power capacity, P^R, in this mechanism is illustrated in Figure 2.4. In this figure, the dotted blue line shows the income for the real-time reserve procurement. It is seen that for $P^R \geq P^{Ro}$, the committed unit receives a constant expected revenue regarding the day-ahead offer. However, the lack of reserve power availability leads to a loss of revenue in real-time. Moreover, as shown by the dotted red line, the participant obtains a constant revenue of $\lambda^{a\uparrow} \theta \, P^{Ro}$ when it passes the availability check

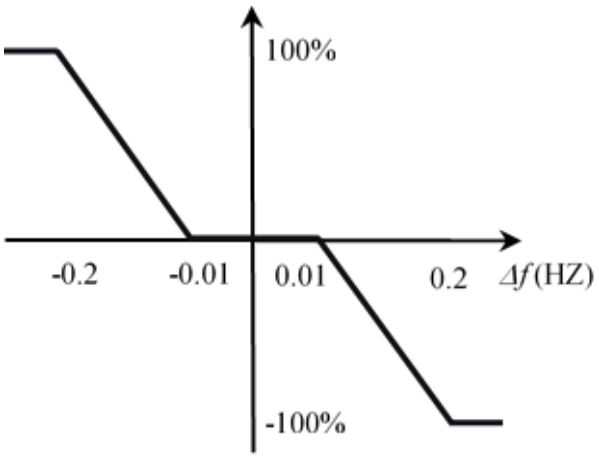

Figure 2.3) Percentage of FCR activation with respect to a frequency deviation.

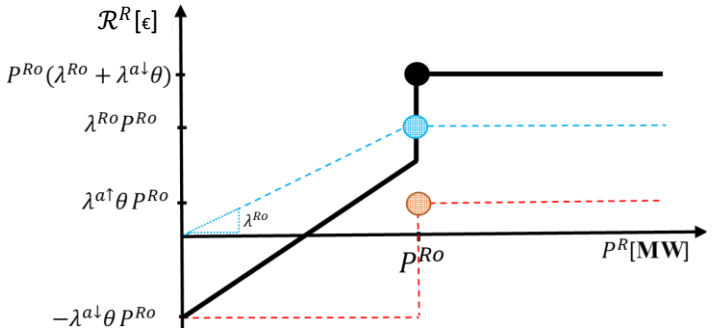

Figure 2.4) Representation of the different revenues from the FCR, i.e., procurement revenue as a function of the offered FCR bid (blue), activation revenue as a function of the percentage of called reserve(Red), and total revenue in the reserve market

in real-time for reserve activation. In contrast, when $P^R < P^{Ro}$, the committed unit is penalized at a higher price factor $\lambda^{a\downarrow}\theta\ P^{Ro}$. Finally, the total revenue of WPP in real-time is obtained by adding both remuneration strategies as shown by the plain black line.

It should be noted that we consider a balancing market wherein one-directional upward FCR bids are also acknowledged. It should be noted that downward reserve provision for WPPs is not economically encouraged since they do not leverage fuel-saving returns as conventional units do.

2.4 State of the art on WPP Bidding Approaches

The growing share of renewable energy resources is a great challenge for power system operators that have to continuously accommodate the resulting intermittent and uncertain power supply while ensuring system stability and security [12]. As discussed, other market floors such as the day-ahead reserve market are complementing the day-ahead energy market so as to help for compensating for the real-time mismatch between generation and demand, thereby improving the frequency regulation of the power systems [13]. These market floors are accompanied by a real-time balancing stage in which the imbalances from the scheduled bids are financially settled [19].

A possible way to tackle the imbalance cost of wind power deviation is to team up with other stable power sources, such as thermal power or hydro technology [32], in order to maximize the portfolio's profit. However, coordinated bidding may not be recognized in some markets [33]. Moreover, owing to the recent developments in wind turbines' technology, market incentives, and forecast tools, the WPPs are seeking to obtain an optimal offering strategy while acting as single Generation Company (GENCO) owners in the electricity market [34]. Accordingly, in this study, the GENCO is considered to be a WPP, where all its generation comes from wind energy, in order to analyze its potential as an active market actor.

In [35] a stochastic bidding algorithm for single and dual imbalance settlement schemes is presented to enhance WPP's profit in the day-ahead energy market while minimizing the imbalance costs considering generation and price uncertainties. An optimal energy bid is obtained in [36] by reducing the commercial risk of imbalance cost using Markov probabilities. In addition, the impact of market closure delays and forecasting window

lengths are studied. In [37], an hourly bidding strategy for a WPP participating in the day-ahead energy and adjustment market is proposed while controlling the risk of profit variability at the expense of a minor decrease in expected profit. In [38] an energy offering curve aiming to maximize the WPP's profit is obtained through the two-dimensional distribution of price and wind power prediction errors. The presented offer curve has greater profitability rather than the offer curve of the marginal distribution. An optimal energy bidding strategy to maximize the operating profit of a WPP in a real-time market is developed in [39], taking into account the uncertainty of other energy sources. The presented model employs a bi-level stochastic optimization scheme in which the lower-level clears the real-time market and the upper-level reduces the negative profit of the WPP. In [40], the negative impact of real-time energy deviations of WPP is mitigated by buying a quantity of energy from the intra-day reserve market which is calculated by the Cauchy-Lorentz distribution model. In [41] two types of offering strategies hedge the risk of profit variability by relying on a naïve use of power forecast and stochastic model. Interestingly, it is shown that the stochastic approach outperforms the bidding strategy based on the naïve forecast in terms of expected profit and its variability.

However, despite the potential ability of wind turbines in reserve provision, limited attention is devoted to the participation of the WPP in the ERM while reducing the imbalances that occur in real-time (for energy and reserve contributions). In [42], an analytical method is applied to increase wind power profit by participating in the ERM. In this model, both WPP and the TSO encounter fewer intra-hour variations in the energy market since part of these variations is absorbed in the reserve market. However, the TSO may further suffer from the risk of real-time reserve power unavailability. Moreover, the wind turbine control strategy is

neglected in their model. Thus, the obtained optimal bids and the expected revenue may not be attainable in practice. In [43], different control strategies for the allocation of energy and reserve power in the bidding strategy are taken into account. The proposed model employs market penalties and wind power uncertainties in an analytical approach based on the newsvendor problem. The optimal bidding strategy of the WPP aiming to maximize its expected profit in the ERM, based on market incentives, considering wind power uncertainty is dealt with as a stochastic programming problem in [44]. The proposed method also evaluates the impact of having better forecast information, close to the real-time stage, on WPP's offering strategy.

2.5 Employed Data in this thesis

This section provides an overview of the data characteristics in this work. In particular, the main data used to conduct the analysis in this study are meteorological, market, and system data. The meteorological data are used to train forecasting and scenario generation models that aim to estimate the future value of wind speed and power. Market data, on the other hand, are used as the core of the decision-making framework. The framework aims to optimize wind energy scheduling by considering market prices along with forecasted wind power. In addition, the performance of all models is evaluated through an extensive out-of-sample analysis using these data.

In Chapters 3 and 4 of this study, we use quarter-hourly resolution wind power data to generate wind power scenarios. We obtain these data from Elia's publicly available database [45], which provides wind power data at quarter-hourly resolution. Similarly, we collect market incentives and system data, such as system frequency, from Elia [45] to perform the analyses.

Notably, at the time of conducting the analysis, we lacked wind power data with a high temporal resolution to assess the influence of wind fluctuations on the decisions made by the models proposed in Chapters 3 and 4. To solve this problem, we used a sophisticated wind field simulator [46]. By generating time series of wind speed fluctuations with a temporal resolution of 0.1 Hz, we were able to perform ex-post analyses to study the impacts of wind fluctuations.

During the development of the scenario generation and forecasting models described in Chapters 5 and 6, the need to acquire real meteorological data with high temporal resolution became more apparent. This was critical because these models capture wind fluctuations at a fine temporal granularity, in contrast to the scenario generation model of Chapters 3 and 4, which only generate wind scenarios at an hourly resolution. Importantly, we use the meteorological data of a wind farm on the island of Frøya [47], for the period 2014 to 2016 with a temporal resolution down to the second. The wind measuring station has a pair of 100-meter-high measuring masts equipped with ultrasonic anemometers. In addition to wind speed data, calendar, and air temperature data are also available in this dataset.

To prepare the data for training and testing the scenario generation model, in Chapter 5, pre-processing techniques are used to eliminate possible outliers. This involves analyzing the data and removing any data points that fall outside of a certain range or that are considered statistical anomalies. Once the pre-processing is complete, a total of 7,560 time series are obtained, each containing 60 instances (dimensions) representing fluctuations in wind speed with minute-by-minute resolution.

In Chapter 6, where a forecasting model is proposed, 6,000 time series with a dimension of 3,600 are extracted from [47]. Each time series represents one hour and contains wind speed data with a second-by-second resolution. These data are supplemented with hourly air temperature and calendar data to train the forecast model.

For the decision-making framework, both chapters use European market data available on the ENTSO-E transparency platform [48]. The extracted data cover the same time period as the meteorological dataset. Out-of-sample evaluation of all models, in both chapters, is performed using a significant amount of real-world data, which is also used for training and tuning the models. Further information on data processing and characteristics can be found in the corresponding chapters.

Chapter 3. Assessment of Fast Wind Fluctuations

3.1 Introduction

It should be pointed out that the actual wind capacity available in real-time, accounting for inherent fast wind speed fluctuations, is not considered in the studies mentioned in subsection 2.4. Such models thereby fail to capture penalties arising from the WPP's inability to deliver the capacity offered at the day-ahead stage, which may potentially lead to ex-post disappointment regarding the actual profit.

In this chapter, we aim to properly evaluate this impact. To that end, we, first, formulate the day-ahead problem of a WPP targeting to maximize its profit in the ERM. Without loss of generality, the WPP is considered to be a price-taker in the electricity markets. It signifies that the energy generated by the WPP has no effect on market prices, which is a reasonable assumption since the generation of a single WPP is dramatically smaller than the total generation at the system level. The schematic diagram of the applied decision model is shown in Figure 3.1. It is seen that the framework receives market prices along with system frequency and hourly wind uncertainties as input and returns the optimal power allocation for participation in the energy and reserve market floors.

In order to investigate the impact of actual intra-period wind speed fluctuations on the obtained results, two different cases are considered. In

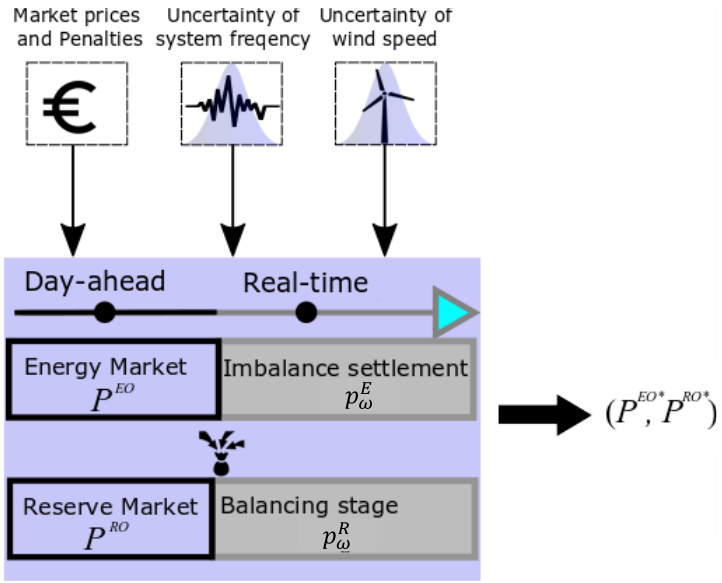

Figure 3.1) Schematic diagram of the applied decision model for assessing the adverse impacts of intra-hour wind variations (the optimal values are shown by * superscripts).

the first one, we consider a single scenario that represents the actual perfect information of the mean wind power (over each time step of the daily optimization horizon). This case shows that, even if a WPP relies on perfect information on the averaged future wind conditions, the intra-period wind fluctuations, which is considered to be 10 seconds in this study, can negatively affect its revenues. The second case is modeled as a more realistic two-stage stochastic model, where wind speed uncertainties are represented through a set of scenarios.

In the presented formulation, the WPP is not allowed to deviate from the contracted reserve capacity, thus leading to conservative strategies in the reserve market. After obtaining the optimal bids in both aforementioned cases, an ex-post analysis is performed. The proposed ex-post analysis employs a set of 15-min synthetic wind speed signals with a 10-sec resolution as well as a set of real-world system frequency data (to represent the real-time activation of balancing reserves). The numerical analysis illustrates

the consequences of intra-period wind speed fluctuations in providing the balancing reserve, as well as the resulting effects on the WPP's expected inflows and losses. The revenue streams in the different market floors are individually compared to their associated expected terms.

The remaining part of the chapter is outlined as follows. In section 3.2, the proposed stochastic model, (which corresponds to the second case mentioned above), for the participation of WPP in ERM is presented. Section 3.3 explains the proposed empirical ex-post analysis and assessment approach. In section 3.4 the numerical results are detailed. Section 3.5 concludes the chapter with some guidelines for the participation of WPPs in the ERM. The material presented in this chapter is predominantly sourced from the author's publication, as referenced in last Section (Related publication), with due respect for the original copyright[1].

3.2 Conservative Stochastic Bidding Formulation

In this section, a stochastic framework is presented to assist WPPs to find the optimal trade-off between energy and reserve in ERM.

The mathematical formulation of this problem is expressed as follows:

$$\max_{X,\Psi} \mathcal{R} = \lambda^{Eo} P^{Eo} \Delta t + \lambda^{Ro} P^{Ro} + \sum_{\omega \in \Omega} \pi_\omega \left\{ \lambda^{E\uparrow} \Delta p_\omega^{E\uparrow} - \lambda^{E\downarrow} \Delta p_\omega^{E\downarrow} + \lambda^{a\uparrow} \theta_\omega p_\omega^R \right\} \Delta t \tag{3.1}$$

$$P^{Eo} + P^{Ro} \leq \overline{P} \tag{3.2}$$

[1] The IET permission grant can be accessed at the following link: https://www.wiley.com/en-us/network/publishing/research-publishing/trending-stories/how-to-clear-permissions-for-a-thesis-or-dissertation [Accessed 10 Feb 2023]

$$P^{Eo} + P^{Ro} \geq \underline{P} \tag{3.3}$$

$$p_\omega^E + p_\omega^R = \tilde{P}_\omega \qquad \forall \omega \in \Omega \tag{3.4}$$

$$\Delta p_\omega^E = P^{Eo} - p_\omega^E \qquad \forall \omega \in \Omega \tag{3.5}$$

$$\Delta p_\omega^E = \Delta p_\omega^{E\downarrow} - \Delta p_\omega^{E\uparrow} \qquad \forall \omega \in \Omega \tag{3.6}$$

$$P^{Ro} - p_\omega^R \leq 0 \qquad \forall \omega \in \Omega \tag{3.7}$$

$$P^{Eo}, P^{Ro}, p_\omega^E, p_\omega^R, \Delta p_\omega^E, \Delta p_\omega^{E\uparrow}, \Delta p_\omega^{E\downarrow} \geq 0 \qquad \forall \omega \in \Omega \tag{3.8}$$

where the objective function $\mathcal{R}$, presented in (3.1), consists of two contributions for the first (day-ahead) stage and 3 terms for the second (real-time) stage. The first term represents the income of the WPP in the day-ahead energy market. In that regard, $\lambda^{Eo}, P^{Eo},$ and Δt denote the day-ahead energy price, the contracted power, and the imbalance period (in hour units), respectively. The second term represents the income for procurement of the reserve capacity (which reflects a pay-as-bid system), and depends on the reserve capacity procurement price λ^{Ro}, and the contracted reserve capacity P^{Ro}. The real-time contributions are weighted by scenario $\omega \in \Omega$, where π_ω is the probability of each scenario. The third and fourth terms indicate the imbalance settlement, where $\lambda^{E\uparrow}$ and $\lambda^{E\downarrow}$ denote the imbalance price associated with a power surplus $\Delta p_\omega^{E\uparrow}$ and power deficit $\Delta p_\omega^{E\downarrow}$ with respect to the day-ahead contract respectively. The last term in (3.1) determines the payment of reserve power activation, where $\lambda^{a\uparrow}$ and θ_ω represent the reserve activation price and the percentage of real-time reserve deployment p_ω^R, respectively.

Constraints (3.2) and (3.3) guarantee that the total contracted bid in the energy and reserve markets is bounded by the physical generation limits of the wind farm. Constraint (3.4) entails the allocated power in the energy market p_ω^E and the reserve market p_ω^R to match the total available power

$\tilde{P}_\omega$ in each scenario. Constraint (3.5) determines the total power deviation in each scenario Δp_ω^E. Constraint (3.6) allows $\Delta p_\omega^{E\downarrow}$ to be the deficit of power in case of real-time generation shortage and $\Delta p_\omega^{E\uparrow}$ to be the surplus of generation in case of over generation. Constraint (3.7) ensures that violation of the scheduled reserve (and its demanded activation) does not occur. Constraint (3.8) guarantees that the first- and second-stage optimization variables, i.e. respectively, denoted by $\mathrm{X} = \{P^{Eo}, P^{Ro}\}$ and $\Psi = \{p_\omega^E, p_\omega^R, \Delta p_\omega^E, \Delta p_\omega^{E\downarrow}, \Delta p_\omega^{E\uparrow}\}$, are non-negative. Additionally, the random variables θ_ω and $\tilde{P}_\omega$ introduce the uncertainties in the model. The framework has been modeled as a linear programming problem.

It is worth noting that, in this model, the expected values of market prices are substituted by random sampling from their estimated distribution. Due to the certainty equivalent theory, this assumption is valid as these prices enter linearly in the objective function and are not influenced by the WPP generation [19], [43]. Moreover, the presented model (3.1)-(3.8) considers one imbalance settlement period for sake of simplicity and reducing the computational burden. Nonetheless, the information regarding market prices and scenarios could be dynamically updated so as to obtain the optimal bids of the succeeding time units.

3.3 The Procedure of Ex-Post Analysis

In this section, the proposed ex-post analysis approach is described to assess the impact of the fast wind speed fluctuations on the actual WPP profit.

Energy market and imbalance settlement

The TSO imposes an imbalance fee on BRPs violating their scheduled power bids on the energy market. In this study, the imbalance settlement of energy takes place at the end of each quarter-of-an-hour, i.e. $\Delta \mathrm{t} = 1/4$ h.

Thus, for each period, depending on the system requirements for upward or downward regulation, an imbalance price is determined, which reflects the real-time value of energy. In order to assess the actual revenue of the WPP, the obtained results of the stochastic model and engaged imbalance prices, along with real-time available power are employed.

At each settlement period, when the mean observed power P^{obs} is higher than the scheduled power in the energy market P^{Eo}, the WPP gets paid for its positive deviation as follows:

$$\mathcal{R}^{\mathrm{E}+} = \Delta t(P^{obs} - P^{Eo})\lambda^{\mathrm{E}\uparrow} \tag{3.9}$$

Consequently, the actual WPP's revenue for participating in the energy market is determined as follows:

$$\mathcal{R}^{DAB} = \lambda^{Eo}\Delta t P^{Eo} + \mathcal{R}^{E+} \tag{3.10}$$

Accordingly, the loss of profit when trading the surplus of power by the imbalance settlement price rather than the day-ahead market price, the so-called opportunity cost, is yielded as follows:

$$\mathcal{R}^{op} = \Delta t(P^{obs} - P^{Eo})\left(\lambda^{Eo} - \lambda^{E\uparrow}\right) \tag{3.11}$$

On the contrary, when the mean available power is lower than the scheduled energy in the energy market, the WPP is responsible for its deficit of generation. The payment for compensating the negative deviation is expressed as follows:

$$\mathcal{R}^{\mathrm{E}-} = \Delta t(P^{obs} - P^{Eo})\lambda^{\mathrm{E}\downarrow} \tag{3.12}$$

Consequently, the income and opportunity cost of the WPP for participating in the energy market are determined by (3.13) and (3.14) respectively, as follows:

$$\mathcal{R}^{DAB} = \Delta t\lambda^{Eo}P^{Eo} + \mathcal{R}^{E-} \tag{3.13}$$

$$\mathcal{R}^{op} = \Delta t(P^{obs} - P^{Eo})\left(\lambda^{Eo} - \lambda^{\mathrm{E}\downarrow}\right) \tag{3.14}$$

Reserve and balance markets

The settlement period for procurement and activation of the reserve is equal to 10 seconds (which is shorter than the 15 minutes of the imbalance energy settlement).

The WPP's net revenue for procuring reserve capacity $\mathcal{R}^{Cap}$ is computed over each 10-second interval δt as follows:

$$\mathcal{R}^{Cap} = P^{Ro}\lambda^{Ro} - \frac{\delta t}{\Delta \acute{t}}\sum_{i=1}^{\frac{\Delta t'}{\delta t}} P^{Ro}\lambda^{Ro}\mathbb{I}\left(P_i^{obs} < P^{Ro}\right) \tag{3.15}$$

In (3.15), $\mathcal{R}^{\mathrm{Cap}}$ consists of two terms including the expected revenue of the WPP for reserve capacity procurement (first term) and the penalty for not being able to meet the contracted reserve capacity in real-time (second term). In this regard, the binary variable $\mathbb{I}$ is equal to 1 when the stated condition in the bracket is satisfied, i.e. observed power being less than the contracted FCR. The constant terms $\Delta t'$ and δt represent the energy and reserve imbalance settlement periods in seconds, respectively.

Additionally, the balancing revenues $\mathcal{R}^{a+}$ for FCR activation is expressed as follows:

$$\mathcal{R}^{a+} = \Delta t\frac{\delta t}{\Delta \acute{t}}\sum_{i=1}^{\frac{\Delta \acute{t}}{\delta t}} P^{Ro}\theta_i\lambda^{a\uparrow}\mathbb{I}\left(P_i^{obs} \geq P^{Ro}\right) \tag{3.16}$$

where $\lambda^{a\uparrow}$ is the price of reserve activation.

Additionally, the WPP is penalized when failing to meet the contracted or demanded reserve capacity as follows:

$$\mathcal{R}^{a-} = -\Delta t\frac{\delta t}{\Delta \acute{t}}\sum_{i=1}^{\frac{\Delta \acute{t}}{\delta t}} P^{Ro}\theta_i\lambda^{a\downarrow}\mathbb{I}\left(P_i^{obs} < P^{Ro}\right) \tag{3.17}$$

where $\lambda^{a\downarrow}$ is the penalty price used in the reserve imbalance settlement. It should be noted that, in this mechanism, the WPP should at least provide

the contracted reserve capacity in order to get paid for its activation. In other words, the penalty term (3.17) is applied when the WPP is unable to provide (in real-time) the reserve capacity scheduled in day-ahead.

3.4 Case Study

The proposed stochastic model and ex-post analysis are implemented in Julia/JuMP [49] and Python, using a 5 MW wind turbine model for simulation purposes. Table 3.1 summarizes the market prices and penalty rates used to evaluate the WPP's profit. Two cases are established to examine the impact of wind speed fluctuations on the WPP's profit. The first case considers the availability of perfect information on mean wind power for each quarter-hour through an ideal forecaster, while the second case takes into account the uncertainty of mean wind speed through a set of scenarios generated by an auto-regressive moving average (ARMA) scenario generation method. To generate scenarios using the ARMA model, the process involves estimating model parameters using historical data, sampling error terms from a normal distribution with mean zero and constant variance, and calculating the value of the time series for each time step and scenario using the ARMA equation (detailed in [50]). The reduced set of wind speed scenarios is then converted to wind power using the wind turbine's power curve. Moreover, an additional set of scenarios representing system frequency are produced from historical data of the last 30 days and reduced using the same scenario reduction method. These scenarios are used to calculate the percentage of actual balancing reserve power activated in real-time. The results of the model are presented through an illustrative example highlighting the effects of wind fluctuations on a single scenario and an extensive out-of-sample analysis that quantifies the financial impacts in a multi-scenario probabilistic environment.

3.4.1 Illustrative Example

First case:

In this case, a single scenario representing the perfect information on the mean wind power along with a set of scenarios representing the percentage of the required reserve activation is fed to the stochastic model. The WPP chooses to allocate all forecasted power, P^{Ro}= 0.8028 MW, in the reserve market due to more favorable prices, resulting in a constant income of € 23.26.

For the sake of illustration, one synthetic wind speed signal, with the same mean as the actual speed (i.e., 5.7 m/s), is generated. The synthetic wind speed signal is then converted to wind power using the power curve of the wind turbine as shown in Figure 3.2 (plain line). In parallel, the real-time amount of activated FCR is simulated by using the system frequency data for the period of interest, as shown in Figure 3.3. Interestingly, we observe that due to fast (10-sec) wind speed fluctuations and the required level of reserve activation, the WPP is not able to provide the contracted reserve capacity for several intervals δt, thereby losing 55.56% of its expected profit. In Figure 3.4, the instantaneous net revenue of the WPP for reserve activation is normalized by the value determined by the day-ahead optimization (plain line).

Second case:

A set of scenarios regarding the mean wind speed and percentage of the activated reserve is fed to the stochastic model (3.1)-(3.8). The obtained expected revenue and optimal bids of the WPP for a range of spot market prices are shown in Figure 3.5. It is seen that the WPP allocates a constant

Table 3.1) Prices and penalty rates of the market

λ^{Eo}	λ^{Ro}	$\lambda^{\mathrm{E}\uparrow}$
30-50	28	30
$\lambda^{\mathrm{E}\downarrow}$	$\lambda^{a\uparrow}$	$\lambda^{a\downarrow}$
50	50	150

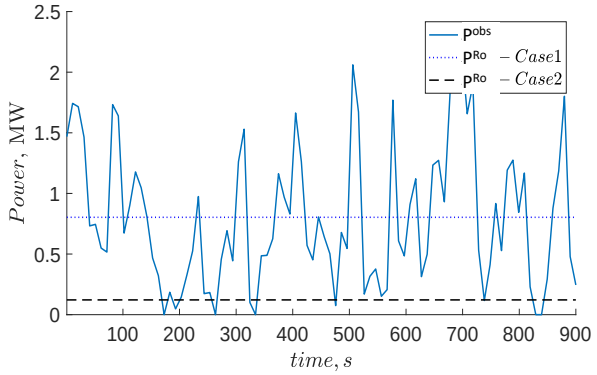

Figure 3.2) Observed power (plain line), contracted FCR for case 1(dotted line), contracted FCR for case 2 (dashed line)

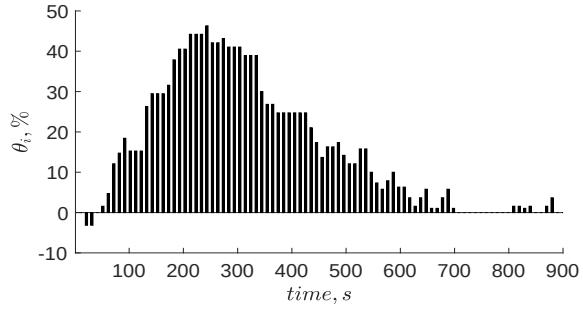

Figure 3.3) Required level of FCR activation

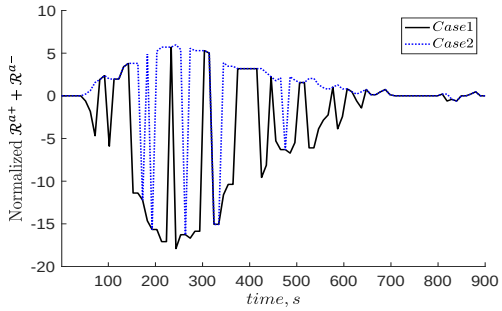

Figure 3.4) Normalized net reserve activation revenue

feasible power in the reserve market, and devotes the rest to the energy market. In this way, the WPP avoids the risk of deviation from the contracted reserve capacity. The same simulated wind speed signal and system frequency data are used for ex-post analysis. It is seen that the available mean power may differ from the power bids of the energy market. As a consequence, imbalance penalties (opportunity costs) are occurring.

The actual revenue of the WPP in the energy markets ($\mathcal{R}^{DAB}$) along with the opportunity cost ($\mathcal{R}^{\text{op}}$) are normalized by their related expected term and shown in Figure 3.6(a)-(b), respectively. One can see that the actual revenue of the WPP in the energy market may deviate more than 20% from the expected value (obtained at the end of the day-ahead optimization).

Moreover, the WPP may face an opportunity cost of more than 10% with respect to its related expected income. Furthermore, for some 10-sec intervals, the wind speed drops sufficiently low so that the WPP fails to deliver the FCR capacity offered in day-ahead.

Therefore, the revenues from the reserve market also deviate from the expected ones. In this regard, the actual revenue of the WPP for reserve capacity procurement is 10% lower than the related income of the day-

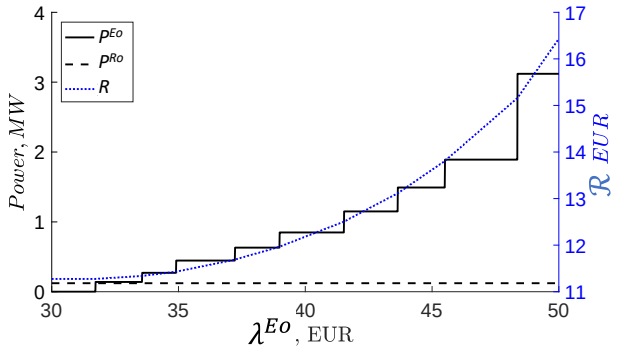

Figure 3.5) (left axis) optimal bids, (right axis) expected revenue

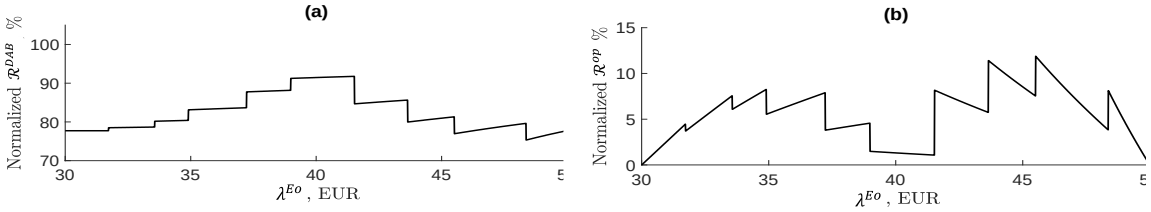

Figure 3.6(a)-(b), (a) Normalized R^{DAB}, (b) Normalized R^{op}

ahead stage. Moreover, the normalized actual net revenue from the reserve deployment is shown in the dotted line in Figure 3.4.

3.4.2 Out-of-sample analysis

The obtained results in Section 3.4.1 merely describe the impact of wind speed fluctuations on the WPP's profit based on one realization of wind speed and system frequency data. To accurately assess the impact of wind speed fluctuations on the WPP's profit, a broader representation of possible wind speed and system frequency realizations is needed for ex-post analysis. 100 wind speed signals and system frequency data are used to generate 10,000 different samples.

First Case:

The expected profit and bids based on perfect information of the available mean power are used. Figure 3.7 displays the normalized mean value of the instantaneous net reserve activation revenue and its standard deviation. On average, the WPP does not meet the required reserve activation and receives a negative revenue of -33.77% of its expected term. The actual revenue for reserve capacity procurement is 42.14% of the expected value (57.86% lower). The overall revenue of the WPP is 39.60% of its expected value (60.40% lower).

***Second case*:**

The results of the stochastic model considering mean power scenarios are used. The wind speed fluctuations result in losses for the WPP compared to its expected revenue in the energy market. Figure 3.8(a) shows the average and standard deviation of the WPP's normalized actual revenue from the energy market and imbalance settlement ($\mathcal{R}^{DAB}$). On average, the WPP loses between 2.27% to 19.09% of its expected revenue. Figure 3.8(b) shows the average and standard deviation of the normalized opportunity

cost over the samples, which is between 1.01% to 11.03% of the expected revenue in the energy market and imbalance settlement.

The WPP misses out on revenues in the reserve market due to its inability to procure or activate the required FCR during certain periods. This is illustrated in Figure 3.9, which shows the mean and standard deviation of the normalized net reserve activation revenue. According to Table 3.2, the wind speed fluctuations result in the WPP receiving only 13.79% of the expected revenue from real-time reserve activation. On average, the actual revenue from reserve capacity procurement is 88.26% of the expected revenue, which is 11.74% lower. The overall revenue of the WPP from activation and procurement of reserve is 85.77% of its expected value, a difference of 14.23%.

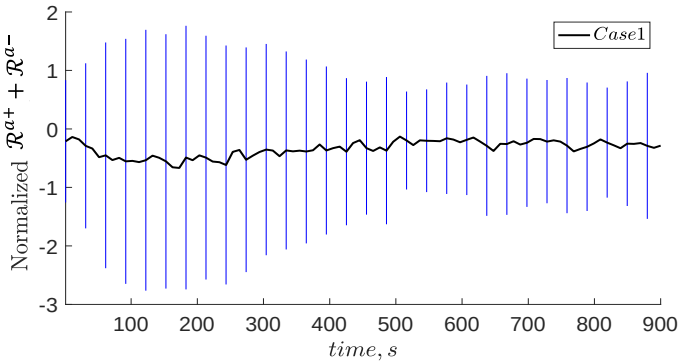

Figure 3.7) Normalized net reserve activation revenue and its standard deviation concerning out-of-sample analysis

Table 3.2) Normalized revenue elements of the reserve market

	$\overline{\mathcal{R}^{a+} + \mathcal{R}^{a-}}$	$\overline{\mathcal{R}^{cap}}$	$\overline{\mathcal{R}^{a+} + \mathcal{R}^{a-} + \mathcal{R}^{cap}}$
Case 1	-33.77%	42.14 %	39.60 %
Case 2	13.79 %	88.26 %	85.77%

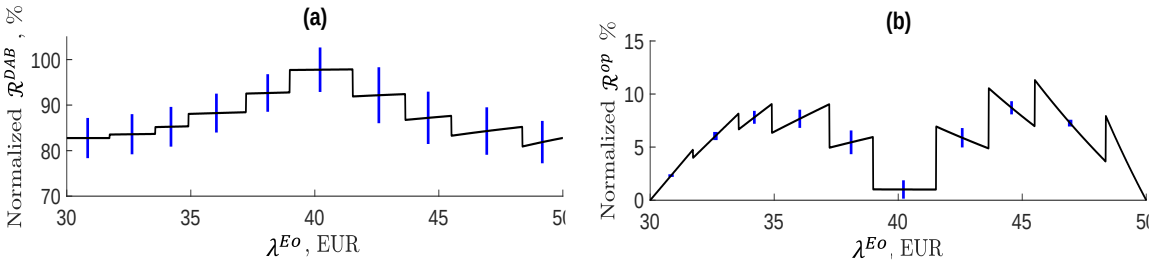

Figure 3.8 (a)-(b)) (a) Normalized R^{DAB}, (b) Normalized R^{op}

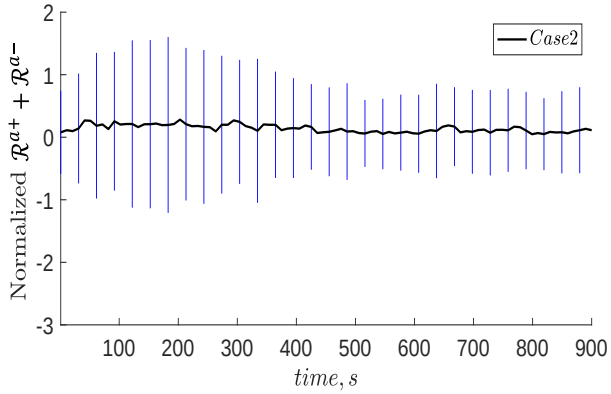

Figure 3.9) Normalized net reserve activation revenue and its standard deviation concerning out-of-sample analysis

3.5 Discussion and Conclusion

The study analyzed the impact of wind speed fluctuations on the profit of a WPP participating in the Energy Reserve Market (ERM). A stochastic model was developed and an ex-post analysis was conducted for two scenarios: one with perfect hourly wind power foresight and the other with wind speed forecast information. Despite using a risk-averse model in dealing with the reserve power violation, the numerical outcomes for both cases confirm that the revenue considerably deviates from its expected value. Additionally, it can be seen that the day-ahead uncertainty of the expected (mean) wind realization (case 2) inadvertently helps the WPP to

hedge against losses from intra-hour wind speed fluctuations (compared to case 1*)*. However, decision-makers should not be misled to use a forecaster with a wide range of scenarios to handle the uncertainty of wind speed fluctuations. On the other hand, they should be cautioned that even exploiting a perfect mean wind power forecaster does not essentially help them to play optimally in ERM.

3.6 Related Publication

S.A. Hosseini, J.-F. Toubeau, N. Singh, J. De Kooning, N. Kayedpour, G. Crevecoeur, Z. De Grève, F. Vallée, L. Vandevelde, "Impact of fast wind fluctuations on the profit of a wind power producer jointly trading in energy and reserve markets," in The 9th Renewable Power Generation Conference (RPG Dublin Online 2021), Dublin, Ireland (Online), 2021, pp. 240–245. doi: 10.1049/icp.2021.1386

Chapter 4. Day-Ahead Wind Power Bidding Considering Reserve Reliability

4.1 Introduction

The current WPP bidding frameworks for participation in the energy and reserve market (mentioned in section 2.4) are merely based on hourly wind speed, without controlling the reliability of the offered bids. In chapter 3, it is shown that such approaches lead to dramatic ex-post disappointment for both WPP and TSO. In order to tackle this problem, this chapter proposes a probabilistic requirement on the availability of the offered reserve bids while still modeling wind stochasticity based on its hourly uncertainty.

It should be noted that, using a deterministic requirement for reserve capacity availability, as currently done in European markets, overlooks the stochastic nature and reliability of the committed units. This may result in a significant loss of load in the power system [22]. Accordingly, several approaches are proposed in the literature to integrate a probabilistic reserve constraint in the market-clearing algorithm [22]. For instance, a probability method is presented in [51] such that the reliability of reserve service, based on the probability of not meeting the load, remains fixed. The authors in [21] explicitly modeled a probabilistic reserve criterion in the unit commitment problem which properly represents the reserve capacity with respect to various risk levels.

Therefore, due to the increased uncertainty in power systems, owing to the high penetration of renewable energy sources, the incorporation of probabilistic reserve constraints in the electricity market could potentially tackle the problem of wind power integration in the reserve market.

Accordingly, reserve market participants should guarantee a certain confidence level of reserve power availability, determined by the TSO, in order to be considered as reserve providers. Nevertheless, while participants ensure a certain Confidence Level of Reserve Power Availability (CLRA), their real-time energy and reserve power deviations should be financially settled.

Remarkably, it should be noted that the classical offering strategy of the WPP in the market, which is merely based on market incentives, does not ensure a firm reliability level. Hence, this chapter aims to address the research gap regarding the optimal bidding strategy of the WPP while fulfilling a required CLRA. Additionally, Table 4.1 briefly provides the readers with the advantages of the proposed method over the methods presented in the literature in the context of the WPP's bidding strategy.

Particularly, in this study, firstly the remuneration and penalty mechanism of the applied ERM model while satisfying the interest of system operators and the WPP is detailed. The model is formulated as a bi-objective two-stage chance-constrained stochastic framework (BTCS), where the first objective is to obtain the optimal bids of WPP in the different day-ahead market floors, while the second one is to ensure the desired real-time CLRA. Additionally, the absolute reserve power

procurement strategy is adapted in the model to make sure that the obtained decisions of the BTCS framework comply with the wind turbine control scheme. Therefore, the obtained efficient Pareto front provides WPP with a powerful model to participate in ERM. To do so, a plausible set of system frequency and hourly wind speed (provided by forecasting models) are considered as uncertain variables in the model. It should be noted that generating a set of discrete scenarios, based on the available information, for simulating the uncertainties of the influencing parameters of the model, e.g. wind speed, and price, in stochastic programming is regularly practiced in power system applications [52], [53]. Then, the effectiveness of the proposed approach is properly evaluated through an extensive out-of-sample analysis containing three wind turbulence intensity levels with a high resolution, i.e. 0.1 Hz, along with the real-time system frequency data. Furthermore, the obtained results are also compared with the results of the state-of-the-art methods to show the effectiveness of the proposed framework. Finally, the impact of market incentives on WPP's risk attitude and bidding strategy is detailed.

The organization of this chapter is as follows. In Section 4.2, the optimal offering strategy for the participation of WPP in ERM is detailed. In Section 4.3, the ex-post analysis methodology is described. Numerical results are provided in Section 4.4 so as to evaluate and discuss the effectiveness and flexibility of the proposed approach. A discussion regarding the advantages and limitations of the proposed framework with respect to the state-of-the-art method along with a conclusion is given in Section 4.5. The material presented in this chapter is predominantly sourced

from the author's publication, as referenced in the last Section (Related publication), with due respect to the original copyright[2] .

4.2 Reliability-Based Offering Strategy of Wind Power Producers

The proposed BTCS framework takes advantage of a multi-objective programming approach to simultaneously optimize WPP's profit and CLRA in the ERM. The idea behind the presented framework is illustrated in Figure 4.1. As seen in this figure, WPP's profit and confidence level of reserve power availability is modeled as a stochastic model, in which system frequency and wind speed uncertainties appear as the inputs of profit maximization problem while the maximization of CLRA only required wind speed uncertainty as to the input. Finally, the bi-objective optimization programming allows us to illustrate the impact of the risk threshold, defined by the TSO, on WPP's revenue.

Table 4.1) Advantages of the proposed strategy over the methods presented in the literature regarding WPP's bidding strategy.

References	Participation in energy market	Participation in reserve market	Control technology of wind turbine	Integrating uncertainty of system frequency	Consideration of reserve reliability
[35]-[41]	✓	×	×	×	×
[42]	✓	✓	×	×	×
[43]-[44]	✓	✓	✓	×	×
[**Proposed**]	✓	✓	✓	✓	✓

[2] The Elsevier permission grant can be accessed at the following link: https://www.elsevier.com/about/policies/copyright/permissions [Accessed 10 Feb 2023]

The first objective function $\mathcal{R}$ of the proposed MOP problem aims to maximize WPP's profit in a two-stage stochastic programming framework, in which the first and second stages respectively represent the day-ahead and real-time market floors. The objective function is formulated as follows:

$$\underset{X,\Psi}{\text{Max}}\ \mathcal{R} = \{\mathcal{R}^{Eo} + \mathcal{R}^{Ro}\} + \left\{\begin{matrix}\sum_{\omega\in\Omega} \pi_\omega(\mathcal{R}_\omega^{E\uparrow} - \mathcal{R}_\omega^{E\downarrow} \\ +\mathcal{R}_\omega^{a+} - \mathcal{R}_\omega^{a-} - \mathcal{R}_\omega^{R\downarrow})\end{matrix}\right\} \tag{4.1}$$

The terms $\mathcal{R}^{Eo}$ and $\mathcal{R}^{Ro}$, respectively, represent the revenue of the WPP in the day-ahead energy and reserve capacity markets, and are given by:

$$\mathcal{R}^{Eo} = \lambda^{Eo}\Delta t P^{Eo} \tag{4.2}$$

$$\mathcal{R}^{Ro} = \lambda^{Ro} P^{Ro} \tag{4.3}$$

Then, the effect of real-time deviations from the contracted day-ahead bids on WPP's revenue is taken into account by the second bracket in (4.1). In that regard, π_ω is the probability of occurrence of scenario $\omega \in \Omega$.

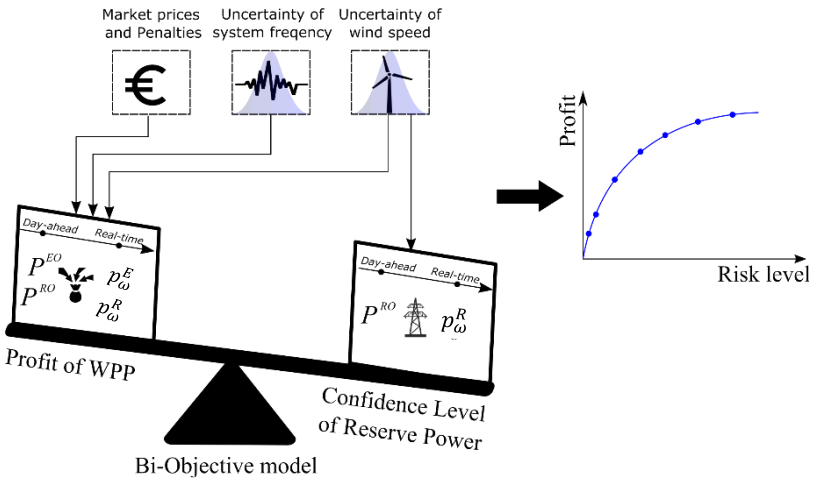

Figure 4.1) Proposed bi-objective two-stage stochastic chance-constrained framework for profit maximization of WPP with respect to risk thresholds

The energy imbalance settlement is represented by $\mathcal{R}_{\omega}^{E\uparrow}$ and $\mathcal{R}_{\omega}^{E\downarrow}$, which respectively indicate the financial compensation regarding real-time surplus and deficit of generation in scenario ω. The mathematical expression of the energy imbalance settlement, as described in Section 2.3, is as follows:

$$\mathcal{R}_{\omega}^{E\uparrow} = \lambda^{E\uparrow}\Delta t\ \Delta p_{\omega}^{E\uparrow} \tag{4.4}$$

$$\mathcal{R}_{\omega}^{E\downarrow} = \lambda^{E\downarrow}\Delta t\ \Delta p_{\omega}^{E\downarrow} \tag{4.5}$$

where $\Delta P_{\omega}^{E\uparrow}$ and $\Delta P_{\omega}^{E\downarrow}$ are, respectively, the positive and negative power imbalances with respect to the day-ahead energy market bid of scenario ω.

The last 3 elements in (4.1) represent the real-time balancing stage in which $\mathcal{R}_{\omega}^{a+}$ and $\mathcal{R}_{\omega}^{a-}$, respectively, indicate payment and penalty for reserve activation, while $\mathcal{R}_{\omega}^{R\downarrow}$ deals for the penalty for unavailability of the FCR in scenario ω. The mentioned elements for a given θ_{ω} , as explained in Section 2.3, are formulated as follows:

$$\mathcal{R}_{\omega}^{a+} = \lambda^{a\uparrow}\Delta t\theta_{\omega}\xi_{\omega}^{\uparrow} \tag{4.6}$$

$$\mathcal{R}_{\omega}^{a-} = \lambda^{a\downarrow}\Delta t\theta_{\omega}\xi_{\omega}^{\downarrow} \tag{4.7}$$

$$\mathcal{R}_{\omega}^{R\downarrow} = \lambda^{R\downarrow}\Delta p_{\omega}^{R} \tag{4.8}$$

where $\xi_{\omega}^{\uparrow}$ and $\xi_{\omega}^{\downarrow}$ are conditional decision variables, which are equal to P^{Ro} regarding the real-time availability and unavailability of the scheduled reserve power, respectively. Also, Δp_{ω}^{R} indicate the negative deviation of the available reserve power p_{ω}^{R} from P^{Ro} in scenario ω.

It should be noted that the model is only considering the provision of upward reserve regulation since WPP is not able to benefit from fuel-saving return in downward regulation (like the conventional units do) [43], [44].

The constraints associated with the first objective function (4.1) are as follows:

$$P^{Eo} + P^{Ro} = P^{qo} \tag{4.9}$$

$$\underline{P} \leq P^{qo} \leq \overline{P} \tag{4.10}$$

$$P^{Eo} - p_{\omega}^{E} = \Delta p_{\omega}^{E\downarrow} - \Delta p_{\omega}^{E\uparrow} \tag{4.11}$$

$$p_{\omega}^{E} + p_{\omega}^{R} = \tilde{P}_{\omega} \tag{4.12}$$

$$p_{\omega}^{R} \leq P^{Ro} \tag{4.13}$$

$$p_{\omega}^{R} \leq \tilde{P}_{\omega} \tag{4.14}$$

$$p_{\omega}^{R} \geq P^{Ro} - M(1 - \mu_{\omega}) \tag{4.15}$$

$$p_{\omega}^{R} \geq \tilde{P}_{\omega} - M\mu_{\omega} \tag{4.16}$$

$$P^{Ro} - p_{\omega}^{R} \leq \Delta p_{\omega}^{R} \tag{4.17}$$

$$m(1 - \delta_{\omega}) \leq \Delta p_{\omega}^{R} \leq M(1 - \delta_{\omega}) \tag{4.18}$$

$$\xi_{\omega}^{\downarrow} \leq P_{max}(1 - \delta_{\omega}) \tag{4.19}$$

$$\xi_{\omega}^{\downarrow} \leq P^{Ro} \tag{4.20}$$

$$\xi_{\omega}^{\downarrow} \geq P^{Ro} - \overline{P}\delta_{\omega} \tag{4.21}$$

$$\xi_{\omega}^{\uparrow} \leq \overline{P}\delta_{\omega} \tag{4.22}$$

$$\xi_{\omega}^{\uparrow} \leq P^{Ro} \tag{4.23}$$

$$\xi_{\omega}^{\uparrow} \geq P^{Ro} - \overline{P}(1 - \delta_{\omega}) \tag{4.24}$$

where P^{qo} is the total bid of the WPP at the day-ahead stage for the energy and reserve market which is limited by (4.9) and (4.10). The power

mismatch in scenario ω is obtained by the power balance equation in (4.11), where p_ω^E is the power fed in the network regarding scenario ω. Equation (4.12) ensures that the allocated power in the energy and reserve market does not exceed the total available power $\tilde{P}_\omega$ of scenario ω. Constraints (4.13)-(4.16) indicate the absolute control strategy of the WPP, where μ_ω is a binary decision variable. In this strategy, a fixed amount of reserve power is allocated to the reserve market providing that sufficient power is available, i.e. $\mu_\omega = 1$. However, when the available power,$\tilde{P}_\omega$, is lower than P^{Ro}, the power is fully allocated to the reserve market, i.e. $\mu_\omega = 0$, such that $p_\omega^R = \min\left(P^{Ro}, \tilde{P}_\omega\right)$. The negative deviation of the allocated FCR from its analogous day-ahead bid is obtained by (4.17). The status of Δp_ω^R is expressed by (4.18), where $\delta_\omega \in \{0,1\}$ is equal to 0 in case of negative deviation ($\Delta p_\omega^R > 0$), and equal to 1 when no deviation from the contracted reserve power bid exists ($\Delta p_\omega^R = 0$). It should be noted that m and M are, respectively, the minimum and maximum bounds of the decision variable. Constraints (4.19)-(4.21) let the conditional decision variable $\xi_\omega^\downarrow$ to be equal to P^{Ro} so as to calculate the penalty for reserve activation failure, provided that a negative deviation between the contracted and allocated FCR exist, i.e. *if* $\Delta p_\omega^R > 0$ *then* $\xi_\omega^\downarrow = P^{Ro}$. However, constraints (4.18)-(4.20) assign $\xi_\omega^\uparrow$ to P^{Ro} when $\Delta p_\omega^R = 0$, so as to calculate the real-time reserve activation revenue of scenario ω . It should be also noted that the first stage decision variables, $\mathrm{H} = \{P^{Eo}, P^{Ro}, P^{qo}\}$, and the second stage variables including $\left\{p_\omega^E, \Delta p_\omega^{E\downarrow}, \Delta p_\omega^{E\uparrow}, p_\omega^R, \Delta p_\omega^R, \xi_\omega^\downarrow, \xi_\omega^\uparrow\right\} \in \Psi$ are non-negative continuous. Additionally, $\{\mu_\omega, \delta_\omega\} \in \Psi$ are binary decision variables of the second stage. Moreover, $\tilde{P}_\omega$ and θ_ω are the uncertainty sources respectively related to the available power and system frequency in scenario ω. The framework has been modeled as a mixed integer linear programming problem.

The presented objective function in (4.1), along with the constraints (4.9)-(4.24), defines the two-stage stochastic optimization problem aiming to maximize WPP's profit in the ERM.

Then, the second objective of the proposed BTCS problem, which maximizes CLRA is formulated as follows:

$$\underset{X,\Psi}{\text{Max}}\ \Phi = \mathbb{P}(\Delta p_{\omega}^{R} = 0, \omega \in \Omega) \tag{4.25}$$

$$\underline{P} \leq P^{Ro} \leq \overline{P} \tag{4.26}$$

$$p_{\omega}^{R} \leq P^{Ro} \tag{4.27}$$

$$p_{\omega}^{R} \leq \tilde{P}_{\omega} \tag{4.28}$$

$$p_{\omega}^{R} \geq P^{Ro} - M(1 - \mu_{\omega}) \tag{4.29}$$

$$p_{\omega}^{R} \geq \tilde{P}_{\omega} - M\mu_{\omega} \tag{4.30}$$

$$P^{Ro} - p_{\omega}^{R} \leq \Delta p_{\omega}^{R} \tag{4.31}$$

$$\Delta p_{\omega}^{R} \geq 0 \tag{4.32}$$

The objective function of the CLRA problem, Φ, is presented in (4.25), where $\mathbb{P}$ is a probability function that computes the probability of real-time reserve availability throughout the scenarios. P^{Ro} is the first-stage decision variable regarding the day-ahead reserve power bid. p_{ω}^{R} and Δp_{ω}^{R} are the second-stage decision variables, which respectively, correspond to the real-time allocated reserve power and violation of p_{ω}^{R} from the contracted bid P^{Ro}. Additionally, μ_{ω} is a binary decision variable that is equal to 1 when sufficient power regarding the contracted reserve bid is available and 0 otherwise. Constraints (4.26)-(4.32) guarantee that the obtained solution is in the feasible space of the problem. However, it should be noted that this single-objective optimization problem does not have a unique solution in

the feasible space since there is no gain to provide a likely high reserve power bid. To better illustrate this effect, let us consider a single scenario where $\tilde{P}_{\omega} = 2.5\ \text{MW}$ with the probability of 100%, and $0 \leq P^{Ro} \leq 5\ \text{MW}$. As shown in Figure 4.2, the maximum value of Φ can be obtained through various decision variables, P^{Ro} and p_{ω}^{R} within the feasible solution space as shown by a blue line.

The concept of Pareto optimality is used in Multi-Objective Programming (MOP) where the goal is to find a set of solutions, rather than a single optimal solution, that cannot be improved in one objective without negatively affecting the other objectives scalarization approaches among the other MOP methods in the power systems literature [55]. The ε-constraint method has advantages over the weighted-sum approach, such as not requiring normalization of objectives and allowing for control of the number of efficient solutions generated by adjusting a resolution parameter. In the ε-constraint [54]. The weighted-sum and ε-constraint methods are the most predominant formulation, one objective is selected as the main objective and the other is considered as an inequality constraint [56]. The generic formulation of ε-constraint method for a bi-objective problem, with objective functions $F_1(x)$ and $F_2(x)$, is as follows:

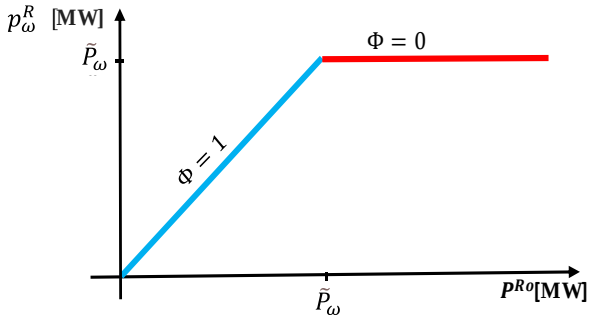

Figure 4.2) Feasible solution space and objective function value of CLRA.

$$\begin{aligned} &\underset{x\in S}{\text{Max}}\ F_1(x) \\ &s.t.\quad F_2(x) \geq \varepsilon_k \\ &\text{where } \varepsilon_k = F_{2min} + k(F_{2Max} - F_{2min})/NP;\ k = 0, \dots, NP \end{aligned} \tag{4.33}$$

where S is the feasible region of the MOP problem and ε_k is a lower bound for $F_2(x)$. Thus, by varying ε_k in a range of minimum and maximum values of the second objective, i.e. F_{2min}, F_{2Max}, $NP+1$ sub-problems are produced. Accordingly, the optimal solution of each sub-problem corresponds to a Pareto solution. However, the sub-problems with an infeasible solution should be ignored in the process of MOP. Moreover, the obtained Pareto front may contain some dominated solutions, which should be filtered out from the optimal set.

In order to plausibly investigate the effect of the risk threshold on the WPP's profit and offered power quantities in the ERM, the problem is recast as a MOP. Accordingly, WPP's profit (4.1) and the confidence level of reserve availability (4.35) are considered as the two competing objectives of the proposed MOP problem, i.e. $\underset{x\in(4.9)-(4.24)}{\text{Max}}\{(4.1),(4.35)\}$. It implies that the proposed BTCS framework concurrently maximizes the WPP's profit in a two-stage stochastic environment while ensuring a sufficient CLRA. Accordingly, equation (4.1) is considered as the primary objective function of the ε-constraint method, while the second objective (4.25), i.e. Φ, is treated as an inequality constraint. Additionally, the feasible space of the problem is defined by constraints (4.9)-(4.24). Also, the minimum and maximum bounds of Φ are 0 and 1, respectively. It should be noted that constraints (4.26)-(4.32) can be discarded in the MOP approach as they either are redundant or not limiting the feasible space. The compact representation of the BTCS model is finally given by:

$$\begin{aligned} &\underset{X,\Psi}{\text{Max}}\ \mathcal{R} \\ &\text{Constraints (4.9)-(4.20)} \\ &\Phi = \mathbb{P}(\Delta p_{\omega}^{R} = 0, \omega \in \Omega) \\ &\Phi \geq \varepsilon_k = \frac{k}{NP} \quad k=0,\ldots,NP \end{aligned} \tag{4.34}$$

Furthermore, the primary objective function and the defined constraints (4.9)-(4.24) sufficiently limit the feasible space of the problem, thereby one decision set per CLRA is returned (as opposed to the earlier description through Figure 4.2).

The probabilistic constraint in (4.34), which controls the real-time provision of the committed reserve, can be expressed as a chance-constrained program, and thus approximated by various approaches such as second-order cone program if the distribution of random variables follows a Gaussian function [57]. When dealing with an unstructured distribution, sampling average approximation technique accompanied by mixed integer programming can be used to estimate (4.34) as follows [58], [59]:

$$\Phi = \sum\nolimits_{\omega \in \Omega} \pi_{\omega} \delta_{\omega} \tag{4.35}$$

Nevertheless, in chance-constrained programming, it is more common to measure the probability of constraint violation, i.e. risk, rather than its confidence level. Therefore, the last two constraints of (4.34) and (4.35) can be reformulated as follows:

$$\bar{\Phi} = 1 - \sum\nolimits_{\omega \in \Omega} \pi_{\omega} \delta_{\omega} \tag{4.36}$$

$$\bar{\Phi} \leq \mathrm{r}_k = \frac{k}{NP} \quad \mathrm{k=0,\ldots,NP} \tag{4.37}$$

where r_k is the analogous parameter to that of ε_k and $\bar{\Phi}$ is the one's complement of Φ, which indicates the optimal risk level regarding the trade-off between competing objectives.

4.3 Ex-post analysis detail

In this section, we evaluate the obtained solutions of the BTCS framework using the out-of-sample approach. To that end, a set of wind speed and system frequency signals with a resolution of τ are employed so as to assess the actual revenue of the WPP.

The actual revenue of WPP for reserve procurement concerning day-ahead remuneration and real-time settlement, with 10-second resolution, is obtained by:

$$\tilde{\mathcal{R}}^{Cap}_{t',w,i} = N^{-1}\lambda^{Ro}P^{Ro}_{i}\left[1 - \mathbb{I}\left(P_{t',w} < P^{Ro}_{i}\right)\right] \tag{4.38}$$

where $\tilde{\mathcal{R}}^{Cap}_{t',w,i}$ is the instantaneous revenue of WPP for Pareto optimal point i at time t' for wind signal w. Then, P^{Ro}_{i} corresponds to the optimal solution i within the Pareto front, while $P_{t',w}$ is the available power at instance t' for wind signal, w. $\mathbb{I}$ is the indicator function that is equal to 1 when the operand in the parenthesis is satisfied and 0 otherwise. N is the number of intervals within one hour with respect to the defined resolution of the reserve market, i.e. $N = 360$. Subsequently, real-time remuneration and settlement for reserve power activation depend on system frequency. Hence, the percentage of the called reserve should be calculated for each instance regarding the frequency samples.

$$\tilde{\mathcal{R}}^{a}_{t',(w,f),i} = N^{-1}\theta_{t',f}P^{Ro}_{i}\left[\lambda^{a\uparrow} - \lambda^{a\downarrow}\mathbb{I}\left(P_{t',(w,f)} < P^{Ro}_{i}\right)\right] \tag{4.39}$$

where $\tilde{\mathcal{R}}^{a}_{t',(w,f),i}$ is the actual instantaneous reserve activation revenue of WPP in which $\theta_{t',f}$ is the percentage of the called reserve at instance t' for frequency signal *f*.

The total actual revenue of WPP in the reserve market, $\tilde{\mathcal{R}}^{R}$, can be assessed using (4.38) and (4.39) for each Pareto point, i.e. risk level. It should be noted that in an ideal situation, the obtained revenue should match its corresponding expected value obtained by BTCS model, i.e. $\mathcal{R}^{Ro} + \sum_{\omega\in\Omega} \pi_{\omega}\left(\mathcal{R}^{a+}_{\omega} - \mathcal{R}^{a-}_{\omega} - \mathcal{R}^{R\downarrow}_{\omega}\right)$.

The real-time energy imbalance should also be settled. In this chapter, it is assumed that the BRP submits its nomination at the end of the day-ahead market with a quarter-hour resolution, $\tau' = 1/4$ h. Consequently, an asymmetric imbalance tariff is imposed for BRPs who violate their nominations. Moreover, nominations of the WPP in this problem for all the intervals within one hour day-ahead market time unit is considered to be $\tau' P^{Eo}_{i}$, since WPP only injects power to the network with no off-takes. Therefore, the fed-in energy to the system for each imbalance settlement interval is obtained by:

$$E_{\tau'_j,w} = \int_{t_j}^{t_{j+1}} \tilde{P}_{t,w} dt \tag{4.40}$$

where $\tilde{P}_{t,w}$ is the real-time available power injected into the network, and $t_j, \forall_{j\in\{0,\dots,3\}}$ defines the boundary of each time interval τ'_j of the imbalance settlement process. $E_{\tau'_j,w}$ is the available energy of wind signal w at an imbalance settlement interval τ'_j.

The actual net revenue of WPP resulting from the day-ahead and imbalance settlement, $\tilde{\mathcal{R}}^{E}_{\tau'_j, w, i}$, regarding each time interval τ'_j, wind signal w and Pareto solution i is obtained as follows:

$$\tilde{\mathcal{R}}^{E}_{\tau'_j, w, i} = \lambda^{Eo}\tau'_j P_i^{Eo} + \lambda^{E\uparrow}\left(E_{T_j,w} - \tau'_j P_i^{Eo}\right)\mathbb{I}\left(E_{T_j,w} \geq \tau'_j P_i^{Eo}\right) - \lambda^{E\downarrow}\left(\tau'_j P_i^{Eo} - E_{T_j,w}\right)\mathbb{I}\left(E_{T_j,w} < \tau'_j P_i^{Eo}\right) \tag{4.41}$$

Finally, for each Pareto point, i.e. risk level, the total ex-post hourly revenue of WPP regarding the day-ahead energy and imbalance settlement stage, $\tilde{\mathcal{R}}^{E}$, can be obtained using (4.41) which should be $\mathcal{R}^{Eo} + \sum_{\omega\in\Omega}\pi_\omega\left(\mathcal{R}^{E\uparrow}_{\omega} - \mathcal{R}^{E\downarrow}_{\omega}\right)$ in an ideal condition.

4.4 Case study

4.4.1 Problem set-up

The performance of the proposed BTCS bidding strategy is verified using a 5.3 MW wind turbine with cut-in, rated, and cut-out wind speeds of 3, 12, and 25 m/s for participation in the ERM. The results of the proposed bidding strategy are compared to the classical bidding strategy method and the impact of market incentives on the WPP's revenue and risk attitude is evaluated. The advantages of the proposed method are discussed and a conclusion is given. The prices and penalties associated with the market are shown in Table 4.2.

Table 4.2) Prices and penalties in the ERM for the base case.

λ^{Eo} [€/MWh]	λ^{Ro} [€/MW]	$\lambda^{E\uparrow}$ [€/MWh]	$\lambda^{E\downarrow}$ [€/MWh]	$\lambda^{a\uparrow}$ [€/MWh]	$\lambda^{a\downarrow}$ [€/MWh]	$\lambda^{R\downarrow}$ [€/MW]
33	36	30	40	40	60	36

4.4.2 Evaluation of The Reliability-Based WPP Bidding

The stochastic process of wind speed is simulated using the ARMA method. To do so, hourly wind speed data, available in [45], are fed into the ARMA model to estimate its statistical parameters. 1000 wind speed scenarios are produced and reduced to 20 scenarios using a reduction technique based on Kantorovich distance [50]. These scenarios, along with 9 system frequency scenarios, and ERM tariffs, are applied to the BTCS framework to obtain the optimal Pareto set. The BTCS model runs in 10.68 seconds on a MacBook Pro with an Intel Core i5 CPU 2.3 GHz.

The resulting decisions of the BTCS framework for the first stage variables with respect to the risk of inability to provide the contracted reserve power are shown in Figure 4.3. In this figure, the horizontal axis is the expected probability of inability to provide the contracted reserve, $\overline{\Phi}$, while the vertical axis represents the scheduled power at each market floor. It can be seen that when the risk level, $\overline{\Phi}$, is between $[0, 0.3]$, the WPP bids a fixed quantity of power in the ERM. As expected, when the risk level rises, WPP submits a higher power quantity in the market (and it faces thus more imbalance penalties). Likewise, risky strategies lead to a prominent share of the available power that is committed to the reserve market while a lower portion is allocated to the energy market, reflecting that bidding in the reserve market is more advantageous than in the energy market (in the studied market conditions). To get a better insight, the penalty paid by the WPP as a function of the risk threshold is shown in Figure 4.4. It can be seen that the induced penalty regarding the reserve market monotonically increases with respect to the risk level.

The proposed BTCS framework results in the in-sample revenue of WPP, as illustrated in Figure 4.5. It shows that increasing the risk level improves the expected revenue in the reserve market (dotted blue line), while decreasing it in the energy market (plain red line), aligned with the power bids shown in Figure 4.3. Above a risk level of 0.3, WPP still earns revenue from its energy imbalance without bidding in the day-ahead energy market. The total expected revenue for WPP in the ERM is shown in Figure 4.6 on a Pareto-efficient front, steadily growing with risk levels. The BTCS model provides WPP with a flexible model for bidding in the ERM according to the desired risk level.

In order to demonstrate the impact of real-time intra-hour wind speed variations on WPP's actual revenue, using the proposed BTCS model, extensive out-of-sample validation is performed. Accordingly, three sets of wind speed signals, embodying different Turbulence Intensity Level (TIL), i.e. 10%, 30%, and 50%, are initially produced using [46]. Each set carries 50 wind speed signals with a resolution of 0.1 Hz on a one-hour span. Furthermore, another set of system frequency realizations, with an equal dimension, is captured by employing real-world frequency deviation data available in [45]. Therefore, regarding each TIL 2500 samples are generated so as to evaluate the obtained results of the BTCS framework.

In this case, the classical bidding strategy approach [42], [43] provides the WPP with the optimal bids of $P^{Eo} = 0$ and $P^{Ro} = 2.375\,[\mathrm{MW}]$, and revenue of € 80.97. However, such a bid demonstrates a high-risk of unavailability in ex-post, which is equal to 0.585, 0.585, 0.569 regarding the TILs of 10%, 30, 50%, respectively.

Therefore, the offered bids may even deteriorate the system's security of supply as the TSO generally considers high reliability for the reserve services. The ex-post revenue of WPP in the reserve and energy market is

shown in Figures 4.7 and 4.8, respectively. The blue, green, and red lines correspond to TIL of 10%, 30%, and 50% while the expected in-sample revenue is shown in black. It can be seen that the actual revenue of WPP in the reserve market is higher than its related expected value for a low TIL, i.e. 10%. In other words, the in-sample BTCS model overestimates the uncertainty around intra-hour wind speed fluctuations for this case, which results into conservative decisions. Conversely, for 30% TIL, the actual reserve market revenue is slightly below the expected term, while TIL of 50% is considerably lower than the expected in-sample revenue due to the inability of the WPP to offer the scheduled reserves.

As seen in Figure 4.8, for a low TIL, i.e. 10%, the actual revenue of WPP in the energy market is lower than the expected in-sample one while the one computed for turbulence level of 30% is really close to the expected in-sample revenue. It is also interesting to observe that the obtained revenue for a high TIL of 50% can even be higher than the expected one. In other words, WPP may compensate for some loss of revenue by leveraging the additional available energy in turbulent wind. However, the loss of revenue in the reserve market is more substantial than the gain of revenue in the energy market concerning the increase of turbulence. As shown in Figure 4.9, the total real-time revenue of WPP in the ERM concerning the expected revenue declines by the increase of turbulence level. To gain insight into this matter, the deviation of actual revenue streams from their expected in-sample values for the different TIL is normalized by the total expected revenue of the same Pareto point.

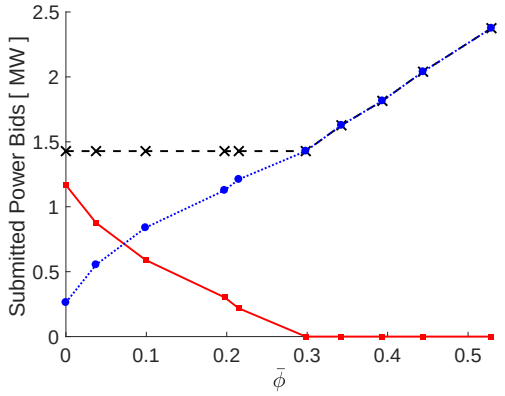

Figure 4.3) First stage decision variables of the BTCS model regarding different risk levels for the base case, P_i^{Ro} (dotted blue line), P_i^{Eo} (plain red line), and P_i^{qo} (dashed black line)

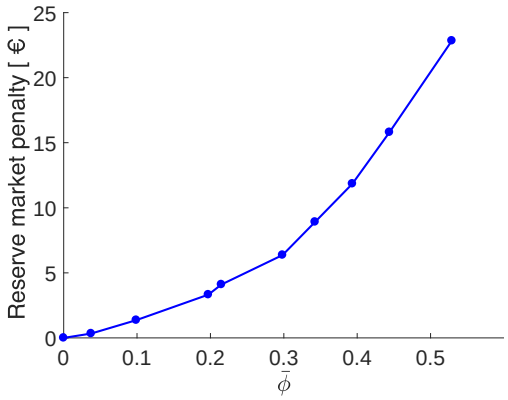

Figure 4.4) The penalty paid by WPP in the reserve market with respect to the inability to provide the contracted reserve bid for the base case

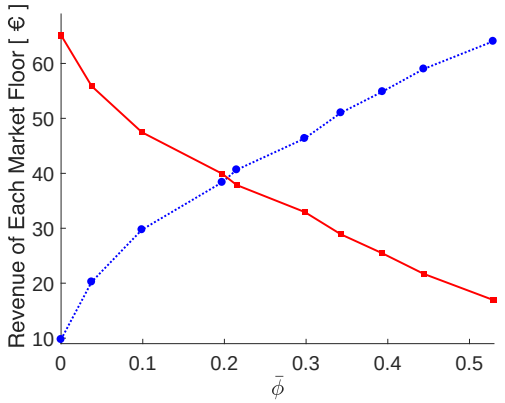

Figure 4.5) The expected revenue of WPP in energy (plain red line) and reserve market (dotted blue line) for the base case

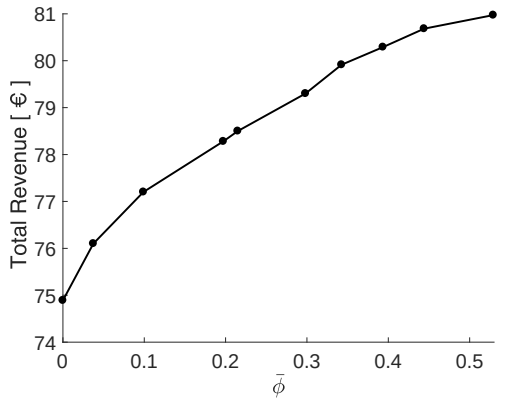

Figure 4.6) The total expected revenue of WPP for participating in the ERM for the base case versus risk levels

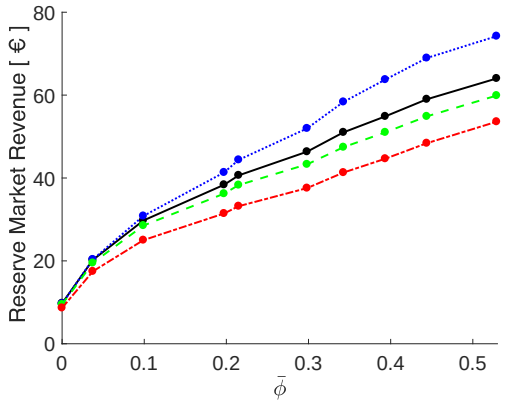

Figure 4.7) The expected revenue of WPP in the reserve market (black line) and its related actual revenue for TIL of 10% (dotted blue line), 30% (dashed green line), and 50% (red dash-dotted line) in the base case.

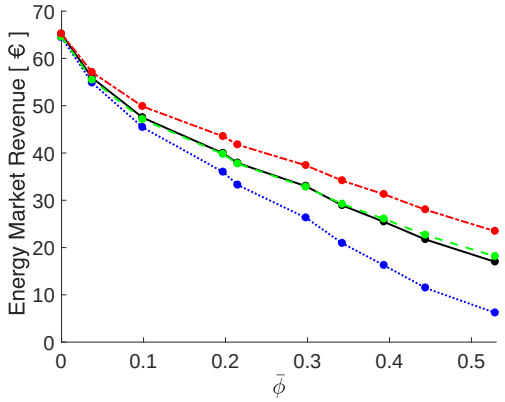

Figure 4.8) The expected revenue of WPP in the energy market (black line) and its related actual revenue for TIL of 10% (dotted blue line), 30% (dashed green line), and 50% (red dash-dotted line) in the base case.

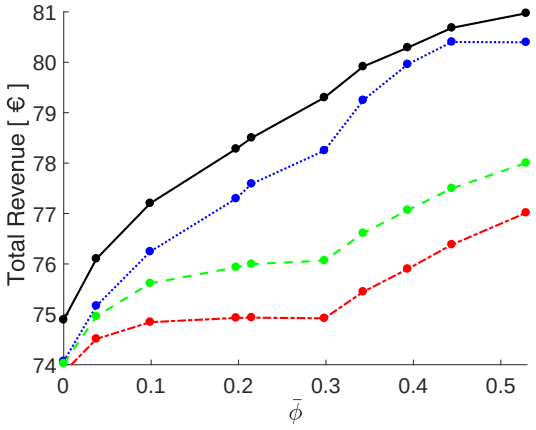

Figure 4.9) The overall expected revenue of WPP in the ERM (black line) and its related actual term for TIL of 10% (dotted blue line), 30% (dashed green line), and 50% (red dash-dotted line).

The results are detailed in Table 4.3. It can be seen that $\Delta\tilde{\mathcal{R}}_n^R\%$, normalized revenue deviation of the reserve market, is between [-0.152, 12.601] for 10% TIL, [-5.118, -0.399] for TIL of 30% and finally [-13.137, -1.485] for 50% TIL. Moreover, $\Delta\tilde{\mathcal{R}}_n^E\%$, normalized revenue deviation of the energy market, for TIL of 10%, 30% and 50% is in range of [-13.313, -0.947], [-0.758, 1.438] and [0.091, 8.015], respectively. It can be observed that when the risk level increases, the actual revenue term is getting farther from the total expected term. Additionally, $\Delta\tilde{\mathcal{R}}_n\%$, i.e. resulting from both markets, for TIL of 10%, 30%, and 50% is in the range of [-1.328, -0.346], [-4.134, -1.501], and [-5.590, -1.394]. It is interesting to see that the wide range of $\Delta\tilde{\mathcal{R}}_n^E\%$ and $\Delta\tilde{\mathcal{R}}_n^R\%$ is shrunk compared to the normalized total revenue deviation $\Delta\tilde{\mathcal{R}}_n\%$. It means that even though the model cannot fairly assess the specific revenue of each market floor with respect to turbulence and high-risk levels, it is still able to sufficiently estimate the entire revenue of the WPP in the ERM with an acceptable range. The obtained results of the BTCS framework regarding the second objective function, $\bar{\Phi}$, is reported in the first column of Table 4.4, which corresponds to the defined risk threshold by the TSO. Additionally, the out-of-sample analysis regarding the real-time inability of FCR procurement for TILs of 10%, 30, 50% , $\tilde{\bar{\Phi}}_{\text{TIL}\%}$, are detailed in the 2nd, 3rd and 4th columns of this Table. It is observed that the actual risk level associated with the inability to procure reserve power for 10% TIL, $\tilde{\bar{\Phi}}_{10\%}$, is lower than the expected risk metrics, for $\bar{\Phi} < 0.529$, while greater for a high TIL, i.e. 30% and 50%. Moreover, it should be noted that setting a high-risk threshold for reserve provision by the TSO, i.e. higher than 0.5, is unrealistic, as these products should be highly reliable.

Table 4.3) Normalized deviation of each revenue stream for different TIL for the base case.

Φ	TIL								
	10%	**30%**	**50%**	**10%**	**30%**	**50%**	**10%**	**30%**	**50%**
	$\Delta\tilde{\mathcal{R}}_n\%$			$\Delta\tilde{\mathcal{R}}_n^E\%$			$\Delta\tilde{\mathcal{R}}_n^R\%$		
0.000	-1.099	-1.157	-1.394	-0.947	-0.758	0.091	-0.152	-0.399	-1.485
0.037	-1.228	-1.501	-2.089	-1.375	-0.543	1.553	0.147	-0.958	-3.641
0.099	-1.241	-2.055	-3.054	-2.664	-0.478	3.079	1.423	-1.577	-6.133
0.197	-1.260	-3.001	-4.283	-5.069	-0.260	4.556	3.809	-2.741	-8.839
0.215	-1.163	-3.192	-4.543	-5.923	-0.201	4.930	4.760	-2.990	-9.473
0.298	-1.328	-4.080	-5.524	-8.419	-0.240	5.547	7.091	-3.840	-11.071
0.343	-0.836	-4.134	-5.590	-10.027	0.355	6.556	9.192	-4.489	-12.146
0.393	-0.414	-4.017	-5.470	-11.464	0.773	7.251	11.051	-4.791	-12.721
0.444	-0.346	-3.946	-5.330	-12.690	1.172	7.807	12.344	-5.118	-13.137
0.529	-0.712	-3.668	-4.890	-13.313	1.438	8.015	12.601	-5.106	-12.905

Table 4.4) The real-time inability of reserve power deployment as a risk metric concerning different TIL for the base case.

$\bar{\Phi}$	0	0.037	0.099	0.197	0.215	0.298	0.343	0.393	0.444	0.529
$\bar{\tilde{\Phi}}_{10\%}$	0	0	0.001	0.014	0.022	0.063	0.132	0.22	0.363	0.585
$\bar{\tilde{\Phi}}_{30\%}$	0.033	0.083	0.183	0.294	0.316	0.373	0.423	0.467	0.518	0.585
$\bar{\tilde{\Phi}}_{50\%}$	0.134	0.201	0.316	0.399	0.414	0.446	0.476	0.5	0.529	0.569

Additionally, it should be further remarked that for $\bar{\Phi} = 0.529$, $\tilde{\bar{\Phi}}_{10\%}$ and $\tilde{\bar{\Phi}}_{30\%}$ is slightly higher than the case of 50% TIL. This is evident since its associated reserve power bid is equal to the deterministic value of power scenarios, i.e. slightly (3%) higher than the mean power of the generated wind signals. In other words, in the turbulent wind, the possibility of reaching this rather high power-bid is higher than wind with a low TIL. Nevertheless, the actual revenue of WPP regarding this bid is still much lower than the case of 10% and 30% TIL because the deviation term Δp_{ω}^{R} in (4.8) is more significant in higher turbulent wind.

4.4.3 Impact of Market Incentives on WPP Bidding

In order to investigate the impact of market incentives on the WPP's revenue and its risk attitude, two cases regarding different market rates are presented. The variability of the total revenue as a function of the risk threshold is shown in Figure 4.10(a)-(b). Also, the associated expected in-sample revenue is shown by a plain black line and the ex-post revenue concerning the TIL of 10%, 30% and 50% are respectively represented by blue, green and red styled lines.

In case 1, the day-ahead reserve procurement price, λ^{Ro}, is increased to 39 [€/MW] in order to investigate the effect of such variation on WPP's risk attitude and associated revenue. The single-objective solution, i.e. neglecting the risk threshold, yields the expected revenue of € 92.49 regarding the optimal offered bids of $P^{Eo} = 0$ and $P^{Ro} = 5.08\,[\mathrm{MW}]$. Remarkably, as the WPP does not meet any risk threshold in the biding strategy, the ex-post analysis shows that the WPP is never able to provide the offered capacity bid throughout the market period, i.e. $\tilde{\bar{\Phi}}_{10\%} = \tilde{\bar{\Phi}}_{30\%} = \tilde{\bar{\Phi}}_{30\%} = 1$.

On the other hand, when using the BTCS model, this favorable incentive allows the WPP to withstand a higher risk regarding the inability to provide the offered FCR service, compared to the base case, as illustrated in Figure 4.10(a). As seen in this figure, the ex-post revenue of the WPP for 10% TIL stays suitably close to the in-sample results, whereas highly diverges from the expected revenue for higher TILs, i.e. 30% and 50%. Moreover, as shown in Table 4.5, for 10% TIL, the actual risk level, obtained by out-of-sample analysis, regarding the inability to procure the offered FCR is lower than the expected risk level for $\bar{\Phi} < 0.529$. It means that, when the defined risk threshold, indicated by the TSO, is higher than 0.529, WPP may not be able to meet this requirement in real-time. However, defining such a high-risk threshold for reserve procurement by the TSO is unrealistic as these services should be highly reliable. The real-time risk level, obtained by ex-post analysis, for high TIL, i.e. 30% and 50%, are detailed in the third and fourth columns of Table 4.5.

In the second case, the reserve activation price, $\lambda^{a\uparrow}$, concerning the real-time energy deployment is augmented to 88 [€/MWh]. In this configuration, when neglecting the risk index (single-objective problem), despite WPP submitting the same bids as the base case, i.e. $P^{Eo} = 0$ and $P^{Ro} = 2.375\ [\mathrm{MW}]$, it expects an increased revenue of 82.61 € compared to the base case, 80.97 €. However, such bids demonstrate a high-risk of unavailability in ex-post, which is equal to 0.585, 0.585, 0.569 regarding the TILs of 10%, 30, 50%, respectively. Nevertheless, when incorporating the allowed risk threshold in the bidding strategy, WPP is able to obtain the optimal bids with respect to the defined risk threshold to improve its

revenue in the ERM, as shown in Figure 4.10(b). As seen in this figure, the ex-post revenue of the WPP closely follows its expected term for TIL of 10% while further deviating for higher TILs. Moreover, as shown in Table 4.6, apart from the case when the allowed risk is impractically high, $\overline{\Phi} = 0.529$, the real-time FCR unavailability is below the expected threshold defined by the TSO for 10% TIL. Also, the real-time risk level, obtained by ex-post analysis, for high TILs, i.e. 30% and 50%, are detailed in the third and fourth columns in Table 4.6.

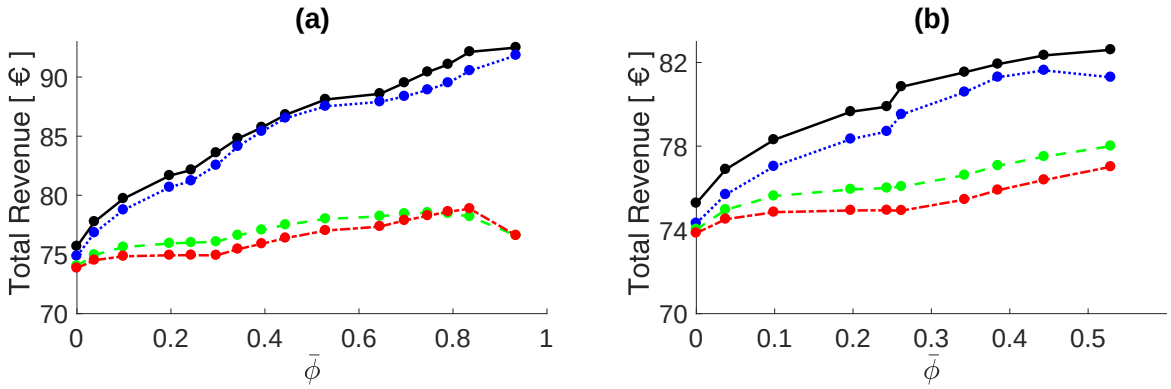

Figure 4.10 (a)-(b)) The impact of reserve market incentives on the risk-taking attitude and WPP's revenue including in-sample and ex-post analysis for TILs of 10%, 30% and 50%, (a) reserve procurement price is set to 39, (b) reserve activation price is set to 88.

Table 4.5) The real-time inability of reserve power deployment as a risk metrics concerning different TIL for case 1.

$\overline{\Phi}$	0	0.037	0.099	0.197	0.243	0.296	0.343	0.393	0.444	0.529	0.645	0.697	0.746	0.79	0.836	0.934
$\tilde{\overline{\Phi}}_{10\%}$	0	0	0.001	0.014	0.022	0.063	0.132	0.22	0.363	0.585	0.709	0.867	0.95	0.983	0.997	1
$\tilde{\overline{\Phi}}_{30\%}$	0.033	0.083	0.183	0.294	0.316	0.373	0.423	0.467	0.518	0.585	0.625	0.689	0.742	0.786	0.843	1
$\tilde{\overline{\Phi}}_{50\%}$	0.134	0.201	0.316	0.399	0.414	0.446	0.476	0.5	0.529	0.569	0.593	0.629	0.665	0.692	0.74	1

Table 4.6) The real-time inability of reserve power deployment as a risk metrics concerning different TIL for case 2.

$\bar{\Phi}$	0	0.037	0.099	0.197	0.243	0.262	0.343	0.385	0.444	0.529
$\tilde{\bar{\Phi}}_{10\%}$	0	0	0.001	0.014	0.022	0.063	0.132	0.22	0.363	0.585
$\tilde{\bar{\Phi}}_{30\%}$	0.033	0.083	0.183	0.294	0.316	0.373	0.423	0.467	0.518	0.585
$\tilde{\bar{\Phi}}_{50\%}$	0.134	0.201	0.316	0.399	0.414	0.446	0.476	0.5	0.529	0.569

Accordingly, the variation of market incentives directly affect the obtained revenue of the WPP. More interestingly, the interaction of these incentives defines the maximum tolerable risk regarding reserve unavailability. In particular, when the penalty rates associated with the reserve market increase, the maximum tolerable risk decrease whereas the increases in the reserve market prices allow the WPP to take a riskier decision regarding maximization of its profit. Therefore, the market incentives alone cannot limit the risk attitude of the WPP. However, by integrating the risk threshold definition in the bidding strategy framework, WPP can maximize its profit while respecting the defined risk threshold.

4.5 Discussion and conclusion

The current advancements in electricity market regulations and control mechanisms of wind turbines motivate wind power producers to participate in the energy and reserve market. It is shown that the classical offering strategy of WPP in the market, which is merely based on the market incentives [42]–[44], does not ensure a firm reliability level. In other words, WPP offers power quantities such that the income resulting from the positive incentives is greater than the negative ones. Also, the TSO is not informed about the confidence level of the contracted bid which deteriorates

the system security. Therefore, their intermittent nature is a great concern of the TSO to consider them as a reserve provider, since these services are expected to be highly reliable (as conventional units). Nevertheless, regarding the advantages of the probabilistic reserve procurement metrics, the TSO can define a risk threshold for the participation of WPP in ERM. In this way, WPP integrates the indicated risk threshold in its bidding strategy algorithm so as to maximize its profit while respecting market policies. The proposed BTCS framework illustrates the potential benefits of WPP's profit improvement while respecting a large range of confidence levels which can be imposed by the TSO.

In this chapter, firstly, a market framework, which incentivizes the wind power producer to participate in the day-ahead energy and reserve market so as to maximize its profit, is described. In this market setting, the transmission system operator also benefits by enhancing system security due to the appropriate penalty settings in the balancing stage, while specifying a new risk metric for the real-time unavailability of the scheduled reserve bids. Consequently, an advanced bidding strategy for the participation of the wind power producer in this market, considering practical constraints of wind turbine and market rules, is proposed. Then, an extensive out-of-sample validation regarding different turbulence intensity levels is performed ex-post to verify the validity of the obtained results. It is shown that, in contrast with traditional models, the obtained results of the proposed bidding strategy improves the availability of the offered bid and the producer's revenue in the market, thereby they could practically be considered as a reliable reserve provider. On the other hand, the risk of unavailability of the reserve power in the classical approach could increase to 100%, depending on market incentives, thus threatening the system's security of supply. Additionally, it is seen that with the increase of turbulence intensity level, the actual revenue of the wind power producer

gets farther from the expected value. However, the deviation is still acceptable, i.e. around -5%.

4.6 Related publication

S. A. Hosseini, J.-F. Toubeau, Z. De Grève and F. Vallée, "An advanced day-ahead bidding strategy for wind power producers considering confidence level on the real-time reserve provision", Appl. Energy, vol. 280, p. 115973, 2020. doi: 10.1016/j.apenergy.2020.115973

Chapter 5. Wind Fluctuations in Bidding: Scenario Generation

5.1 Introduction

The real-time financial compensation for certain reserve services, (e.g., FCR) occurs at a much shorter time interval than the financial compensation for energy deviations in the imbalance settlement mechanism, e.g., minute-wise versus hour-wise [19], [60]. However, all models mentioned in section 2.4 and the one presented in chapter 4 neglect this fact. In particular, due to the difficulty of ultra-short-term wind forecast as well as developing a multi time-scale bidding framework, the mentioned studies in section 2.4 have merely employed hourly wind uncertainty for the remuneration of real-time energy and reserve deviation. This strong assumption may incur opportunity losses due to the poor representation of the wind speed dynamics [60]. More importantly, when ultra-short-term wind variations are high, as shown in chapters 3 and 4, there is a high risk that the scheduled reserves cannot be deployed in real-time, thus exposing the WPPs to high financial penalties.

Therefore, a novel multi-resolution probabilistic bidding framework is first developed to optimize the profit of WPPs in ERM markets. Compared with existing works, the proposed WPP bidding strategy also considers the fluctuations of wind power at the minute level to accurately model the planned reserve bids in the balancing stage. Moreover, the model is enriched with a probabilistic constraint that controls the probability that the wind power capacity offered in day-ahead can be actually delivered in real-time, in the reserve market, using minute-wise variations (as opposed to chapter 4 which uses hourly variations).

With respect to wind uncertainty modeling, there is an increasing need to properly represent the quick dynamics of the wind power behavior and feed this information into dedicated decision models. Several model-based scenario generation approaches such as copula and auto-regressive moving average are presented in the literature to characterize wind uncertainty [61]. However, the quality of the generated scenarios in such approaches is highly limited by modeling and statistical assumptions [61], [62]. For instance, ARMA models face considerable limitations in modeling non-linear and non-stationary patterns due to their inherent assumptions of linear processes and data stationarity [63]. Wind power patterns, in particular, exhibit strong nonlinearity and non-stationarity [64], which become even more pronounced when dealing with very short timescales at long horizons (e.g., day-ahead). Additional ARMA models' assumptions, such as predefined distribution for uncertainty, and difficulty in selecting appropriate model orders, further contribute to their suboptimal performance [65]. For copula method, the quality of the generated scenarios is extremely sensitive to the copula function chosen to capture the dependence features [66]. Also, the use of copula in higher dimensions is challenging and known to be a difficult problem , as it is inflexible in defining multiple dependency structures among features [67]. Therefore, generating ultra-short-term wind scenarios using copula is extremely challenging as each intra-period time step appears as a new dimension.

The recent advancements in Generative Adversarial Networks (GANs) draw wide attention to their application regarding model-free scenario generation for renewable energy sources [61], [62], [68], [69]. The term "model-free" refers to methods that are independent of any prior assumptions about the data distribution [61], [62]. These models can return efficient scenarios by directly learning the diversity and stochasticity of the

historical data [62]. In [62], it is shown that conditional GAN (CGAN) can produce higher quality photovoltaic scenarios in comparison with model-based methods such as copula and auto-regression. In [61], the Wasserstein GAN (WGAN) model, which has higher training stability compared to GAN, is utilized to produce scenarios for wind and solar power variations with hourly and 5-min temporal resolutions. It is also shown that WGAN produces more effective scenarios compared to the copula method. Additionally, the Lipschitz continuity constraint of Wasserstein distance is imposed by the weight clipping method. In [68], an improved technique to enforce Lipschitz continuity constraint based on gradient penalty is employed in conditional WGAN (CWGAN) to improve the training process. In [69], CWGAN is used to model load forecast uncertainty based on temperature, historical load measurements, and calendar information. However, the performance of CWGAN can be further improved by exploiting an auxiliary classifier (ACWGAN) in the network design to predict the class labels instead of feeding them as an input to the network. It is shown in [70], [71] that such a design can return high-quality outputs for the classification problem of wireless signals. This advanced architecture will be used and optimized in this chapter to generate representative forecast scenarios of wind generation with high temporal granularity, which requires advanced adaptation based on wind power expertise. Specifically, we utilise the wind deviation level as the class label, which can vary from high to low. In this way, our model can produce realistic and diverse wind scenarios with the appropriate features by conditioning the generation process on the contextual information provided as class labels.

The overall schematic diagram of the proposed multi-resolution bidding framework is shown in Figure 5.1. It is seen that the bidding approach receives the wind uncertainty with different temporal resolutions regarding energy and reserve bids settlement (respectively, 1 hour and 1 minute). It

is seen that the role of ACWGAN is to generate zero mean wind deviation scenarios, which should be added to hourly mean wind scenarios to obtain wind scenarios with ultra-short term granularity. Also, the risk constraint regarding reserve availability, as a requirement for participation in the reserve market, is shown by a black arrow.

We analyse real-world data to measure profit loss and deviation from the allowed threshold for unavailability risk in real-time reserves. Our study compares GAN-based scenario generation techniques and direct random sampling methods. Our proposed framework outperforms classic single-resolution and non-probabilistic methods for reserve availability.

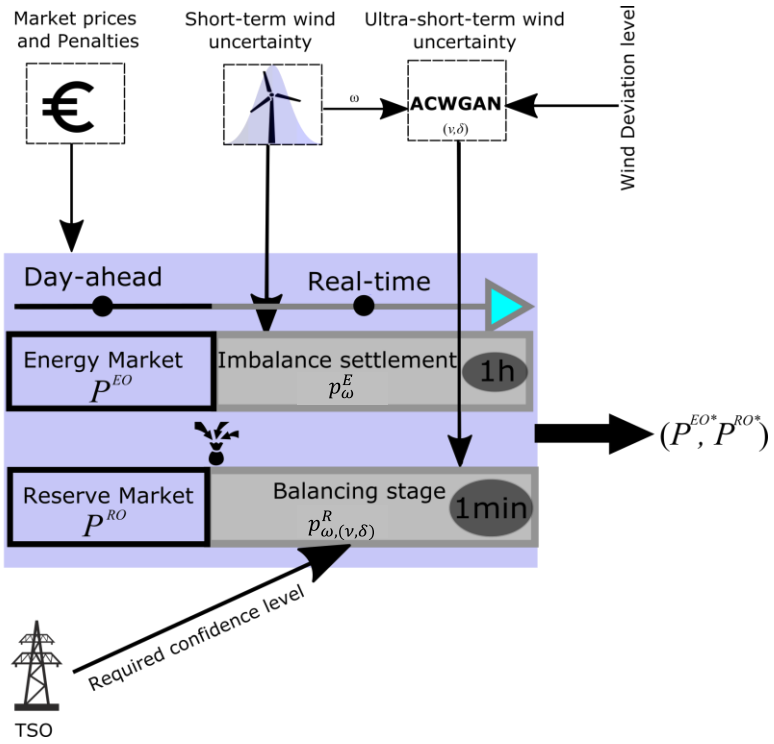

Figure 5.1) The schematic diagram of the proposed multi-resolution bidding framework.

The remainder of this chapter is organized as follows. Section 5.2. describes the proposed multi-resolution two-stage stochastic WPP bidding framework with probabilistic constraints. Section 5.3 presents the details of the proposed ACWGAN model used to generate wind speed time trajectories with a one-minute resolution. Section 5.4 provides the numerical results. Section 5.6 concludes the chapter. The material presented in this chapter is predominantly sourced from the author's publication, as referenced in last Section (Related publication), with due respect for the original copyright[3].

5.2 Multi-Resolution Stochastic Bidding Framework

The revenue of a WPP in the ERM, $\mathcal{R}$, consists of its contribution to day-ahead market and real-time compensation mechanisms. The bidding framework models day-ahead revenue in the first stage and real-time compensation in the second stage using mixed integer linear programming. The objective of the proposed WPP bidding strategy is:

$$\max_{X,\Psi} \mathcal{R} = \sum_{t\in T}\Bigg[\underbrace{\lambda_t^{Eo}P_t^{Eo} + \lambda_t^{Ro}P_t^{Ro}}_{\text{(i)}} + \sum_{\omega\in\Omega}\pi_{\omega,t}\Big(\underbrace{\lambda_t^{E\uparrow}\Delta p_{\omega,t}^{E\uparrow} - \lambda_t^{E\downarrow}\Delta p_{\omega,t}^{E\downarrow}}_{\text{(ii)}} \underbrace{- \lambda_t^{R\downarrow}|\Delta|^{-1}\sum_{\nu\in V}\mu_{\omega,\nu,t}\sum_{\delta\in\Delta}\Delta p_{\omega,(\nu,\delta),t}^{R}}_{\text{(iii)}}\Big)\Bigg] \tag{5.1}$$

[3] The IEEE permission grant can be accessed at the following link: https://journals.ieeeauthorcenter.ieee.org/choose-a-publishing-agreement/avoid-infringement-upon-ieee-copyright [Accessed 10 Feb 2023]

The decision variables of the optimization problem include non-negative decision variables of the first stage $\mathrm{X} = \{P_t^{Eo}, P_t^{Ro}\}$, and second-stage decision variables $\Psi = \{p_{\omega,t}^{E}, \Delta p_{\omega,t}^{E\downarrow}, \Delta p_{\omega,t}^{E\uparrow}, p_{\omega,(\nu,\delta),t}^{R}, \Delta p_{\omega,(\nu,\delta),t}^{R}, r_t, z_{\omega,(\nu,\delta),t}\}$, which comprise non-negative variables at the second stage $\{p_{\omega,t}^{E}, \Delta p_{\omega,t}^{E\downarrow}, \Delta p_{\omega,t}^{E\uparrow}, p_{\omega,(\nu,\delta),t}^{R}, \Delta p_{\omega,(\nu,\delta),t}^{R}, r_t\}$ and the auxiliary binary variables $\{z_{\omega,(\nu,\delta),t}\}$. The first term in (5.1), (i), presents the day-ahead profit of bidding in the ERM. λ_t^{Eo} and λ_t^{Ro} represent the day-ahead energy and reserve prices, respectively, at market period *t*; P_t^{Eo} and P_t^{Ro} are the energy and reserve power bids in the day-ahead stage, respectively. The second term (ii) represents the financial compensation in the energy imbalance settlement. $\pi_{\omega,t}$ is the probability of the hourly mean scenarios of wind power. $\lambda_t^{E\uparrow}$ and $\lambda_t^{E\downarrow}$ are energy imbalance prices for generation surplus $\Delta p_{\omega,t}^{E\uparrow}$ and generation deficit $\Delta p_{\omega,t}^{E\downarrow}$ regarding the hourly mean wind scenario ω at time *t*, respectively. The last term (iii) reflects the balancing stage penalties. The reserve unavailability penalty rate for market period *t* in (iii) is indicated by $\lambda_t^{R\downarrow}$. $\Delta p_{\omega,(\nu,\delta),t}^{R}$ represents the non-provided capacity regarding wind mean deviation scenario ν at the balancing period δ with respect to ω and *t*. $|\bullet|$ indicates the cardinality of its set argument. All instances of time-series scenario ν, (ν, δ), have an identical probability for a given hourly wind scenario and market time unit. $\mu_{\omega,\nu,t}$ is the probability of mean deviation scenarios of wind power. It is worth noting that, from this chapter onward, compared to former chapters, the remuneration for FCR activation is implicitly incorporated into the procurement prices. This approach not only simplifies the settlement process at the balancing stage but also ensures consistency and adherence to widely-accepted standards within the FCR market landscape in European countries, such as Belgium [29].

At this stage, it is important to note that a forecaster is firstly used to generate $|\Omega|$ hourly wind power scenarios to hedge against the uncertainty

regarding real-time energy deviations. Then, an ACWGAN model is used to construct, around each mean hourly scenario $\omega \in \Omega$, $|V|$ scenarios of wind deviations, with length $|\Delta|$, regarding each one-minute interval $\delta \in \Delta$.

The constraints of the proposed WPP bidding framework are presented in the following. The total submitted bids to the day-ahead market, $P_t^{Eo} + P_t^{Ro}$, should be within the upper $\overline{P}$ and lower $\underline{P}$ capacity limits of the WT. Thus, the physical capacity constraint, which belongs to the first stage of the problem, is as follows:

$$\underline{P} \leq P_t^{Eo} + P_t^{Ro} \leq \overline{P} \qquad \forall\, t \in T \qquad (5.2)$$

Then, it should be ensured that the allocated reserve in scenario ω and interval δ of mean deviation scenario ν for the given market period t, does not exceed the available power $\tilde{P}_{\omega,(\nu,\delta),t}$ and submitted reserve power in the day-ahead market P_t^{Ro}, respectively. Constraints (5.3) and (5.4), respectively, limit $p^R_{\omega,(\nu,\delta),t}$ to $\tilde{P}_{\omega,(\nu,\delta),t}$ and P_t^{Ro} as follows:

$$p^R_{\omega,(\nu,\delta),t} \leq \tilde{P}_{\omega,(\nu,\delta),t} \qquad \forall\, t \in T; \forall\, \omega \in \Omega;\ \forall\, (\nu,\delta) \in V \times \Delta \qquad (5.3)$$

$$p^R_{\omega,(\nu,\delta),t} \leq P_t^{Ro} \qquad \forall\, t \in T; \forall\, \omega \in \Omega;\ \forall\, (\nu,\delta) \in V \times \Delta \qquad (5.4)$$

Along with (5.3)-(5.4), the following constraints, i.e., (5.5)-(5.6), enable that the allocated real-time reserve power is the minimum of real-time total available power $\tilde{P}_{\omega,(\nu,\delta),t}$ and the day-ahead reserve bid P_t^{Ro} through the auxiliary binary variable $z_{\omega,(\nu,\delta),t}$ and a sufficiently large positive constant M.

$$p^R_{\omega,(\nu,\delta),t} \geq P_t^{Ro} - \mathrm{M} z_{\omega,(\nu,\delta),t} \qquad \forall\, t \in T; \forall\, \omega \in \Omega;\ \forall\, (\nu,\delta) \in V \times \Delta \qquad (5.5)$$

$$p^{R}_{\omega,(\nu,\delta),t} \geq \tilde{P}_{\omega,(\nu,\delta),t} - \mathrm{M}\left(1 - z_{\omega,(\nu,\delta),t}\right) \qquad \forall\, t \in T; \forall\, \omega \in \Omega; \forall\, (\nu,\delta) \in V \times \Delta \qquad (5.6)$$

Therefore, when available power is adequate, $\tilde{P}_{\omega,(\nu,\delta),t} \geq P^{Ro}_{t}$, $z_{\omega,(\nu,\delta),t}$ becomes zero to comply with (5.4) and avoid inconsistent constraints (5.4)-(5.6). In this regard, (5.4) imposes an upper limit, which is P^{Ro}_{t}, on $p^{R}_{\omega,(\nu,\delta),t}$ and thus the real-time allocated reserve power $p^{R}_{\omega,(\nu,\delta),t}$ matches the day-ahead reserve bid. However, when the available power is lower than the scheduled bid, $z_{\omega,(\nu,\delta),t}$ becomes equal to one, and (5.3) becomes an active constraint, thereby imposing an upper limit, i.e., $\tilde{P}_{\omega,(\nu,\delta),t}$, on $p^{R}_{\omega,(\nu,\delta),t}$. Thus, all available power is allocated to the reserve market, so as to reduce the reserve deviation penalty as much as possible. In other words, the set of constraints (5.3)-(5.6) enforce the absolute reserve allocation control strategy of the WPP where its maximum power production is derated by the day-ahead reserve bid P^{Ro}_{t}. In this way, WPP acts close to conventional units since it prioritizes power delivery to the reserve market [19], [43].

Then, the non-provided allocated reserve in scenario ω and instance δ of the mean deviation scenario ν for the given market period t with respect to P^{Ro}_{t} is obtained by (5.7).

$$P^{Ro}_{t} - p^{R}_{\omega,(\nu,\delta),t} \leq \Delta p^{R}_{\omega,(\nu,\delta),t} \qquad \forall\, t \in T; \forall\, \omega \in \Omega; \forall\, (\nu,\delta) \in V \times \Delta \qquad (5.7)$$

Importantly, since the proposed bidding framework considers wind uncertainty with two different time-scales, constraint (5.8) links the minute-wise and hourly scenarios, as follows:

$$p^{E}_{\omega,t} = \widetilde{\overline{P}}_{\omega,t} - \left(|V|.|\Delta|\right)^{-1} \sum_{(\nu,\delta)\in V\times\Delta} p^{R}_{\omega,(\nu,\delta),t} \qquad \forall\, t \in T;\ \forall\, \omega \in \Omega \qquad (5.8)$$

where, $\widetilde{\overline{P}}_{\omega,t}$ is the available hourly mean wind power in scenario ω at time t, and $p^{E}_{\omega,t}$ is the allocated power to the energy market in scenario ω at period t.

The deficit and surplus of the allocated power to the energy market, used for energy imbalance settlement, are obtained by (5.9).

$$P^{Eo}_{t} - p^{E}_{\omega,t} = \Delta p^{E\downarrow}_{\omega,t} - \Delta p^{E\uparrow}_{\omega,t} \qquad \forall\, t \in T; \forall\, \omega \in \Omega \qquad (5.9)$$

Furthermore, as the proposed framework aims to satisfy the reliability of the offered reserve bids, the following constraint is given to approximate the risk of reserve unavailability:

$$r_t = |\Delta|^{-1} \sum_{\omega \in \Omega} \pi_{\omega,t} \sum_{(\nu,\delta) \in V \times \Delta} \mu_{\omega,\nu,t}\, z_{\omega,(\nu,\delta),t} \quad \forall\, t \in T \qquad (5.10)$$

where r_t is the risk of reserve unavailability at market period t.

As seen in (5.10), the probability-weighted average of the instances of power scarcity, $z_{\omega,(\nu,\delta),t} = 1$, with respect to the probability of hourly $\pi_{\omega,t}$ and minute-wise $\mu_{\omega,\nu,t}$ scenarios, estimates r_t.

Finally, the risk behavior of the WPP is controlled by defining an upper bound on the allowed risk threshold, ρ^{o}_{t}, for each market time-unit, as follows:

$$r_t \leq \rho^{o}_{t} \qquad \forall\, t \in T \qquad (5.11)$$

It should be noted that although it is the TSO that defines a risk threshold regarding reserve unavailability, WPP may take a lower risk depending on market incentives and wind power uncertainty to obtain the optimal allocation trade-off in each market floor. Also, the single-resolution

model, i.e., the classic model, can be interpreted as a simplified version of the proposed framework wherein the ultra-short-term wind stochasticity is ignored.

The inter-temporal dependency of wind power between market time units is implicitly considered in the framework through the use of hourly scenarios. Also, reserve availability constraints are considered separately for each market period, ensuring reserve reliability for each individual period instead of for the entire day-ahead market. This allows for decomposing the framework into |T| mixed-integer linear subproblems for each time period t, making the bidding framework more manageable.

5.3 Modeling Wind Uncertainty with High Resolution

A wind speed time-trajectory $\widetilde{ws}_t$ with $|\Delta|$ samples per hour at a given hourly period t can be explicitly expressed via its hourly mean value $\overline{ws}_t$ and ultra-short-term mean deviations $\widehat{\varepsilon s}_t$ by $\widetilde{ws}_t = \mathbf{1}\overline{ws}_t + \widehat{\varepsilon s}_t$; where $\mathbf{1}$ is a vector of all ones; $\mathbf{1}$ and $\widehat{\varepsilon s}_t$ are both $|\Delta|\times 1$ dimension.

A great effort is devoted to hourly wind forecast and scenario generation models in the literature [11]. In general, since hourly wind variations and the required prediction horizon are both tractable, these methods yield acceptable performance [11]. The required hourly wind scenarios Ω for the proposed bidding framework can be obtained by any of those effective methods, e.g., random sampling from the empirical hourly wind distribution [72] or probabilistic hourly wind speed forecast [73]. In this study, without loss of generality, the distribution of hourly wind forecast errors is used to represent the stochasticity of wind regarding $\overline{ws}_t$. Remarkably, the distribution of wind frequency, especially in the medium- and long-term horizons, is conventionally fitted to the Weibull distribution [74]. Also, it can be modeled with the non-parametric approaches, e.g., those proposed

in [75]. However, it is important to notice that the distribution of hourly wind speed forecast errors is better fitted to normal distribution [74]. Therefore, in this study, the hourly wind uncertainty is represented by a normal distribution as in the wind-related literature on stochastic programming [72].

Nevertheless, generating efficient zero mean wind deviation scenarios with a high temporal resolution, concerning $\widehat{\varepsilon s}_t$, is challenging [19]. This increased difficulty is primarily due to the higher randomness and volatility of wind over ultra-short time periods (e.g., minute-wise) compared to short-term periods (e.g., hourly) [11], [20]. Moreover, in this study, the required prediction horizon for the wind deviation scenarios with high temporal granularity is $|\Delta|$ (i.e., 60) times more than the short-term scenarios. Therefore, as the prediction lead-time increases, the performance of conventional prediction models deteriorates [11], [20]. Therefore, this section proposes a new model to capture the time-varying and nonlinear dynamics of high-dimensional weather data regarding ultra-short-term wind variations by directly learning their distribution without making any modeling assumptions.

5.3.1 Wasserstein GAN With Gradient Penalty

A GAN consists of an interconnected network comprising a generator $G_\alpha(\cdot)$ and discriminator $D_\beta(\cdot)$ which simultaneously compete in a zero-sum game. The trainable parameters of the generator and discriminator neural networks, during training, are, respectively, shown by α and β subscripts. The generator $G_\alpha(\cdot)$ samples a latent noise vector z from the latent space with the probability distribution $\mathcal{P}_Z$, i.e., $z \sim \mathcal{P}_Z$, as input and attempts to map it to realistic-looking data s_g , e.g., scenario of wind time-series, in the output $G_\alpha(z)$. Notably, z should have a relatively low dimension $|z|$ to facilitate the generator's task in mapping the latent space to real data

distributions $\mathcal{P}_r$ [76]. Discriminator $D_\beta(\cdot)$ receives either a real sample s_r drawn from the original dataset, e.g., actual wind dataset, with distribution $\mathcal{P}_r$, i.e., $s_r \sim \mathcal{P}_r$, or synthesized sample s_g from the generator with distribution $\mathcal{P}_g$, i.e., $s_g \sim \mathcal{P}_g$, as input and identifies the realness or fakeness of the received sample in the output. On the other hand, $G_\alpha(\cdot)$ aims to generate realistic-looking samples, e.g., scenario of wind time-series, to deceive $D_\beta(\cdot)$. The discriminator is trained directly via a binary classifier loss function while the generator is updated indirectly by the gradient of the discriminator loss.

Remarkably, the loss function of GAN can be interpreted as minimizing the distance between the probability distribution of real data $\mathcal{P}_r$ and synthesized data $\mathcal{P}_g$ using Jensen-Shannon Divergence (JSD) criterion. However, JSD fails to provide a sensible gradient in GAN training when two distributions, $\mathcal{P}_r$ and $\mathcal{P}_g$, have non-overlapping support [77]. This undesirable characteristic of JSD leads to several issues, such as training instability and mode collapse in GAN's training process [77]. To circumvent these drawbacks, a Wasserstein distance-based loss function is proposed in [78]. Also, adopting such a loss function prevents the potential overfitting problem of the model [78]. The Wasserstein distance, WD, between two distributions $\mathcal{P}_r$ and $\mathcal{P}_g$ is given as follows:

$$WD(\mathcal{P}_r, \mathcal{P}_g) = \inf_{\gamma \in \Gamma(\mathcal{P}_r, \mathcal{P}_g)} \mathbb{E}_{(s_r, s_g)\sim\gamma} \left\| s_r - s_g \right\| \tag{5.12}$$

where Γ is the set of all joint distributions γ with marginals $\mathcal{P}_r$ and $\mathcal{P}_g$.

Considering the numerous joint distributions γ in Γ, (5.12) is computationally intractable. Therefore, using the duality theory, the Wasserstein distance primal problem (5.12) is converted to the following form [77]:

$$WD(\mathcal{P}_r, \mathcal{P}_g) = \sup_{\|\varphi\|_L \leq 1} \mathbb{E}_{s_r \sim \mathcal{P}_r}[\varphi(s_r)] - \mathbb{E}_{s_g \sim \mathcal{P}_g}[\varphi(s_g)] \tag{5.13}$$

where φ is the set of 1-Lipschitz functions [77].

In WGAN, $D_\beta(\cdot)$, the so-called critic in WGAN terminology, takes the role of φ to find the distance between distributions. The 1-Lipschitz regularity condition of $D_\beta(\cdot)$ can be effectively imposed by restricting the gradient norm of $D_\beta(\cdot)$, $\nabla\|D_\beta(\cdot)\|_2$, to be at most one through adding a penalty term in the loss function [79].

Accordingly, while the critic measures the discrepancy between $\mathcal{P}_r$ and $\mathcal{P}_g$, e.g., the discrepancy between actual and generated wind time-series, using (5.13), the generator tries to produce realistic-looking data to minimize $WD(\mathcal{P}_r, \mathcal{P}_g)$. The improved loss function in WGAN, $\mathcal{L}_W(D_\beta, G_\alpha)$, is as follows:

$$\begin{aligned}\mathcal{L}_W(D_\beta, G_\alpha) = \min_\alpha \max_\beta\ & \mathbb{E}_{s_r \sim \mathcal{P}_r}[D_\beta(s_r)] - \mathbb{E}_{s_g \sim \mathcal{P}_g}[D_\beta(s_g)] \\ & - \eta_{GP}\mathbb{E}_{\hat{s} \sim \hat{\mathcal{P}}}\left[\left(\nabla_{\hat{s}}\|D_\beta(\hat{s})\|_2 - 1\right)^2\right]\end{aligned} \tag{5.14}$$

where η_{GP} is the gradient penalty coefficient concerning the 1-Lipschitz regularity condition and $\hat{s}$ symbolizes the linearly interpolated data points belonging to $\mathcal{P}_r$ and $\mathcal{P}_g$, which is defined as follows:

$$\hat{s} = \varrho s_r + (1 - \varrho)s_g \qquad s_r \sim \mathcal{P}_r\ ;\ s_g \sim \mathcal{P}_g \tag{5.15}$$

where ϱ is sampled from a standard uniform distribution, $\varrho \sim U[0,1]$.

5.3.2 Conditional Wasserstein GAN

While discussed generative models offer realistic scenarios, they lack control over specific features or modes, such as wind deviation levels. However, this can be overcome by incorporating additional information, such as class labels, which are considered to be wind deviation levels in our problem, into the adversarial training process of GANs.

Particularly, in the critic's network $D_\beta(\cdot|c)$ of CWGAN, the class labels $c \sim \mathcal{P}_c$ are merged with the actual $s_r \sim \mathcal{P}_r$ and generated $s_g \sim \mathcal{P}_g$ samples to obtain a joint hidden representation of samples and class labels. Furthermore, in the generator's network, these class labels are merged with the latent noise vectors $z \sim \mathcal{P}_z$. The loss function of CWGAN, $\mathcal{L}_{CW}(D_\beta, G_\alpha)$, is then expressed as follows:

$$\begin{aligned}\mathcal{L}_{CW}(D_\beta, G_\alpha) &= \min_{\alpha} \max_{\beta} \mathbb{E}_{s_r \sim \mathcal{P}_r}\left[D_\beta(s_r|c)\right] - \mathbb{E}_{s_g \sim \mathcal{P}_g}\left[D_\beta(s_g|c)\right] \\ &\quad - \eta_{GP}\mathbb{E}_{\hat{s} \sim \hat{\mathcal{P}}}\left[\left(\nabla_{\hat{s}}\left\|D_\beta(\hat{s}|c)\right\|_2 - 1\right)^2\right]\end{aligned} \tag{5.16}$$

The input-output diagram of the CWGAN is shown in Figure 5.2(a). The input to the critic in CWGAN consists of class labels (denoted by a bold black arrow) and the joint hidden representation of class labels and input samples. The training process of CWGAN involves sequential updates to the critic and generator parameters, based on loss feedback (dashed lines), via the inner maximization problem and outer minimization problem, respectively, defined in (5.16).

5.3.3 Proposed Wasserstein GAN with Auxiliary Classifier

CWGAN learns a representation of z that depends on class labels as it receives them as input to the network. In other words, CWGAN requires $D_\beta(\cdot|c)$ to return an estimate of the distance between generated and real joint distributions of class labels and samples, by merging c to either z or s_r, since it receives them as input. The complicated task of $D_\beta(\cdot|c)$, measuring the discrepancy between the real and generated joint distributions, and $G_\alpha(\cdot|c)$, mapping the latent space (which is further entangled by merging the class labels into $z \sim \mathcal{P}_Z$) to real data distribution, can be alleviated by incorporating a new agent into the adversarial training process.

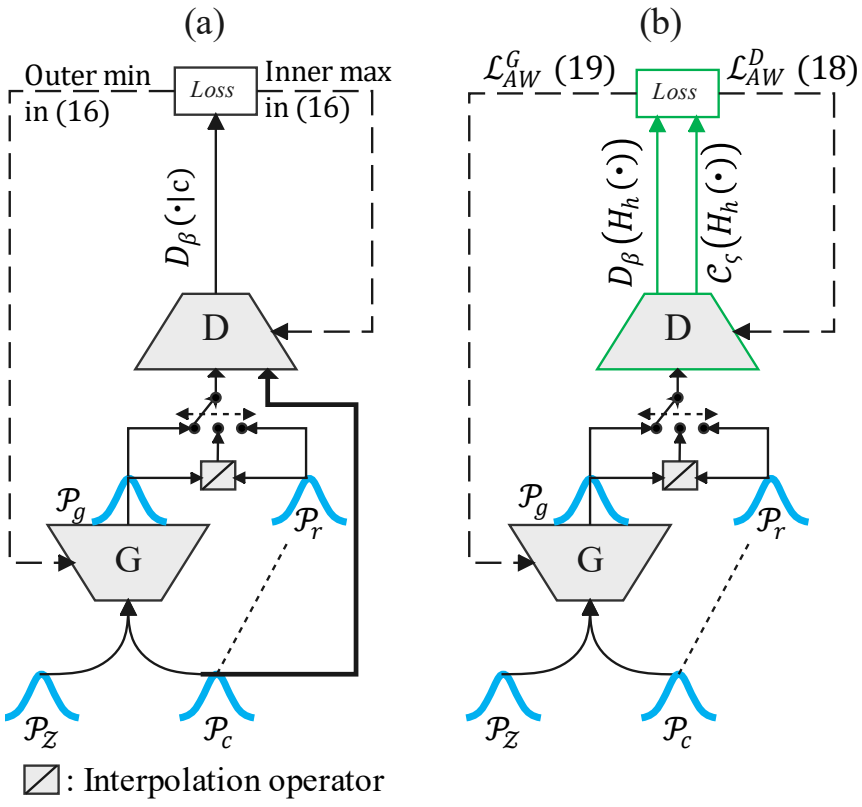

Figure 5.2) Input-output diagram of (a): CWGAN, (b): ACWGAN.

The additional agent, which is a classifier $\mathcal{C}_\varsigma(\cdot)$ and cooperates with $D_\beta(\cdot)$ and $G_\alpha(\cdot)$, estimates the conditional probability of the class labels given the received samples. Thus, the critic now merely estimates the distance between real and generated data distributions, through $WD(\mathcal{P}_r, \mathcal{P}_g)$, which is independent of the class labels, e.g., wind deviation levels.

Moreover, the generator can better map $\mathcal{P}_Z$ to $\mathcal{P}_r$ through $G_\alpha(\cdot)$ as its loss function, $\min_\alpha -\mathbb{E}_{s_g\sim\mathcal{P}_g}\left[D_\beta\left(s_g|c\right)\right]$, depends on the critic's performance as well. Nevertheless, both the generator and critic should still contribute to enhance the ability of $\mathcal{C}_\varsigma(\cdot)$ to predict the class labels of the samples correctly. The proposed three-player adversarial loss function of ACWGAN, $\mathcal{L}_{AW}\left(G_\alpha, \mathcal{C}_\varsigma, D_\beta\right)$, can be formulated as:

$$\begin{aligned}\mathcal{L}_{AW}&\left(G_\alpha, \mathcal{C}_\varsigma, D_\beta\right)\\ &= \min_\alpha \min_\varsigma \max_\beta \ \mathbb{E}_{s_r\sim\mathcal{P}_r}\left[D_\beta(s_r)\right] - \mathbb{E}_{s_g\sim\mathcal{P}_g}\left[D_\beta\left(s_g|c\right)\right]\\ &- \eta_{GP}\mathbb{E}_{\hat{s}\sim\hat{\mathcal{P}}}\left[\left(\nabla_{\hat{s}}\left\|D_\beta(\hat{s}|c)\right\|_2 - 1\right)^2\right]\\ &- \eta_c\mathbb{E}_{s_r\sim\mathcal{P}_r}\left[\log\mathbb{P}\left(\mathcal{C}_\varsigma(s_r) = c\right)\right]\\ &- \eta_c\mathbb{E}_{s_g\sim\mathcal{P}_g}\left[\log\mathbb{P}\left(\mathcal{C}_\varsigma(s_g) = c\right)\right]\end{aligned} \tag{5.17}$$

where ς indicates the classifier's trainable parameters, c is the true class label of the received sample, and η_c is a hyperparameter regarding the weight of the log-likelihood loss, $\log\mathbb{P}(\cdot)$, of the correct class prediction.

The first three terms in (5.17) correspond to the WD of the generated and real data distributions which should be estimated by $D_\beta(\cdot)$ through the inner maximization and minimized by $G_\alpha(\cdot)$ via the outer minimization problem. The last two terms in (5.17) minimize the negative log-likelihood loss of the correct class prediction through the middle minimization problem.

In practice, the ACWGAN three-player game can be implemented by two neural networks comprising a new critic, which also embeds an auxiliary classifier layer as its secondary output, and a generator. In this way, the auxiliary classifier $\mathcal{C}_\varsigma(\cdot)$ and critic $D_\beta(\cdot)$ in (5.17) share the same hidden layers H_h, parameterized by h, in the new critic. Importantly, the multi-task learning framework [80] enhances the three-player ACWGAN learning performance and reduces its complexity by leveraging the shared information among related tasks. In estimating the class label of generated time series, a low WD indicates that the generated scenario closely resembles real data, suggesting it shares similar contextual information as the given class labels. This ensures that the class labels of the generated scenarios should fall within the expected range, providing a reliable basis for label estimation.

Particularly, the new critic receives an input sample, either from $\mathcal{P}_r$ or $\mathcal{P}_g$, and, in contrast to CWGAN, returns two outputs $\left[D_\beta\left(H_h(\cdot)\right), \mathcal{C}_\varsigma\left(H_h(\cdot)\right)\right]$. The first output, $D_\beta\left(H_h(\cdot)\right)$, obtains the WD between real and generated distributions through the inner maximization in (5.17). However, the second output of the new critic in ACWGAN, $\mathcal{C}_\varsigma\left(H_h(\cdot)\right)$, predicts the class label of each provided sample rather than merely receiving it as an input (as in the case of CWGAN). The new critic's loss function is as follows:

$$\begin{aligned} \mathcal{L}_{AW}^{D} = \max_{\{h,\beta,\varsigma\}} & \mathbb{E}_{s_r\sim\mathcal{P}_r}\left[D_\beta\left(H_h(s_r)\right)\right] - \mathbb{E}_{s_g\sim\mathcal{P}_g}\left[D_\beta\left(H_h\left(s_g|c\right)\right)\right] \\ & - \eta_{GP}\mathbb{E}_{\hat{s}\sim\hat{\mathcal{P}}}\left[\left(\nabla_{\hat{s}}\left\|D_\beta\left(H_h(\hat{s}|c)\right)\right\|_2 - 1\right)^2\right] \\ & + \eta_c\mathbb{E}_{s_r\sim\mathcal{P}_r}\left[\log\mathbb{P}\left(\mathcal{C}_\varsigma\left(H_h(s_r)\right) = c\right)\right] \\ & + \eta_c\mathbb{E}_{s_g\sim\mathcal{P}_g}\left[\log\mathbb{P}\left(\mathcal{C}_\varsigma\left(H_h\left(s_g\right)\right) = c\right)\right] \end{aligned} \tag{5.18}$$

In (5.18), $WD\left(\mathcal{P}_r, \mathcal{P}_g\right)$ is estimated by the first three terms. The last two terms in (5.18) optimize the auxiliary classifier layer by inverting the sign

of negative log-likelihood loss, regarding the middle minimization problem in (5.17), and expressing it as a maximization problem.

Nevertheless, in the same fashion as in CWGAN, the generator receives latent noise vectors along with class labels, e.g., wind deviation levels, and returns synthesized samples, e.g., scenario of wind time-series, holding desired class attributes. Accordingly, the generator aims to produce quality samples to reduce the discrepancy between the generated and real data distributions, i.e., by solving the outer minimization problem in (5.17). It is seen that only the second term in (5.17), $-\mathbb{E}_{s_g\sim\mathcal{P}_g}\left[D_\beta\left(s_g|c\right)\right]$, involves the generator's parameters regarding the minimization of $WD\left(\mathcal{P}_r,\mathcal{P}_g\right)$. By inverting its sign, the minimization problem can be converted to a maximization one. Notwithstanding, the synthesized samples by the generator should also have the correct class attributes. It is seen that only the last term in (5.17), $-\eta_c\mathbb{E}_{s_g\sim\mathcal{P}_g}\left[\log\mathbb{P}\left(\mathcal{C}_\varsigma\left(s_g\right)=c\right)\right]$, contains the generator's parameters regarding the correct class prediction error. Thus, by inverting its sign, the two mentioned contributing elements can be combined as follows to construct a single loss function $\mathcal{L}_{AW}^{G}$ for training the generator:

$$\begin{aligned}\mathcal{L}_{AW}^{G} = \max_{\alpha}\ & \mathbb{E}_{s_g\sim\mathcal{P}_g}\left[D_\beta\left(H_h\left(s_g|c\right)\right)\right] \\ & +\ \eta_c\mathbb{E}_{s_g\sim\mathcal{P}_g}\left[\log\mathbb{P}\left(\mathcal{C}_\varsigma\left(H_h\left(s_g\right)\right)=c\right)\right]\end{aligned} \tag{5.19}$$

The input-output diagram of ACWGAN is shown in Figure 5.2(b). It is seen that the new critic of ACWGAN, shown by a green block, does not receive class labels as input. Nevertheless, in contrast with the critic of CWGAN, the new critic of ACWGAN has two outputs, shown by green arrows. The first output, $D_\beta\left(H_h(\cdot)\right)$, obtains the WD between real and generated distributions while the second output, $\mathcal{C}_\varsigma\left(H_h(\cdot)\right)$, predicts the

class label of the provided sample. Finally, ACWGAN is trained by sequentially updating the parameters of the new critic and generator through loss feedbacks $\mathcal{L}_{AW}^{D}$ and $\mathcal{L}_{AW}^{G}$, (shown by dashed lines), respectively.

The training process of ACWGAN is elaborated in detail in Algorithm 5.I. Importantly, as seen in Algorithm 5.I, at each training step, the new critic is first trained by few iterations, typically $n_d = 5$ [79], to estimate $WD(\mathcal{P}_r, \mathcal{P}_g)$ and improve the classifier ability to correctly predict class labels of $s_r \sim \mathcal{P}_r$ and $s_g \sim \mathcal{P}_g$. During this step, the generator's parameters are not updated, since $\mathbb{E}_{s_g \sim \mathcal{P}_g}\left[D_\beta\left(H_h(s_g|c)\right)\right]$ has different signs in the loss functions (5.18) and (5.19). Thus, after the new critic training, the generator is trained for one iteration to minimize the obtained WD through the first term in (5.19), i.e., maximizing $-WD(\mathcal{P}_r, \mathcal{P}_g)$, while satisfying the correct class property of the generated samples as it is also considered in $\mathcal{L}_{AW}^{G}$. Notably, the new critic's parameters are not updated at this step, since training the critic with $\mathcal{L}_{AW}^{G}$ results in an inaccurate estimate of $WD(\mathcal{P}_r, \mathcal{P}_g)$ due to their conflicting objectives. This procedure is continued until the model is converged and desired outputs are achieved.

Once ACWGAN is trained by labeled samples, the generator is capable of producing plausible wind speed mean deviation scenarios with a high temporal resolution, e.g., minute-wise time granularity, and desired class labels, e.g., deviation levels. In this regard, the generator is fed by K noise vectors z of dimension $|z|$ and desired class label c to obtain K scenarios of wind speed mean deviation with $|\Delta|$, e.g., = 60, samples per hour. These effectively-controlled wind speed scenarios are then converted to wind power scenarios through an intermediate conversion layer.

Training Algorithm 5.I: Proposed ACWGAN Model.

Default values: $n_b = 64$, $n_d = 5$, $\eta_{GP} = 10$, $\eta_c = 1$, Gradient descent optimizer = Adam, l_r =0.00006.

Require: n_b, Batch size. n_d, Number of critic's updates in ACWGAN. η_{GP}, Gradient penalty. η_c, Log-likelihood weight loss. Gradient descent optimizer. l_r, Learning rate.

Require: Initialize model's weights $\{\alpha, h, \beta, \varsigma\}$.

while weights have not converged **do:**

▸**Execute n_d training steps for the combined discriminator and classifier network.**

for $n = 1, \dots, n_d$ **do:**

for $i = 1, \dots, n_b$ **do:**

Take a real sample along with its class label from $\mathcal{P}_r$.

s_r and $c \sim \mathcal{P}_r$

sample a noise vector from latent space $\mathcal{P}_z$.

$z \sim \mathcal{P}_z$

Generate fake sample using G_α.

$s_g \leftarrow G_\alpha(z|c)$

Obtain the interpolated sample $\hat{s}$.

$\hat{s} \leftarrow \varrho s_r + (1-\varrho)s_g$, where $\varrho \sim U[0,1]$

Compute the combined discriminator and classifier loss regarding s_r, s_g and $\hat{s}$.

$$L_D(i) \leftarrow D_\beta\left(H_h(s_r)\right) - D_\beta\left(H_h\left(s_g|c\right)\right) - \eta_{GP}\left(\nabla_{\hat{s}}\left\|D_\beta\left(H_h(\hat{s}|c)\right)\right\|_2 - 1\right)^2 + \eta_c \log \mathbb{P}\left(\mathcal{C}_\varsigma\left(H_h(s_r)\right) = c\right) + \eta_c \log \mathbb{P}\left(\mathcal{C}_\varsigma\left(H_h\left(s_g\right)\right) = c\right)$$

end for

Update discriminator and classifier layer parameters $\{h, \beta, \varsigma\}$ using gradient descend algorithm.

$$\{h, \beta, \varsigma\} \leftarrow \text{Adam}\left(-\nabla_{\{h,\beta,\varsigma\}} n_b^{-1} \sum_{i=1}^{n_b} L_D(i)\right)$$

end for

▸**Execute a single generator training step.**

Sample a batch of noise vectors and class labels.

$\{z(i)\}_{i=1}^{n_b} \sim \mathcal{P}_z$; $\{c(i)\}_{i=1}^{n_b} \sim \mathcal{P}_c$

Generate a batch of fake samples using the generator network.

$\{s_g(i)\}_{i=1}^{n_b} \leftarrow G_\alpha\left(\{z(i)\}_{i=1}^{n_b} | \{c(i)\}_{i=1}^{n_b}\right)$

Update generator parameters α using gradient descend algorithm.

$$\alpha \leftarrow \text{Adam}\left(-\nabla_\alpha\, n_b^{-1} \sum_{i=1}^{n_b} D_\beta\left(H_h\left(s_g(i)|c(i)\right)\right) + \eta_c \log \mathbb{P}\left(\mathcal{C}_\varsigma\left(H_h\left(s_g(i)\right)\right) = c(i)\right)\right)$$

end while

In this study, a penalized cubic B-spline method which better controls the curvature of the fitted power curve is employed. In this method, a penalty term is added to the least square fitting objective in order to control the smoothness of the power curve. The details of this method are given in [81]. Nevertheless, more advanced techniques, e.g., neural networks, can be incorporated into the proposed speed to power conversion layer, to deal with a wind farm where its total production is significantly affected by other factors such as wake effects.

Eventually, the WPP not only receives K realistic-looking wind power scenarios with a high temporal resolution but also has control over the desired characteristics, e.g., deviation levels, of the generated samples as input to the stochastic bidding model.

5.4 Case Study

In this section, a comprehensive case study analysis is performed using real-world datasets. The focus is on evaluating the performance of the proposed ACWGAN model for generating wind power variation scenarios, which serve as inputs for the multi-resolution probabilistic bidding framework. Also, the advantages of the proposed data-driven probabilistic WPP energy and reserve scheduling framework over the classic single-resolution model are investigated. Finally, the benefits of using ACWGAN in the presented decision model, in contrast to the other alternative scenario representation methods, are further investigated. The scenario generation models are developed in TensorFlow [82], and the wind power scheduling framework is developed in Julia/JuMP [49].

A WPP owning a 5.3 MW wind turbine with cut-in and cut-off speed of, respectively, 3 and 25 $m.s^{-1}$ is studied here. It should be noted that even with this limited wind power capacity, portfolios are still able to participate

at both day-ahead energy and reserve market floors. For example, in the electricity markets operated by EPEX-Spot and Nord Pool (which include several countries, such as Belgium), the minimum bid size in the day-ahead energy market is 0.1 MW [10]. Also, in many countries, such as Belgium, Denmark, and France, the portfolios with at least 1 MW of flexible power are allowed to participate in the balancing market as BSP [83]. The hourly wind scenarios are obtained by sampling from a normal distribution with the mean wind speed of 9 $m.s^{-1}$ and standard deviation of 1.5 $m.s^{-1}$. Furthermore, the ultra-short-term wind scenarios are obtained by ACWGAN and evaluated by other benchmark algorithms including direct random sampling from the training set, CGAN, and CWGAN. Both hourly and ultra-short-term scenarios, employed in the proposed bidding framework, are considered equiprobable. Market prices and penalties for one market period are reported in Table 5.1. These market rates are in a similar and comparable range as in the related literature [19], [43] and in several European electricity markets, such as in Denmark, Norway, and Belgium [48].

The reserve unavailability penalty rate during each imbalance settlement period is constant. The proposed scheduling problem is solved for one market period. This reduction is not limiting as one can solve the problem for $|T|$ market periods by decomposition of (1)-(11) as detailed in subsection II.B. Moreover, this setting allows us to better demonstrate the effectiveness of the proposed approach by detailing various aspects of in- and out-of-sample results.

Table 5.1) Prices and penalty rates of the studied ERM period

λ^{Eo} [€/MWh]	λ^{Ro} [€/MW]	$\lambda^{\uparrow}$ [€/MWh]	$\lambda^{\downarrow}$ [€/MWh]	λ^{R} [€/MW]
33	35	31	36	40

In this study, a sufficiently large dataset regarding minute-wise and hourly wind variations from 2014 to 2016 is collected from a wind site located in Frøya island [46]. Specifically, the wind dataset contains 453,600 instances regarding 7,560 hours of minute-wise wind data. The processed dataset is then divided into training and test sets with a 4:1 ratio.

For a fair comparison, the same neural network architecture is used for the critic and generator of all GAN-based methods. The generator network has three fully connected layers and the critic uses three 1D convolution layers. The number of neurons in each network's hidden layer is fine-tuned based on 50 trial runs. The networks are trained on 362,880 samples, each with 1 minute-resolution (6,048 hours) and corresponding labels, including wind fluctuation level, divided into 5 categories. In particular, the fluctuation levels belonging to intervals [0, 0.5), [0.5, 1), [1, 1.5), [1.5, 2) and [2, S_{max}] $m.s^{-1}$ corresponds to the class labels C_0, C_1, C_2, C_3, and C_4, respectively. S_{max} denotes the maximum wind deviation value and is 5 $m.s^{-1}$ in our dataset. Notably, C_0, C_1, and C_2, with the probability of, respectively, 0.37, 0.40, and 0.15, are the dominant events in the dataset. On the other hand, C_3 and C_4, with the probability of, respectively, 0.03, and 0.05 are less probable events. After training the models, the standalone generator is supplied with K=1000 noise vectors, accompanied by the desired class labels, to create suitable wind mean deviation scenarios in the form of time trajectories. To thoroughly evaluate the method, a large number of samples—specifically, 5,000 samples—are generated, with K=1000 samples allocated to each class. This extensive sampling ensures a comprehensive assessment of the method's performance. Subsequently, an

out-of-sample analysis is conducted on the 75,650 instances derived from 1,513 hours of wind data in the test set. This analysis helps to validate the effectiveness of the generated scenarios and the overall approach for modeling wind data.

5.4.1 Evaluation of the Proposed Scenario Generation Model

Although the evaluation of GAN-based models with image output is rather straightforward, their evaluation for non-image data is still an open topic [84]. Therefore, various similarity and statistical metrics, based on specific applications, are employed in the literature to assess the performance of time-series generative models. In this study, first, Wasserstein distance (5.12), *WD*, between the probability distributions of the generated and test set instances of wind trajectories, for each label, is calculated. This measure compares the overall variability of the synthesized and actual wind time-series (in the test set). Then, the root-mean-square error (RMSE) of the generated and test sets are computed. The RMSE between two temporal sequences, g and $\hat{g}$, is defined as follows:

$$\text{RMSE} = \sqrt{|\Delta|^{-1} \sum_{\delta \in \Delta} (g[\delta] - \hat{g}[\delta])^2} \tag{5.20}$$

Finally, dynamic time-warping (DTW), a well-known time-series similarity metric, is also used to analyze the similarity of time-series in the generated and test sets with respect to the optimal alignment of time warps [85]. Let's $d_{i,j} = \|g[i] - \hat{g}[j]\|,\ i,j \in \Delta$ be the local cost of alignment between the i^{th} element of g and the j^{th} element of $\hat{g}$. A warping path $\langle W = \langle w_1, \dots, w_L \rangle \mid L \in [|\Delta|, 2|\Delta| + 1] \rangle$, encodes a global alignment between the two time-series, g and $\hat{g}$, by defining a sequence of L pairs $w_l = (i,j)$,

which assign element i of g to element j of $\hat{g}$. The DTW distance between two time-series is the total cost of alignment for the optimal (i.e., minimum cost) warping path:

$$\mathrm{DTW}[g,\hat{g}] = \min_{W} \sum_{l=1}^{L} \tilde{d}_l \qquad W = \langle w_1, \ldots, w_L \rangle \tag{5.21}$$

where $\tilde{d}_l = d_{i,j}$ is the local alignment cost encoded by the l^{th} pair $w_l = (i,j)$ of the warping path W.

DTW and RMSE are conventionally used to evaluate the quality of the generated signals in GAN models [85]. Two real wind trajectories are randomly chosen from the test dataset as shown by black lines in the first and second columns of Figure 5.3. Then, after generating a set of wind trajectories by using ACWGAN, CWGAN, and CGAN, the most similar synthesized wind time-series based on RMSE and DTW metrics are found. The actual wind time-series in the first and the second columns are used to obtain the most similar synthesized sample with respect to RMSE and DTW metrics, respectively. The obtained synthesized trajectories using ACWGAN, CWGAN, and CGAN regarding RMSE metric are, respectively, shown in Figure 5.3(a), (c), and (e) by dashed blue lines. Also, the dashed blue lines in Figure 5.3(b), (d), and (f) correspond to the obtained trajectories using ACWGAN, CWGAN, and CGAN regarding DTW, respectively. It is seen that while the synthesized samples in the right column emphasize the static time alignment, the ones in the left column relax this assumption by using dynamic time alignment. Additionally, the corresponding generated trajectories using ACWGAN, as shown in Figure 5.3(a)-(b), are visually similar to the ones belonging to the real dataset for both RMSE and DTW metrics. On the other hand, the generated samples using CWGAN are visually less similar to the ones belonging to the real dataset, compared with the generated samples by ACWGAN, regarding

both similarity metrics. Also, the obtained samples by CGAN even look farther than their corresponding real samples compared with the ones obtained by ACWGAN and CWGAN. In particular, the RMSE between the real signals (first column) and the generated signals by ACWGAN, CWGAN, and CGAN are 0.47, 0.63, 0.75, respectively. Also, the DTW between the real signals (second column) and the generated signals by ACWGAN, CWGAN, and CGAN are 21.70, 28.62, 30.17, respectively. Nevertheless, DTW and RMSE merely find the distance of two temporal sequences, which are used for qualitative visual assessment in Figure 5.3. Thus, it is required to obtain representative scores based on these metrics for the whole generated scenarios on the test dataset. For this purpose, a brute-force search on the synthesized and test sets is performed to find the most similar time-series based on the desired metric. Then, the average of the obtained cost values, i.e., RMSE and DTW, of the corresponding similar signals in real and generated datasets are considered to obtain the representative RMSE and DTW distance of two sets. The acquired results for the mentioned evaluation metrics on the whole datasets are recorded in tuples (WD, RMSE, and DTW) in Table 5.2. The performance of each presented method should be compared with other methods for each class label individually.

It is seen that CGAN has poor performance compared with the conditional Wasserstein-based GAN models regarding all measures. Moreover, compared with CWGAN, the performance of the proposed ACWGAN is considerably better. For instance, as seen in the 4^{th} row of Table 5.2, i.e., C_3, the WD, RMSE, and DTW of ACWGAN are 1.89, 1.55, 1.30 times lower than those of the CWGAN method. The ACWGAN model is further compared with the benchmark models in terms of classification performance. For this purpose, the 5000 generated samples, i.e., 1000

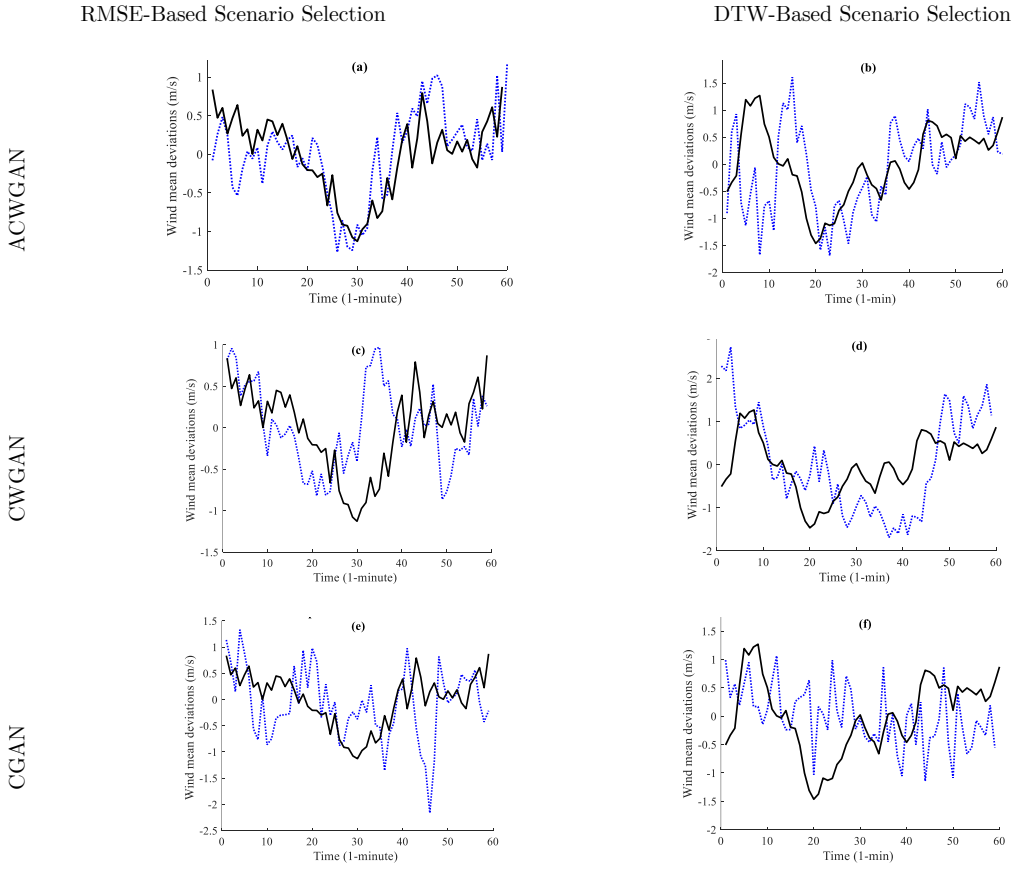

Figure 5.3) Generated wind mean deviation time-series versus the actual time-series. The first and second columns correspond to the scenarios selected based on RMSE and DTW metrics, respectively.

samples for each class, are analysed ex-post in order to obtain their confusion matrix, as shown in Figure 5.4. The predicted classes are color-coded in this figure.

The horizontal axis shows the true class labels. Hence, each bar segment in a given stacked bar indicates the percentage of predicted classes for each true class label. It is graphically seen that CGAN has poor performance compared to the Wasserstein-based models for C0, C1, C2, and C3. However, its performance regarding generating wind time-series with class

label C4 is better than the Wasserstein-based models. Its reason can be described as below. Notably, C4 has a much wider interval [2, Smax] compared to other classes (3 m.s-1 vs. 0.5 m.s-1). Meanwhile, the deviation levels of wind time-series belonging to C4 in the real dataset are mostly concentrated toward the beginning, and middle of this interval. On the other hand, the deviation levels of the generated time-series by CGAN are mostly concentrated on the right tail of C4 interval (higher deviation level). Thus, although the classification accuracy of CGAN regarding C4 seems to be improved, as the deviation levels still fall in this wide interval, they do not maintain the quality of the real wind signals of this class. This can be further confirmed by the poor results of CGAN regarding C4, with respect to the similarity metrics, as reported in Table 5.2. Therefore, when comparing the performance of these approaches, one should be careful to look at classification accuracy and similarity metrics together. Interestingly, it is seen that by leveraging an auxiliary classifier, the classification performance of ACWGAN is significantly improved for all class labels compared to CWGAN. In particular, the accuracy of ACWGAN is 0.8%, 27.4%, 30.5%, 24.3%, and 8.2% higher than CWGAN for class labels C_0, C_1, C_2, C_3, and C_4 in Figure 5.4, respectively.

5.4.2 Advantages of the Proposed WPP Scheduling Model

The obtained results of the classic and proposed WPP energy and reserve scheduling frameworks are summarized in Table 5.3. The WPP's bidding performance with respect to three upper bounds on reserve unavailability risk, $\rho^{o} = \{0\%, 20\%, 40\%\}$, defined by TSO, for both classic and proposed frameworks is detailed. The comparative results are presented for very low, C_o, and high, C_4, wind fluctuation levels in Table 5.3. The in-sample results, including the submitted energy bid P^{Eo} and reserve bid P^{Ro}

to the market as well as the expected revenues from energy $\mathcal{R}^E$ and reserve $\mathcal{R}^R$, are provided in Table 5.3. Moreover, the out-of-sample results regarding the real-time risk of reserve unavailability $\tilde{r}$, and revenues from energy $\tilde{\mathcal{R}}^E$ and reserve $\tilde{\mathcal{R}}^R$ are shown in Table 5.3. The last column details the normalized total profit deviation, and risk of reserve unavailability deviation, which are calculated, respectively, by (5.22) and (5.23):

$$\overline{\Delta\mathcal{R}}\% = \frac{\left(\tilde{\mathcal{R}}^E + \tilde{\mathcal{R}}^R\right) - \left(\mathcal{R}^E + \mathcal{R}^R\right)}{\left(\mathcal{R}^E + \mathcal{R}^R\right)} \times 100\% \tag{5.22}$$

$$\overline{\Delta r}\% = \tilde{r} - r \tag{5.23}$$

where r is the expected risk of reserve unavailability and dropped from Table 5.3 for the sake of brevity. However, in the case of the experiment with the proposed framework on $\rho^{\mathrm{o}} = 40\%$, the expected risk r is 39.53% and 31.45% regarding C_0 and C_4, respectively. It means that the WPP takes a risk lower than the one allowed by the TSO, ρ^{o}, in order to avoid the negative penalties associated with reserve unavailability. For the other experiments, the values of r and ρ^{o} are identical. As seen in Table 5.3, the in-sample results of the classic bidding model are invariable to the wind deviation levels, i.e., C0 and C4.

Table 5.2) Comparison of the proposed scenario generation approach with the other GAN-based techniques

Method / **Class**	**CGAN**	**CWGAN**	**ACWGAN**
C_0	(0.14, 0.24, 18.20)	(0.04, 0.11, 9.33)	(0.04, 0.10, 8.95)
C_1	(0.07, 0.43, 23.97)	(0.05, 0.37, 17.19)	(0.05, 0.31, 16.84)
C_2	(0.15, 1.44, 42.94)	(0.07, 0.95, 30.22)	(0.06, 0.89, 28.75)
C_3	(0.17, 3.64, 67.17)	(0.17, 2.73, 49.52)	(0.09, 1.76, 38.22)
C_4	(0.96, 12.61,138.50)	(0.20, 3.87, 57.64)	(0.13, 3.31, 55.22)

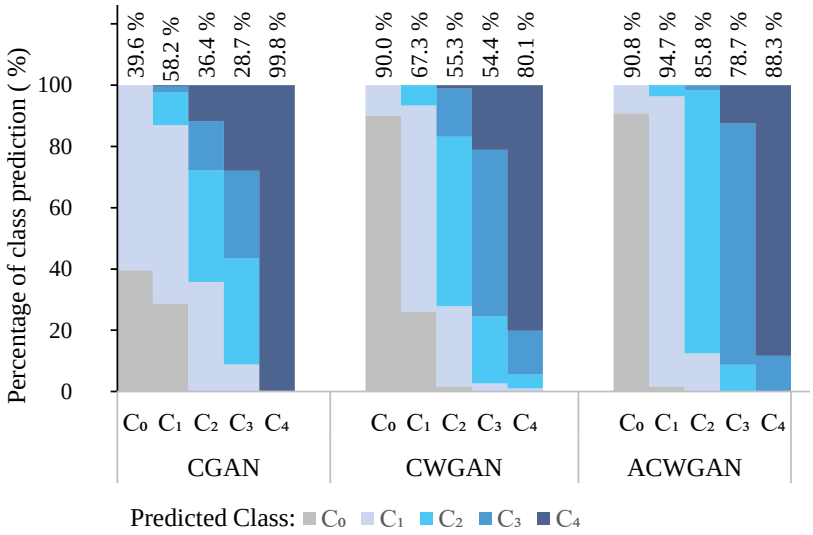

Figure 5.4) Confusion matrix of CGAN, CWGAN, and ACWGAN regarding class labels C_0, C_1, C_2, C_3, and C_4

Its reason is that the classic model merely receives hourly wind uncertainty as input. However, the decisions are different concerning the allowed risk level. On the other hand, the proposed bidding framework returns different

and relevant decisions based on both the wind deviation level and the upper bound of the risk level. For both models, as the permitted risk increases, a higher bid is submitted to the reserve market floor, whereas a lower bid is devoted to the energy market floor. That arises from the fact that the incentives for reserve procurement are more encouraging for the WPP in the presented market setting (see Table 5.1).

Interestingly, it can be observed that $\overline{\Delta r}\%$ for the proposed framework is very small, i.e., its out-of-sample risk result is close to the expected risk level. On the other hand, the classic method fails to stay reasonably close to the expected risk level. In particular, the maximum risk deviation for the proposed method is -0.4%, whereas for the classic method is 35.15%.

Table 5.3) The in- and out-of-sample results of the proposed and classic bidding approaches for different risk thresholds and wind deviation classes.

			In-sample				Out-of-sample			Evaluation	
	ρ^o [%]	Method	P^{Eo} [MW]	P^{Ro} [MW]	$\mathcal{R}^E$ [€]	$\mathcal{R}^R$ [€]	$\tilde{r}$ [%]	$\tilde{\mathcal{R}}^E$ [€]	$\tilde{\mathcal{R}}^R$ [€]	$\overline{\Delta\mathcal{R}}$ [%]	$\overline{\Delta r}$ [%]
C_o	0	Classic	0.54	1.42	27.84	49.79	10.22	28.83	49.18	0.49	10.22
		Proposed	**1.28**	**0.71**	**51.87**	**24.89**	**0.00**	**51.77**	**24.89**	**-0.13**	**0.00**
	20	Classic	0.13	1.96	13.94	64.34	35.84	15.31	63.26	0.37	15.84
		Proposed	**0.46**	**1.65**	**22.88**	**55.54**	**19.71**	**22.70**	**55.62**	**-0.13**	**-0.29**
	40	Classic	0.00	2.09	11.51	66.82	43.91	12.77	65.75	0.24	3.91
		Proposed	**0.14**	**2.02**	**14.35**	**64.31**	**39.54**	**14.12**	**64.45**	**-0.11**	**0.01**
C_4	0	Classic	0.54	1.42	27.84	49.79	35.15	40.95	40.71	5.19	35.15
		Proposed	**2.33**	**0.00**	**81.30**	**0.00**	**0.00**	**80.95**	**0.00**	**-0.43**	**0.00**
	20	Classic	0.13	1.96	13.94	64.34	47.89	30.43	50.54	3.44	27.89
		Proposed	**1.55**	**0.88**	**54.91**	**27.70**	**19.64**	**54.56**	**27.66**	**-0.47**	**-0.36**
	40	Classic	0.00	2.09	11.51	66.82	50.18	28.10	52.55	2.96	10.18
		Proposed	**1.26**	**1.27**	**45.37**	**37.39**	**31.05**	**44.96**	**37.42**	**-0.46**	**-0.40**

The same pattern applies to real-time profit deviation $\overline{\Delta\mathcal{R}}\%$ as shown in Table 5.3. Notably, using the proposed bidding framework, the WPP does not bid any power quantity to the reserve market while the ultra-short-term wind fluctuations are too high, C_4, and the allowed reserve unavailability risk threshold is zero $\rho^o = 0$. In contrast, the classic model, by neglecting the ultra-short-term wind fluctuations, submit a rather high-power bid, $P^{Ro} = 1.42\ \text{MW}$, to the reserve market floor. Accordingly, the classic model is unable to maintain the real-time reserve reliability leading to $\overline{\Delta r} = 35.15\%$.

Similarly, the WPP's bidding behavior with the non-binding reserve unavailability risk constraint in both models can be interpreted from Table 5.3. When the upper risk bound of reserve unavailability is sufficiently high (40% in this study), (5.11) becomes non-binding. Thus, both models bid in such a way that the trade-off between the day-ahead revenue and the real-time penalty is profitable regardless of the confidence level of reserve availability. The values regarding the wind power bidding, with reserve unavailability risk constraint non-binding, are underlined in Table 5.3. It is seen that when the wind deviation level is low, C_0, the classic model obtains the expected total profit of 78.33 €, corresponding to $\mathcal{R}^E + \mathcal{R}^R$, and 78.52 € for the out-of-sample analysis. Also, the proposed framework yields a slightly higher profit of 78.66 € and 78.57 € concerning the in- and out-of-sample analysis, respectively. In addition, for high wind fluctuation level, C_4, the advantage of using the proposed method is more significant. The classic method obtains 78.33 € and 80.65 € regarding the in- and out-of-sample analysis, whereas the proposed framework attains a higher profit of 82.76 € and 82.38 € for the in- and out-of-sample analysis, i.e., 2.1% higher in the ex-post analysis.

Remarkably, by removing the probabilistic constraint (5.11), the proposed framework loses the reserve provision confidence, which has the probability of 1-39.54% = 60.46% and 1-31.05% = 68.95% regarding C_o and C_4 classes, respectively. The classic model has lower reserve provision confidence levels of 1-43.91%= 56.09% and 1-50.18%= 49.82% regarding C_o and C_4, respectively, which are similarly lost when (5.11) is removed. In this case, in both models, the TSO is not aware of the probability of the real-time reserve unavailability. However, by requiring the WPPs to fulfill a confidence level regarding the offered capacity, the proposed framework is able to respect the defined upper risk bound, as seen from $\tilde{r}$ results in Table 5.3. On the other hand, the classic model does not have this capability as seen from its $\tilde{r}$ results in Table 5.3.

Thus, adopting a risk metric regarding reserve unavailability in the proposed WPP multi-resolution probabilistic bidding framework enables the TSO to have reliable insight on the real-time wind power share in reserve provision.

Meanwhile, the proposed multi-resolution bidding framework solves, for an hourly period and a single risk threshold, between 0.07 to 3.94 seconds on a DELL hardware set with Intel Core i7 CPU 2.6 GHz and 16 GB of RAM. This is a low computation time on a simple hardware set.

5.4.3 Advantage of Exploiting ACWGAN in WPP Bidding Framework

In this section, the superiority of employing ACWGAN in the proposed bidding framework, in comparison with other scenario representation methods, is illustrated. Reserve unavailability risk deviation $\overline{\Delta r}\%$ and normalized profit deviation $\overline{\Delta \mathcal{R}}\%$ are used as evaluation metrics and are illustrated in Figure 5.5(a) and 5.5(b), respectively. The horizontal

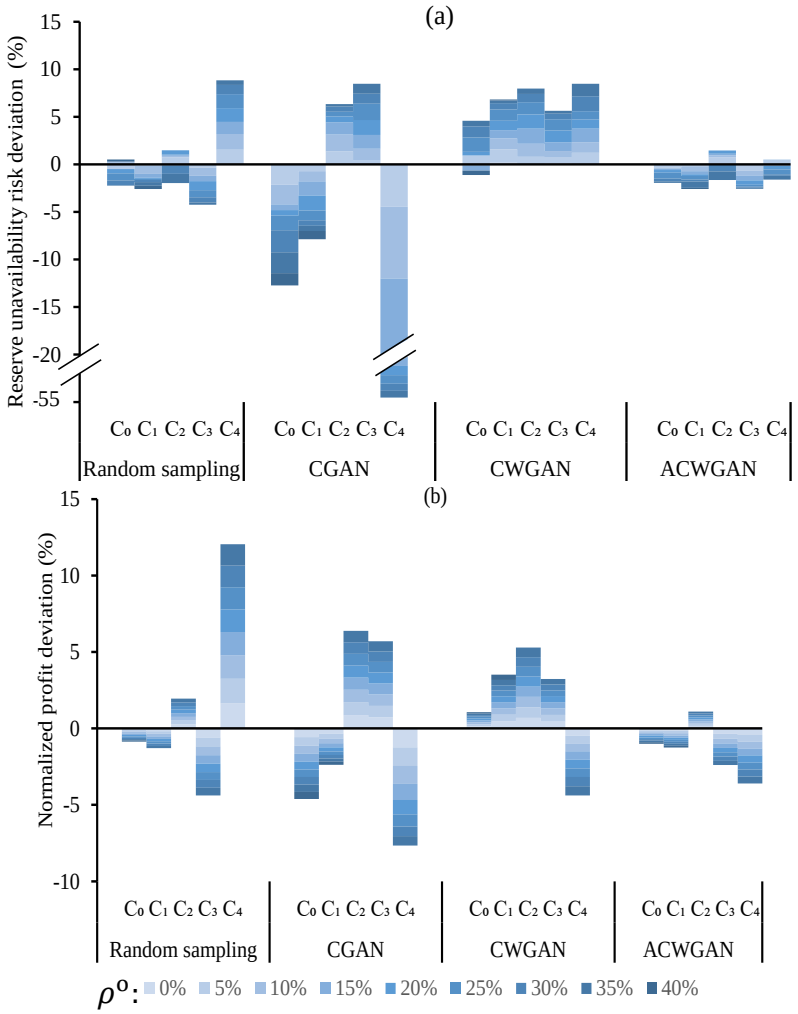

Figure 5.5) Comparison of the proposed ACWGAN scenario generation method with direct sampling, CGAN, and CWGAN using the proposed WPP multi-resolution probabilistic bidding approach based on (a) reserve unavailability risk deviation metric (b) normalized profit

categorical axis shows 5 class labels regarding the wind mean deviation levels, C_0 to C_4, and four scenario generation schemes.

The benchmark scenario generation methods presented for comparison with the proposed ACWGAN approach include direct random sampling from the training set, CGAN, and CWGAN. The vertical axis in Figure 5.5(a) and 5.5(b) corresponds to $\overline{\Delta r}\%$ and $\overline{\Delta \mathcal{R}}\%$, respectively. Each bar segment within

a stacked bar represents the value of the evaluation metric ($\overline{\Delta r}\%$ or $\overline{\Delta \mathcal{R}}\%$), regarding the allowed reserve unavailability risk threshold $\rho^{\mathbf{o}}$. It should be noted that a smaller magnitude of each stacked bar, regardless of its direction, corresponds to a better-performing approach. In this study, a fine resolution, i.e., 5%, concerning the allowed risk bound from 0 to 40% is considered.

As seen in Figure 5.5(a), direct sampling from the training set obtains a lower deviation regarding reserve unavailability risk for all wind fluctuation levels, C_0 to C_4, compared to CGAN. This observation can be explained considering that CGAN has a poor performance regarding the statistical and similarity metrics as well as classification accuracy.

Performance of the CWGAN regarding $\overline{\Delta r}\%$ is better than CGAN for all wind deviation levels while is nonetheless worse than the direct sampling method concerning C_0, C_1, C_2, and C_3. However, it can be seen that the CWGAN yields a lower deviation compared to the direct sampling approach for C_4 and almost a similar deviation concerning C_3. That is because these are less-probable classes in the training set. Thus, since enough samples are not available, direct sampling cannot provide a good approximation to represent the wind deviation uncertainty for these classes. Besides, CGAN does not perform well for the less-probable classes as it is known to suffer from mode collapse. Remarkably, it is seen that the ACWGAN scenario generation method outperforms other GAN-based and direct sampling methods regarding reserve unavailability risk deviation in all classes.

Regarding the normalized profit deviation, as shown in Figure 5.5(b), direct sampling performs better than CGAN for wind deviation levels C_0 to C_3. On the other hand, CWGAN performs better than CGAN for C_0, C_2, C_3, C_4 and is very close to CGAN in the case of C_1. Specifically, regarding less-probable classes, CWGAN performs significantly better than direct

sampling and CGAN. Finally, ACWGAN outperforms direct sampling and the other GAN-based scenario generation schemes since the magnitude of its stacked bar corresponding to each class label is lower than the other alternatives.

5.5 Discussion and Conclusion

Participation of wind power producers in the energy and reserve market requires designing dedicated decision models that consider the stochastic process of the wind at both low and high temporal resolutions. Accordingly, an efficient scenario generation model based on the auxiliary classifier Wasserstein GAN is firstly proposed to produce the wind mean deviation scenarios regarding the ultra-short-term wind uncertainty. The superiority of the proposed scenario generation technique over the conditional GAN and its Wasserstein-based counterpart using statistical and similarity metrics is illustrated. Then, a multi-resolution probabilistic WPP bidding framework, comprising a novel probabilistic constraint, regarding the reliability of the reserve bids, and the proposed ultra-short-term scenario generation approach, is devised. It is shown that compared to the outcomes of the single-resolution model, the profit loss and reserve reliability are significantly improved by the proposed data-driven WPP decision-making framework. Finally, the significance of the devised modules in the proposed framework is shown by comparing deviations from the expected revenue and reserve unavailability risk with the results obtained by other scenario generation alternatives.

5.6 Related Publication

S. A. Hosseini, J.-F. Toubeau, Z. De Grève, Y. Wang, N. Amjady and F. Vallée, "Data-Driven Multi-Resolution Probabilistic Energy and Reserve Bidding of Wind Power," *in IEEE Transactions on Power Systems,* vol. 38, no. 1, pp. 85-99, Jan. 2023, 10.1109/TPWRS.2022.3155865.

Chapter 6. Wind Fluctuations in Bidding: Temporal Distribution Forecasting

6.1 Introduction

Although scenario generation methods provide insights into possible uncertain outcomes, they have several limitations that should be considered. These limitations include an incomplete representation of uncertainty and a lack of reflection of true probability distributions, which can result in ex-post over or underconfidence. Additionally, some scenario generation techniques, such as the one presented in Chapter 5, have difficulty in capturing time-dependent relationships between successive periods of generated scenarios. This is because it is typically trained on large amounts of data without considering inter-sample temporal relationships. Nonetheless, traditional forecasting models can effectively capture time dependencies, but they are not well-suited for predicting wind variability with high temporal resolution over the day-ahead horizon. To highlight the targeted research gap, in this chapter, a detailed overview of the state-of-the-art Wind Power Forecasting (WPF) models is given in the following.

Several deterministic and probabilistic models for WPF have been proposed in various studies. In [86], a WPF framework combining empirical mode decomposition and deep learning with ℓ_1 and ℓ_2 norms for 24 to 48 hours ahead with a time scale of 1 hour is presented. [87] proposes a multi-

to-multi-mapping network using a stacked denoising autoencoder trained with modified cross-entropy for 24-72 hours ahead for WPF with a time scale of 10 minutes. [88] uses a numerical weather prediction and neural network for 4-hour WPF with a time scale of 15 minutes and minimizes the pointwise error. [89] presents a deterministic hierarchical WPF with optimal tuning using ℓ_2 norm losses for 10 to 60 minutes with a 10-minute time scale. [90] proposes a temporal convolutional network for ultra-short-term WPF trained by ℓ_1 norm for point forecasts and a probabilistic approach using quantile losses. [91] proposes a kernel density estimation method for 36-hour WPF with a 1-hour resolution. [92] uses variational recurrent autoencoders with a log-likelihood loss for 48-hour WPF with a 1-hour time scale. [93] uses a sparse vector autoregression method with maximum likelihood and Bayesian information criterion for very short-term probabilistic WPF with a time scale of 5 minutes and one step ahead.

Two main observations are made in the aforementioned studies. First, WPF models are capable of predicting multiple time steps with some temporal resolution. However, the forecast horizon to forecast step (timescale) ratio is usually limited in the previous works, as its high values can have negative impacts on the model's performance. This is due to the accumulation of errors in recursive multi-step approaches or complications in model selection and tuning in direct multi-step approaches [94], also known as the curse of dimensionality [95]. Notably, to the best of the authors' knowledge, the largest forecast horizon to timescale ratio in the literature is 72h$\times$60 min/10 min=432 in [87]. Nevertheless, for some applications (such as wind power reserve scheduling), it is relevant to obtain complementary information regarding wind variation with high temporal granularity (e.g., second-wise) while predicting at day-ahead horizon [96]. This is because neglecting intra-period variability leads to high opportunity losses for a WPP participating in the reserve market since settlement

periods at the balancing stage are typically much shorter than market periods (e.g., from minutes to seconds) [19], [96]. In this case, WPF with a 36-hour horizon (from 12:00 in the day-ahead to 24:00 of the next day) and a second-wise timescale leads to a forecast horizon to timescale ratio of 36h$\times$3600s/1s=129600.

Secondly, the reviewed models use either point forecasts or variants of probabilistic forecasts. The point forecast predicts the mean value of wind power for the next periods. The most frequently used loss for these approaches is the ℓ-norm, which determines the pointwise distance between the actual and predicted values. The probabilistic approach, on the other hand, provides probability information around the expected value, i.e., the mean value in the point forecast. Common losses for these approaches include quantile loss and maximum likelihood estimation, which are also based on the pointwise operation. None of these methods provides complementary information regarding intra-period wind variations with high temporal granularity (e.g., the second-wise timescale for day-ahead WPF).

This chapter focuses on Day-ahead WPF (DWPF) which is an instance of forecasting on a short-term horizon [97]. We enrich the traditional DWPF problem to acquire additional information regarding intra-period wind variations with high temporal granularity. To this end, while using a multistep DWPF model within the day-ahead horizon, the high-dimensional intra-period information is translated into a temporal distribution representing a concise space. Notably, the predicted temporal distribution provides valuable information on the volatility within the time periods of interest, which differs from the traditional probabilistic forecasts that are only able to quantify the uncertainty around the mean value.

The main challenge in accomplishing this task is to develop an effective loss that is capable of comparing temporal distributions. We first tailor various classical loss functions, i.e., a parametric loss as well as entropy-based ones, to the proposed DWPF, in order to investigate their effectiveness. The parametric loss function trains a neural network to estimate the Weibull distribution parameters for each day-ahead period. The entropy-based losses, including cross-entropy (CE), forward/reverse Kullback-Leibler divergence (FKL/RKL), and Jensen–Shannon divergence (JSD), are frequently used in classifications [98], variational autoencoders [99], and generative models [96], respectively. Although these classical losses are suitable to deal with certain distributions (e.g., one-hot encoded distribution for classification tasks using CE), we note some limitations when dealing with temporal distributions.

Wasserstein Distance (WD) is an effective measure for comparing distribution functions. This work proposes a DWPF that uses a special form of WD, which can be computed using a closed-form equation for univariate distributions. However, this equation requires extensive samples and a non-differentiable sorting operator. To address these challenges, the proposed mapping reduces the model's output dimension and enables differentiable tensor operations for end-to-end gradient learning.

The obtained distributions by the proposed DWPF model can indeed help decision-makers take better-informed decisions when wind variability at high-resolution matters. For instance, the proposed high-resolution wind forecasting model can significantly improve reserve sizing decisions in power systems. By using the model's detailed forecasts, TSOs can optimize their decisions regarding the reserve capacity needed to procure in day-ahead markets. As a result, they avoid both over-procurement, which leads to higher operational costs, and under-procurement, which can compromise system reliability.

Another instance where the proposed model can be particularly useful is for wind power portfolios participating in energy and reserve markets. In general, TSOs expect stable availability of the scheduled reserve powers in real-time. Therefore, WPP should be aware of wind variability on very-short timescales (e.g., seconds) to avoid penalties related to real-time deviations in the balancing stage. The high-resolution wind variability forecasts provided by the DWPF model enable WPPs to better predict and manage these deviations, ensuring that their energy and reserve commitments are met, while minimizing the risk of penalties. In particular, through an extensive analysis of real-world market data, the added value of employing the proposed WD loss is demonstrated by presenting a wind power trading framework in the energy and reserve market in Section 6.4.

The structure of the remaining chapter is as follows: Section 6.2 formulates the DWPF problem with temporal distribution. Section 6.3, first, explains the adaptation of the classical ML losses to the problem at hand and then introduces a WD-based loss that addresses the limitations of the classical losses. A dedicated bidding framework that directly employs the predicted distributions as input, is presented in Section 6.4. Numerical results are presented in Section 6.5, and the chapter is concluded in Section 6.6. The material presented in this chapter is predominantly sourced from the author's submitted paper, as referenced in last Section (Related publication).

6.2 Proposed DWPF Model

In a deep-learning-based prediction problem, a model Q_κ, with trainable parameters κ, is constructed using the available data up to the forecast origin T to predict a random variable (e.g., wind power production in DWPF). Specifically, the constructed model Q_κ aims to predict the random

variable for the lead-time $\mathrm{T}+\mathrm{h}$, i.e., $\hat{y}_{\mathrm{T+h|T}}$. The DWPF model uses a set of input features $\Psi_{\mathrm{T+h|T}}$ such as power measurements and explanatory variables to predict $\hat{y}_{\mathrm{T+h|T}}$. The input features $\Psi_{\mathrm{T+h|T}}$ are determined manually or by a feature selection technique, denoted as FS, using the dataset up to T and their predictions up to $\mathrm{T}+\mathrm{h}$, denoted as $X_{1:\mathrm{T}}$ and $\hat{X}_{\mathrm{T+1:T+h}}$, respectively. Notably, $\Psi_{\mathrm{T+h|T}}$ is then mapped to intermediate features via the hidden layers of Q_κ. A DWPF model can be stated as follows:

$$
\begin{aligned}
&Q_\kappa: \mathbb{R}^{\mathrm{I}} \rightarrow \mathbb{R}^{\mathrm{o}} \\
&\Psi_{\mathrm{T+h|T}} = FS\left(X_{1:\mathrm{T}}, \hat{X}_{\mathrm{T+1:T+h}}\right) \qquad \forall\, \mathrm{h} \in \{1, \ldots, \mathrm{H}\} \qquad (6.1) \\
&\hat{y}_{\mathrm{T+h|T}} = Q_\kappa\left(\Psi_{\mathrm{T+h|T}}\right)
\end{aligned}
$$

where $\mathbb{R}^{\mathrm{I}}$ and $\mathbb{R}^{\mathrm{o}}$, respectively, indicate the dimensions of the inputs $\Psi_{\mathrm{T+h|T}}$ and the outputs $\hat{y}_{\mathrm{T+h|T}}$ of the forecast model. H is the forecast horizon. Typically, in European electricity markets (e.g., in Belgium), participants should submit their bids for the 24 hours of day-ahead market for day *d*, spanning from 00:00 to 24:00, before the market closure time of day *d-1*, e.g., at 12:00 [100]. Therefore, H for the DWPF problem becomes 36 hours, including the second half of day *d-1* and day *d*. In (6.1), assuming that second-wise information regarding forecasting period $\mathrm{T}+\mathrm{h}$ is desired, the output dimension of the model is drastically expanded by 3600 times, $\hat{y}_{\mathrm{T+h|T}} \in \mathbb{R}^{3600\times \mathrm{o}}$. This leads to error accumulation and model complexity. For this reason, conventional DWPFs map all intra-period variability onto one or a few dimensions (which only provide information regarding the mean or uncertainty around the mean using point or probabilistic forecast models, respectively). However, the high-dimensional intra-period information can be mapped to a more informative and low-dimensional space to facilitate the learning task of the neural network. Temporal distributions can serve as translatable target mapping to reduce dimensions

while preserving valuable intra-period variability information.

The output representation of the DWPF model, using real wind data, with a horizon of 36 hours is shown in Figure 6.1. The output dimension of each period for a conventional point forecaster without considering intra-period variability is one (black dots), while considering intra-period variability is 3600 (black trajectories). This means that predicting the second-wise intra-period variability with a classical point forecaster with a timescale of one second requires a horizon to timescale ratio of $36 \times 3600 = 129600$, which is impractical. However, by predicting the temporal distribution of intra-period variability (blue surface), the output dimension of the DWPF model can be effectively reduced, as explained in more detail below.

The proposed DWPF trains Q_κ to map the input features $\Psi_{T+h|T}$ to the actual temporal distribution object of wind power for lead-time $T + h$, Y_{T+h}. The actual and predicted distribution objects, $Y_{T+h|T}$ and $\widehat{Y}_{T+h|T}$, are, respectively, characterized by $y_{T+h|T}$ and $\hat{y}_{T+h|T}$ as the target and output of Q_κ. $y_{T+h|T}$ and $\hat{y}_{T+h|T}$ can be parameters of a predefined parametric distribution (e.g., Weibull) or a quantized version of a non- parametric distribution, i.e., the so-called histogram. Notably, histograms are obtained by counting the relative frequency, R.F., of the data within an ordered set of non-overlapping and ascending intervals (so-called bins, i.e., $b \in \mathcal{B}$).

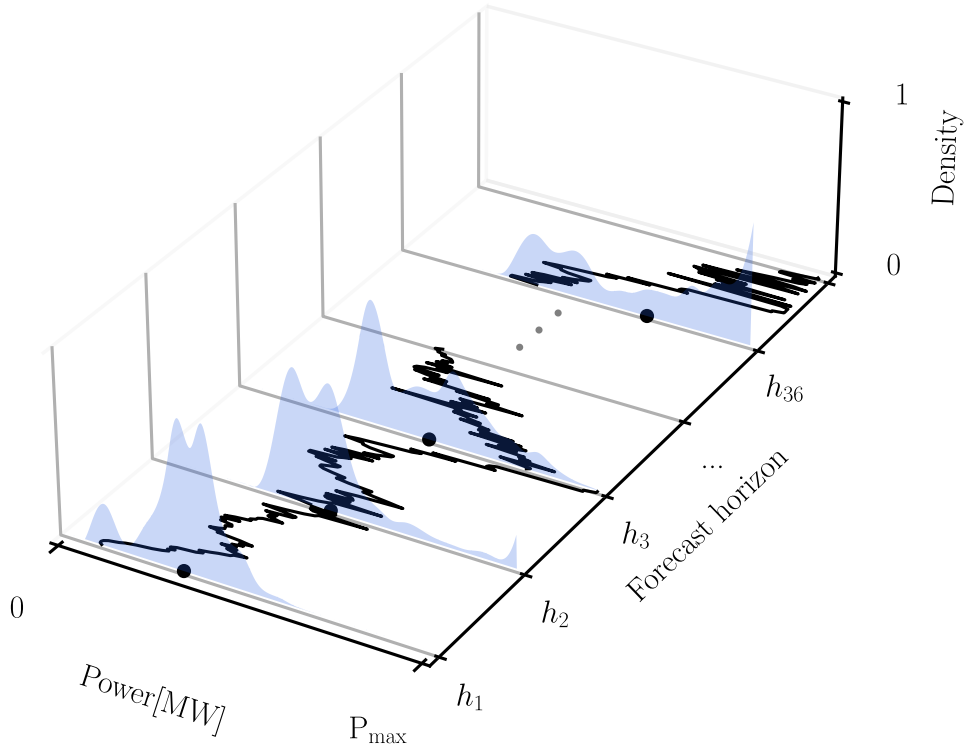

Figure 6.1) The output representation of DWPF model. The black trajectories show intra-period wind variability while the black dots show the mean prediction for each period. The blue surfaces represent the intra-period wind distribution.

In the proposed model, Q_κ takes the wind power histogram of previous periods, temperature, and timestamp along with predictions of temperature and hourly mean wind speed of the target period as input. It should be noted that the bin resolution for input and output are not necessarily the same. The input bin resolution is derived from the feature engineering, while the resolution of the output bin is determined based on the desired accuracy. Consequently, in the inference phase, to obtain predictions over the day-ahead horizon, the predicted distributions are mapped to a compatible dimension with respect to the input bin resolution.

6.3 Tailored Distribution-Based Losses

A deep-learning model is trained through an optimization algorithm

(e.g., gradient descent) by minimizing a loss function $\mathcal{L}: \mathbb{R}^{o} \rightarrow \mathbb{R}$ that measures the error between the ground truth and the predictions. The prevalent loss functions for DWPF, as discussed in Section 6.1, are not suitable for the proposed problem (see Section 6.2), since we are dealing with distributions. A distribution-based loss should compare distributions and return a meaningful error, which provides useful gradient information for training Q_{κ}. The literature on distribution-based losses is limited to parametric and entropy-based losses used for specific ML tasks, such as classification problems. Therefore, in this section, we show how classical losses can be tailored to the proposed DWPF problem.

6.3.1 Parametric-Based Loss

This approach is based on an assumption that wind power variability follows a Weibull distribution, as a fairly accepted simplified approach [101]. A Weibull distribution, $\mathfrak{F}_x(a, \acute{a}) = a(x\acute{a}^{-1})^{a-1}\exp[-(x\acute{a}^{-1})^{a}]$, for a random variable x>0, is characterized by its scale a>0 and shape $\acute{a}$>0 parameters [101].

In this method, for each period t, a Weibull distribution is fitted to intra-period variations of wind power. The ground truth y_t encompasses the Weibull parameters for Y_t. The model Q_{κ} is trained with T samples to map the input features to y_t, and the mapping output is represented by $\hat{y}_t$. The parametric-based loss $\mathcal{L}_{\mathrm{WB}}$, for a single batch T', aims to minimize the distance between the ground truth and predicted parameters, as follows:

$$\min_{\kappa \in \mathrm{M}} \mathcal{L}_{\mathrm{WB}(y,\hat{y})} = |T'|^{-1} \sum_{t \in T'} \sum_{i \in \{1,2\}} \left| y_t^i - \hat{y}_t^i \right| \tag{6.2}$$

where $i = 1$ and $i = 2$ correspond to the scale and shape coefficients of the Weibull distributions. $\mathrm{M} = \{\kappa | \hat{y}_t^i > 0;\ t \in T', i \in \{1,2\}\}$ entails that the scale and shape coefficients satisfy the Weibull distribution definition. $\kappa \in \mathrm{M}$ is implemented by a ReLU layer [102] in the output of Q_κ. The model then forecasts the parameters associated with $\mathrm{Y_{T+h}}$, i.e., $\hat{y}_{\mathrm{T+h|T}}$. The prediction error in the inference phase can also be obtained by (6.2), without gradient calculation. Importantly, this loss suffers from a potential misrepresentation of the wind variability with a structured distribution (e.g., because of the limited number of parameters).

6.3.2 Cross-Entropy Loss

CE measures the discrepancy between a target distribution and its prediction. In particular, CE returns the average number of total bits required to represent an event using predicted distribution, $\hat{y}^b$, instead of the target distribution, y^b, by calculating $\mathrm{CE}(y, \hat{y}) = -\sum_{b \in \mathcal{B}} y^b \log \hat{y}^b$ (where b is the index of distribution's quantized support $\mathcal{B}$) [98].

The CE function implemented in most ML packages is adapted for classification problems where the target distribution has a special one-hot encoded form (i.e., one element in y, associated with the correct class, is one and zero elsewhere). Therefore, $\mathrm{CE}(y, \hat{y})$ for this special case is simplified to $-\log \hat{y}^{\bar{b}}$, where $\bar{b}$ is the index of the correct class. Moreover, during inference, the model's output is passed to an *argmax* operator to return the index of the element with the highest probability as the class prediction.

Remarkedly, this is not the case in our problem as we are interested in the temporal distribution over the entire support. In other words, in the presented problem, a relative frequency, regarding wind power variations, is assigned to each element of the distribution's support ($b \in \mathcal{B}$). The CE loss, $\mathcal{L}_{\mathrm{CE}}$, for the proposed DWPF problem is adjusted as follows:

$$\min_{\kappa \in N} \mathcal{L}_{\mathrm{CE}(y,\hat{y})} = -|T'|^{-1} \sum_{t \in T'} \sum_{b \in \mathcal{B}} y_t^b \log \hat{y}_t^b \tag{6.3}$$

where $|T'|$ is the batch size where its samples are indexed by t. $\mathrm{N} = \{\kappa | \sum_{b \in \mathcal{B}} \hat{y}_t^b = 1, \hat{y}_t^b \geq 0;\ t \in T', b \in \mathcal{B}\}$ constrains the output layer of Q_κ.

Note that $\kappa \in N$ ensures that the relative frequencies of wind power variations over the entire support sum up to unity and are non-negative. In practice, this constraint is modeled by a softmax layer [103] in order to normalize the output space and ensure the non-negativity of elements. This constraint is also used in Sections 6.3.3-6.3.5, since the output form is the same. Also, to avoid numerical instability due to $\log 0$, a small mass is added to zero-valued bins.

As Gibbs' inequality suggests [98], the smallest possible value for $\mathcal{L}_{CE}$ occurs when the learned and target distributions are equal, i.e., $\hat{y}_t^b = y_t^b : \forall\, t \in \acute{T}, \forall\, b \in \mathcal{B}$. Thus, by minimizing $\mathcal{L}_{\mathrm{CE}}$, Q_κ learns to map the input features to a distribution that approximates the target distribution. Notably, the prediction error during inference is obtained by (6.3) without gradient updating (unlike classification problems where *argmax* operator is used).

6.3.3 Kullback-Leibler Divergence Loss

Given two distributions y and $\hat{y}$, the FKL divergence between them, $\mathrm{KL}(y, \hat{y})$, measures the extra bits required to represent an event using $\hat{y}$, instead of y, by calculating $\sum_{b \in \mathcal{B}} y^b \log(y^b / \hat{y}^b)$ [99]. The function $\mathrm{KL}(y, \hat{y})$ reaches zero for $y^b = \hat{y}^b : \forall\, b \in \mathcal{B}$. The model's loss function for a single batch T' using $\mathrm{KL}(y, \hat{y})$ is as follows:

$$\min_{\kappa \in N} \mathcal{L}_{\mathrm{KL}(y,\hat{y})} = |T'|^{-1} \sum_{t \in T'} \sum_{b \in \mathcal{B}} y_t^b \log \frac{y_t^b}{\hat{y}_t^b} \tag{6.4}$$

where $\mathcal{L}_{\mathrm{KL}(y,\hat{y})}$ in (6.4) is the model's loss function that should be minimized.

It can be seen that the inner log term in (6.4) is weighted by y_t^b. This means that $\mathcal{L}_{\mathrm{KL}(y,\hat{y})}$ is not penalized when $\hat{y}$ assigns a mass on zero-valued bins of y. This leads to zero-avoiding behavior and thus wider coverage of the support [95].

In this context, it can be shown that minimizing the Kullback-Leibler divergence between the true distribution y and the predicted distribution $\hat{y}$ is equivalent to minimizing the cross-entropy loss between y and $\hat{y}$. This equivalence follows from a mathematical relationship between the two measures. To show this, consider $\mathrm{KL}(y,\hat{y}) = \sum_{b\in\mathcal{B}} y^b \log(y^b/\hat{y}^b)$. This term can be decomposed into the summation of $-\sum_{b\in\mathcal{B}} y^b \log \hat{y}^b$, and $\sum_{b\in\mathcal{B}} y^b \log \mathrm{y}^b$. The first term is $\mathrm{CE}(y,\hat{y})$ and the second term is $-\mathrm{CE}(y,y)$, which is the entropy of the actual data. Since the second term is fixed for the dataset, $\min \mathcal{L}_{\mathrm{KL}(y,\hat{y})}$ and $\min \mathcal{L}_{\mathrm{CE}(y,\hat{y})}$ lead to the same result.

Importantly, KL divergence is not a symmetric measure, and thus cannot be considered as a distance metric. By swapping y_t^b and $\hat{y}_t^b$ in (6.4), $\mathcal{L}_{\mathrm{KL}(\hat{y},y)}$, RKL loss can be obtained to train the model. In this case, the inner log term is weighted by $\hat{y}_t^b$. It means that $\mathcal{L}_{\mathrm{KL}(\hat{y},y)}$ is not penalized when $\hat{y}$ does not assign mass on modes of y, i.e., ignores some bins. This leads to zero-seeking behavior and a concentration only on some modes [95].

Additionally, for the KL score to be finite, it is necessary that the support of y and $\hat{y}$ overlaps. To ensure this condition, the same support quantization of y is used for $\hat{y}$. Also, a small mass is added to zero-valued bins to avoid infinity. Although numerical issues can be solved by this adjustment, still, the gradient of KL loss is not sensitive to the distance of non-overlapping distributions' supports, thereby limiting the efficiency of the model's learning process.

6.3.4 Jensen–Shannon Divergence Loss

The JSD of y and $\hat{y}$, $\mathrm{JS}(\hat{y}, y)$, is the average of $\mathrm{KL}(y, w)$ and $\mathrm{KL}(\hat{y}, w)$ scores, where $w = 0.5(\hat{y} + y)$ is a mixture distribution [95]. The model's loss function for a single batch using $\mathrm{JS}(y, \hat{y})$ is as follows:

$$\min_{\kappa \in N} \mathcal{L}_{\mathrm{JS}(y,\hat{y})} = 0.5|T'|^{-1} \sum_{t \in T'} [\mathrm{KL}(y_t, w_t) + \mathrm{KL}(\hat{y}_t, w_t)] \tag{6.5}$$

Contrary to the KL divergence, JSD is a symmetric measure and has the properties of distance metrics [95]. Moreover, JSD is bounded by [0, log 2]. The lower bound is obtained when distributions are identical $\hat{y} = y$. Also, unlike KL divergence, where an infinite score is returned for non-overlapping distributions, JSD returns a finite score, log 2, for this case. Although the boundedness of JSD is useful for some problems, e.g., GAN, it is a shortcoming for the problem at hand. Namely, when distributions are on non-overlapping supports, JSD returns a fixed score regardless of the horizontal distance between the distributions. Therefore, JSD loss does not provide a usable gradient to push the model's output toward the target distribution.

6.3.5 Proposed Wasserstein-Based Loss Function

Apart from the aforementioned problems of entropy-based losses, they share another common shortcoming. Namely, they all neglect the cross-bin correlation of the distributions since they compare each bin in isolation. Wasserstein distance loss addresses this limitation and other limitations mentioned earlier. First, WD does not require the distributions to have a predefined structure [104]. In addition, WD is symmetric and defined in metric space, thereby providing a useful gradient (even for non-overlapping

supports) [105]. It also accounts for the cross-bin dependence of the distributions [106]. Consider two distributions $\mathrm{Y}: Z \to \mathbb{R}^+$ and $\widehat{\mathrm{Y}}: \hat{Z} \to \mathbb{R}^+$, where both Z and $\hat{Z}$ are defined on $\mathbb{R}^n$. The objective is to find an optimal transport plan $\lambda^*: Z \to \hat{Z}$, in which the transport cost, i.e., $|a - \hat{a}|$; $(a, \hat{a}) \in Z \times \hat{Z}$, is the least among all transport plans. Accordingly, the WD definition is given by [107]:

$$\mathrm{W}\big(\mathrm{Y}, \widehat{\mathrm{Y}}\big) = \min_{\lambda \in \Lambda} \int_Z |\lambda(a) - a|\, \mathrm{Y}(a)\, da \tag{6.6}$$

where $W\big(\mathrm{Y}, \widehat{\mathrm{Y}}\big)$ is the WD. Λ denotes the set of all transport plans λ.

The standard WD definition in (6.6) is, by itself, an optimization problem. Hence, the absence of an analytical solution for (6.6) hinders its exact application in the ML context. Nevertheless, due to the uniqueness of a monotone increasing map for univariate distributions, i.e., $n = 1$, an explicit formulation can be obtained for $\mathrm{W}\big(\mathrm{Y}, \widehat{\mathrm{Y}}\big)$ [106]. Let, for a distribution Y, $\mathrm{C}_{\mathrm{Y}}(a) = \int_{-\infty}^{a} \mathrm{Y}(x)dx$ and $\mathrm{C}_{\mathrm{Y}}^{-1}(\alpha) = \inf\{a \in \mathbb{R}; \mathrm{C}_{\mathrm{Y}}(a) \geq \alpha\}$ be the cumulative density function and its generalized inverse, respectively. The unique transport plan, for univariant distributions, is obtained by $\lambda^* = \mathrm{C}_{\widehat{\mathrm{Y}}}^{-1} \circ \mathrm{C}_{\mathrm{Y}}$, where $\circ$ indicates the function composition operator [106]. Accordingly, by the change of variable, $\alpha = \mathrm{C}_{\mathrm{Y}}(a)$, the closed-form solution for WD is obtained by:

$$\begin{aligned} \mathrm{W}\big(\mathrm{Y}, \widehat{\mathrm{Y}}\big) &= \int_Z |\lambda^*(a) - a|\, \mathrm{Y}(a) da \\ &= \int_0^1 \left|\mathrm{C}_{\widehat{\mathrm{Y}}}^{-1}(\alpha) - \mathrm{C}_{\mathrm{Y}}^{-1}(\alpha)\right| d\alpha \end{aligned} \tag{6.7}$$

Moreover, $\mathrm{W}\big(\mathrm{Y}, \widehat{\mathrm{Y}}\big)$ in (6.7), can be expressed in terms of cumulative distribution:

$$W\left(\mathrm{Y},\widehat{\mathrm{Y}}\right)=\int_{\mathbb{R}}|\mathrm{C}_{\widehat{\mathrm{Y}}}(a)-\mathrm{C}_{\mathrm{Y}}(a)|da \tag{6.8}$$

To conclude representation (6.8) by (6.7), consider $\mathrm{C}_{\mathrm{Y}}^{-1}(\alpha)$ and $\mathrm{C}_{\widehat{\mathrm{Y}}}^{-1}(\alpha)$ in Figure 6.2, respectively, shown by dashed green and solid blue lines. The range of abscissa, in Figure 6.2, is divided into two sets, $\mathrm{S}=\left\{\alpha\in[0,1]:\mathrm{C}_{\widehat{\mathrm{Y}}}^{-1}(\alpha)\geq\mathrm{C}_{\mathrm{Y}}^{-1}(\alpha)\right\}$ and $\bar{\mathrm{S}}=[0,1]-\mathrm{S}$. For any point in set S, $\mathrm{C}_{\mathrm{Y}}^{-1}(\alpha)\leq a\leq\mathrm{C}_{\widehat{\mathrm{Y}}}^{-1}(\alpha)\Leftrightarrow\mathrm{C}_{\widehat{\mathrm{Y}}}(a)\leq\alpha\leq\mathrm{C}_{\mathrm{Y}}(a)$, e.g., see a_1 and α_1 in Figure 6.2. Similarly, for any point in $\bar{\mathrm{S}}$, $\mathrm{C}_{\widehat{\mathrm{Y}}}^{-1}(\alpha)\leq a\leq\mathrm{C}_{\mathrm{Y}}^{-1}(\alpha)\Leftrightarrow\mathrm{C}_{\mathrm{Y}}(a)\leq\alpha\leq\mathrm{C}_{\widehat{\mathrm{Y}}}(a)$, e.g., see a_2 and α_2 in Figure 6.2. Thus, (6.8) can be recast as a summation of two areas A_S and $A_{\bar{S}}$ as follows:

$$A_{\mathrm{S}}=\int_{S}\int_{\mathrm{C}_{\mathrm{Y}}^{-1}(\alpha)}^{\mathrm{C}_{\widehat{\mathrm{Y}}}^{-1}(\alpha)}da\,d\alpha=\int_{\mathbb{R}}\int_{\mathrm{C}_{\widehat{\mathrm{Y}}}(a)}^{\mathrm{C}_{\mathrm{Y}}(a)}\mathbb{I}_{\alpha\in\mathrm{S}}\,\mathbb{I}_{\mathrm{C}_{\mathrm{Y}}(a)\geq\mathrm{C}_{\widehat{\mathrm{Y}}}(a)}\,d\alpha\,da \tag{6.9}$$

$$\begin{aligned}A_{\bar{\mathrm{S}}}&=\int_{\bar{S}}\int_{\mathrm{C}_{\widehat{\mathrm{Y}}}^{-1}(\alpha)}^{\mathrm{C}_{\mathrm{Y}}^{-1}(\alpha)}da\,d\alpha\\&=\int_{\mathbb{R}}\int_{\mathrm{C}_{\mathrm{Y}}(a)}^{\mathrm{C}_{\widehat{\mathrm{Y}}}(a)}\mathbb{I}_{\alpha\in\bar{\mathrm{S}}}\,\mathbb{I}_{\mathrm{C}_{\widehat{\mathrm{Y}}}(a)\geq\mathrm{C}_{\mathrm{Y}}(a)}\,d\alpha\,da\end{aligned} \tag{6.10}$$

where the indicator function $\mathbb{I}$ is one if its condition, expressed as a subscript, is satisfied and zero otherwise. Therefore, $W\left(\mathrm{Y},\widehat{\mathrm{Y}}\right)$ can simply amount to perform data analysis on the space of cumulative distribution functions. In the literature, e.g., of sliced Wasserstein GAN [108], to estimate cumulative distribution or its generalized inverse, in (6.7)-(6.8), numerous samples are first predicted and then ascendingly rearranged by a sorting operator. Predicting 3600 points for the proposed DWPF problem is not practical since it negatively impacts the learning process due to the curse of dimensionality in ML [95].

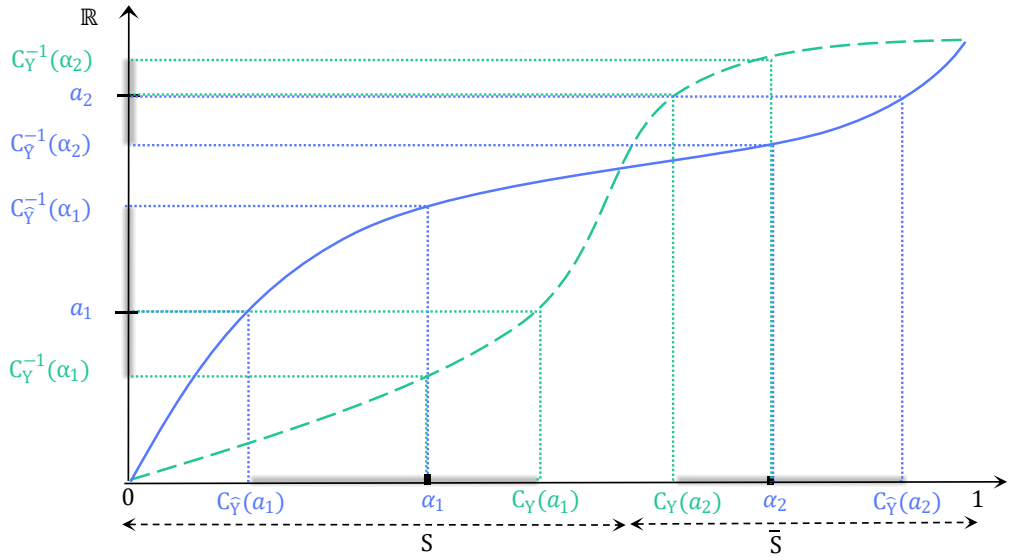

Figure 6.2) Obtaining WD for univariate distributions using L-1norm cost.

Secondly, the non-differentiability of the sorting operator causes a bottleneck in the end-to-end gradient learning of the model [109]. However, the proposed output representation space of Q_κ, presented in Section 6.2, concurrently circumvents both problems. The problem of dimensionality is directly alleviated as the proposed output space summarizes the intra-period wind power variability in a low dimensional space (where each dimension represents one bin). For instance, using 30 bins, the output dimension is reduced by (3600/30=) 120 times. Moreover, since the bins are, by nature, in ascending order, the cumulative sum of the model's output $\hat{y}$ (which represents the relative frequency of each bin) estimates the cumulative distribution $C_{\hat{y}}$. Notably, by using linear algebra for computing cumulative sum, $C_{\hat{y}}$ can be efficiently obtained by $C_{\hat{y}} = \mathbb{L}\hat{y}$ ($\mathbb{L}$ is a unit lower triangular matrix, where its elements are defined on $\{0,1\}$). Thus, using (6.8), the discrete representation of WD, denoted as $\widetilde{\mathrm{W}}(y, \hat{y})$, is efficiently obtained by:

$$\widetilde{\mathrm{W}}(y, \hat{y}) = \langle \Delta_{\mathrm{B}} , |\mathbb{L}(y - \hat{y})|'_{\odot} \rangle \tag{6.11}$$

where y and $\hat{y}$ are column vectors on $[0,1]^o$. Δ_B is a row vector containing intervals width of y (which is the same for $\hat{y}$). $|\ |'_{\odot}$ applies elementwise absolute value and transpose operations on a vector. $\langle\ \rangle$ is the dot product between the vectors.

The validity of the proposed dimensionality reduction is shown by an example. Two real-world wind power time series, obtained from [47], are represented by the blue and green lines on the left side of Figure 6.3. The dashed lines on the right side of Figure 6.3 correspond to the cumulative distribution estimations obtained by sorting 3600 points, while the solid lines are those obtained by the proposed low-dimensional representation space using linear algebra operations. The WD between the green and blue wind power time series is obtained 0.5055 and 0.5056 by the sorting operator and proposed approach, respectively (i.e., less than 0.02% error, which is very small).

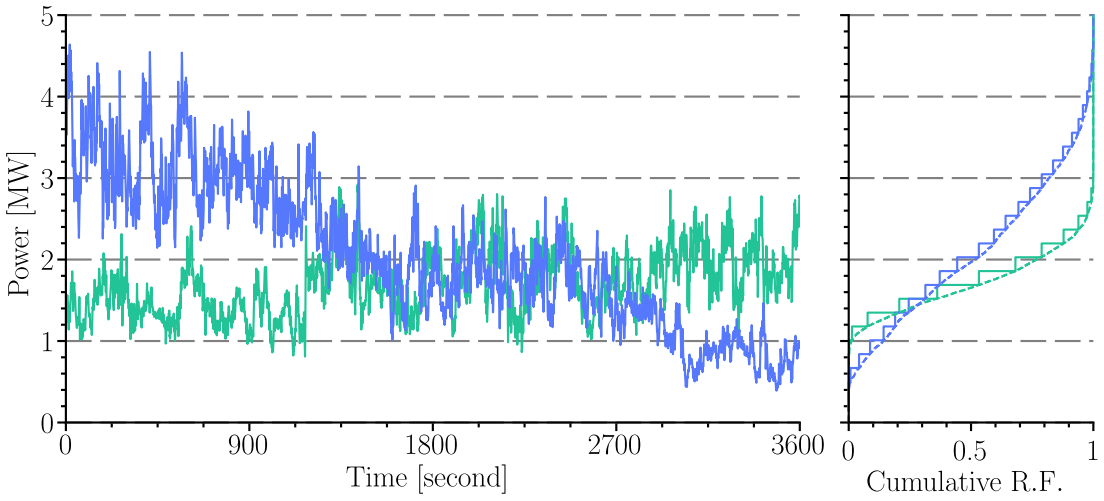

Figure 6.3) Obtaining WD of two real-world wind time series (left) using the sorting operator and proposed dimension reduction (right).

Consequently, the model's loss function using (6.11) for a single batch T' is as follows:

$$\min_{\kappa \in N} \mathcal{L}_{\mathrm{W}(y,\hat{y})} = |T'|^{-1} \sum_{t \in T'} \langle \Delta_{\mathrm{B}} \, , |\mathbb{L}(y_t - \hat{y}_t)|'_{\odot} \quad \rangle \tag{6.12}$$

where $\mathcal{L}_{\mathrm{W}(y,\hat{y})}$ is the WD-based loss function that should be minimized. Notably, the prediction error during inference is obtained by (6.12) without gradient updating.

Finally, Figure 6.4. connects various elements of the proposed DWPF methodology to better illustrate the relationships between the contributions described in Sections 6.2-6.3. The presented deep-learning-based DWPF model, described in Section 6.2, receives a set of input features to predict a representation of high-dimensional wind power variability (with a second-wise granularity) using a low-dimensional compact space, i.e., a temporal distribution. As described in Section 6.2, this output representation can have a parametric or non-parametric form. However, the non-parametric representation of the temporal distribution avoids the potential problem of misinterpreting wind variability with a structured distribution.

The target wind power data are also transformed into a compatible form with respect to the predicted mapping. As shown in Figure 6.4., a loss function is then used to compare the predicted and target distributions. For this task, a parametric and several nonparametric entropy-based loss functions are presented in Sections 6.3.1- 6.3.4.

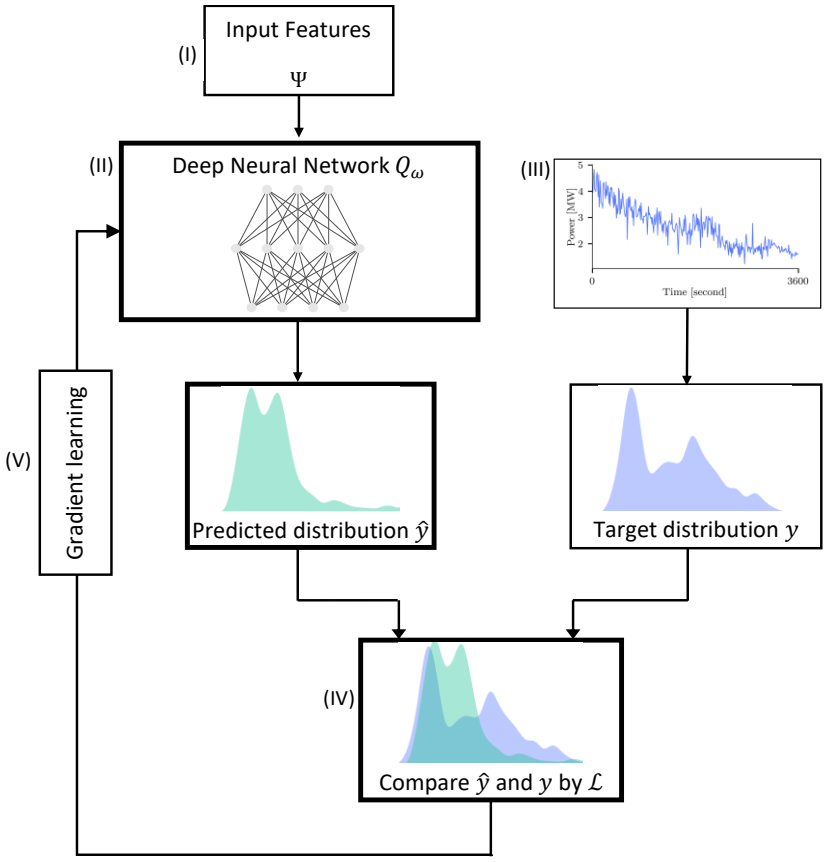

Figure 6.4) The schematic of the learning process of the proposed DWPF.

However, these losses have some shortcomings. Furthermore, as presented in Section 6.3.5, an effective loss, using WD, is developed for this task to address the limitations of the tailored parametric and entropy-based losses.

The gradient of the loss score is then used to train the model. The WD-based loss provides more reliable gradient information for training the model because it does not consider a predefined structure for the wind distribution and also considers the cross-correlation of the intervals of the distributions.

6.4 WPP Bidding via Wind Power Temporal Distribution

In this section, we present a WPP trading framework for day-ahead energy and reserve bidding. The framework directly utilizes forecasted wind power temporal distributions as input to maximize total day-ahead profits. The proposed framework is formulated as follows:

$$\max_{\mathrm{X},\Psi} \mathcal{R} = \sum\nolimits_{t\in T} \mathcal{R}_t^E + \mathcal{R}_t^R \tag{6.13a}$$

$$\mathcal{R}_t^E = \lambda_{\mathrm{t}}^{\mathrm{Eo}} p_t^{Eo} + \lambda_{\mathrm{t}}^{\mathrm{E}\uparrow} \Delta p_t^{E\uparrow} - \lambda_{\mathrm{t}}^{\mathrm{E}\downarrow} \Delta p_t^{E\downarrow} \qquad t \in T \tag{6.13b}$$

$$\mathcal{R}_t^R = \lambda_{\mathrm{t}}^{\mathrm{Ro}} p_t^{Ro} - \lambda_{\mathrm{t}}^{\mathrm{R}\downarrow} \sum\nolimits_{b\in\mathcal{B}} \hat{y}_t^b \Delta p_{t,b}^R \qquad t \in T \tag{6.13c}$$

$$\underline{P} \le p_t^{E\mathrm{o}} + p_t^{R\mathrm{o}} \le \overline{P} \qquad t \in T \tag{6.13d}$$

$$p_{t,b}^R \le P_b \qquad t \in T; b \in \mathcal{B} \tag{6.13e}$$

$$p_t^{R\mathrm{o}} - p_{t,b}^R \le \Delta p_{t,b}^R \qquad t \in T; b \in \mathcal{B} \tag{6.13f}$$

$$p_t^E = \sum\nolimits_{b\in\mathcal{B}} \hat{y}_t^b \, P_b - \sum\nolimits_{b\in\mathcal{B}} \hat{y}_t^b \, p_{t,b}^R \qquad t \in T \tag{6.13g}$$

$$p_t^{E\mathrm{o}} - p_t^E = \Delta p_t^{E\downarrow} - \Delta p_t^{E\uparrow} \qquad t \in T \tag{6.13h}$$

$$\Psi = \left\{ p_t^{\mathrm{Eo}}, p_t^{R\mathrm{o}}, p_t^E, p_{t,b}^R, \Delta p_t^{E\uparrow}, \Delta p_t^{E\downarrow}, \Delta p_{t,b}^R \right\} \in \mathbb{R}^+$$
$$\mathrm{X} = \{ \mathcal{R}_t^E, \mathcal{R}_t^R \} \in \mathbb{R} \tag{6.13i}$$

(6.13j)

The total profit $\mathcal{R}$ consists of WPP's hourly contributions to the energy and reserve markets, denoted $\mathcal{R}_t^E$ and $\mathcal{R}_t^R$, respectively. The energy contribution, given in (6.13b), is a function of the hourly day-ahead power bid p_t^{Eo} as well as real-time power surplus $\Delta p_t^{E\uparrow}$ and deficit $\Delta p_t^{E\downarrow}$

(remunerated with an hourly timescale). The day-ahead energy price, as well as imbalance settlement prices for the surplus and deficit in generations, are, respectively, shown by λ_t^{Eo}, $\lambda_t^{\mathrm{E}\uparrow}$, and $\lambda_t^{\mathrm{E}\downarrow}$. As shown in (6.13c), WPP's contribution to the reserve market, $\mathcal{R}_t^R$, depends on the relative frequency of wind power for each interval $\hat{y}_t^b$ and day-ahead reserve bid p_t^{Ro}, paid by the reserve price λ_t^{Ro}, as well as real-time reserve deficit $\Delta p_{t,b}^R$, penalized by $\mathcal{R}_t^{\mathrm{R}\downarrow}$ within a second-wise timescale. The total energy and reserve bid is constrained by the minimum $\underline{P}$ and maximum capacity $\overline{P}$ of the wind turbine in (6.13d). The allocated real-time reserve power $p_{t,b}^R$ is bounded by potential available power P_b for each interval ($b \in \mathcal{B}$) of wind power distribution, as given by (6.13e). The real-time reserve power deficit is determined by (6.13f). Constraint (6.13g) obtains the hourly injected wind power p_t^E by subtracting the allocated hourly mean reserve power $\sum_{b\in\mathcal{B}} \hat{y}_t^b \, p_{t,b}^R$ from the total hourly mean wind power $\sum_{b\in\mathcal{B}} \hat{y}_t^b \, P_b$. Finally, the deficit and surplus of generation are obtained by (6.13h). The set of decision variables is indicated by Ψ and X in (6.13i) and (6.13j). The framework has been modeled as a mixed integer linear programming problem.

To compare the effectiveness of each loss, used in the proposed DWPF problem, the cumulative absolute day-ahead profit deviations between WPP contributions under perfect and forecast information are calculated as follows:

$$\Delta\mathcal{R}^R = \sum_{D=1}^{30} \left| \sum_{t=13}^{36} \left(\mathcal{R}_t^{R*} : y_t^b\right)_D - \sum_{t=13}^{36} \left(\mathcal{R}_t^{R*} : \hat{y}_t^b\right)_D \right| \tag{6.14a}$$

$$\Delta\mathcal{R}^E = \sum_{D=1}^{30} \left| \sum_{t=13}^{36} \left(\mathcal{R}_t^{E*} : y_t^b\right)_D - \sum_{t=13}^{36} \left(\mathcal{R}_t^{E*} : \hat{y}_t^b\right)_D \right| \tag{6.14b}$$

$$\Delta\mathcal{R} = \sum_{D=1}^{30} \left| \sum_{t=13}^{36} \left(\mathcal{R}_t^*: y_t^b\right)_D - \sum_{t=13}^{36} \left(\mathcal{R}_t^*: \hat{y}_t^b\right)_D \right| \tag{6.14c}$$

where $\Delta\mathcal{R}^R$, $\Delta\mathcal{R}^E$ and $\Delta\mathcal{R}$, are, respectively, the deviation in reserve, energy, and total profits. The superscript * represents the optimal decision resulting from (6.13). Also, $: y_t^b$ / $: \hat{y}_t^b$ indicate the decisions made using perfect/forecasted wind temporal distributions. D and t are, respectively, the day and hour indices.

6.5 Numerical Results

The performance of the proposed methodology is verified in this section through a comprehensive analysis of real-world data. To this end, Section 6.5.1 demonstrates the effectiveness of the proposed losses as an error metric, using an intuitive example. Furthermore, Section 6.5.2 investigates the prediction performance of a naive model, ACWGAN model, parametric and entropy-based losses, as well as the proposed WD-based loss to forecast the temporal distribution of wind power within the developed DWPF problem. Finally, the obtained predictions are used in a WPP day-ahead bidding problem (presented in Section 6.4) to compare the effectiveness of each model, including ACWGAN, within a decision-making framework. The study is conducted for one month using real-world wind and market data [47]-[48].

6.5.1 Intuitive Example

The effectiveness of the proposed WD metric compared to tailored parametric and entropy-based measures is demonstrated by three illustrative cases, each containing three distributions. These cases are shown in Figure 6.5. The horizontal axis represents the power intervals, whereas the vertical axis indicates the relative frequency of each interval (also,

indicated at the top of the bars). Table 6.1 summarizes the distances obtained with different error measures. The distance between distributions is denoted by the superscript ↔, e.g., $\overleftrightarrow{\alpha\beta}$ indicates the distance between distributions α and β. In case 1, distributions are supported on the same domain. The R.F. of the first interval in α is under/over predicted by β/γ, and the corresponding mass change is equally distributed across other intervals. Intuitively, it is expected that $\overleftrightarrow{\alpha\beta} = \overleftrightarrow{\alpha\gamma} < \overleftrightarrow{\beta\gamma}$. In this case, while all losses fairly satisfy the expectation, WD satisfies it exactly (0.15=0.15<0.3). Nevertheless, all measures are still relatively able to provide meaningful error feedback for this case. In case 2, although distributions have still the same support, the R.F. of the first interval in α is shifted one/two interval/s to the right (which is shown by β/γ). In this case, it is expected that $\overleftrightarrow{\alpha\beta} = \overleftrightarrow{\beta\gamma} < \overleftrightarrow{\alpha\gamma}$. The parametric measure Par, opposing the intuitive expectation, obtains different values for $\overleftrightarrow{\alpha\beta}$ and $\overleftrightarrow{\beta\gamma}$, i.e., 2.68 and 2.42, respectively. This can be explained by errors in fitting the given distributions to a structured one.

Nonetheless, it returns a larger value regarding $\overleftrightarrow{\alpha\gamma}$, 5.1, as compared to $\overleftrightarrow{\alpha\beta}$ and $\overleftrightarrow{\beta\gamma}$. Moreover, the next four entropy-based measures obtain an equal value for three distances in this case, while $\overleftrightarrow{\alpha\gamma}$ should be greater than $\overleftrightarrow{\beta\gamma}$ and $\overleftrightarrow{\alpha\beta}$. This insensitivity arises from the fact that entropy-based measures compare intervals of distributions in isolation, thus neglecting the cross-interval information. On the other hand, WD returns a reasonable value regarding the distances, i.e., 0.4=0.4<0.8, as intuitively expected.

Case 3 assumes that the distributions are not supported by the same domain. Distribution β is the shifted version of all intervals of α by one step to the right. In addition to the right shift, compared to α, the R.F. is also changed in γ. To avoid getting unbounded value due to zeros in distributions, the proposed treatment in Section 6.3 is applied to entropy-

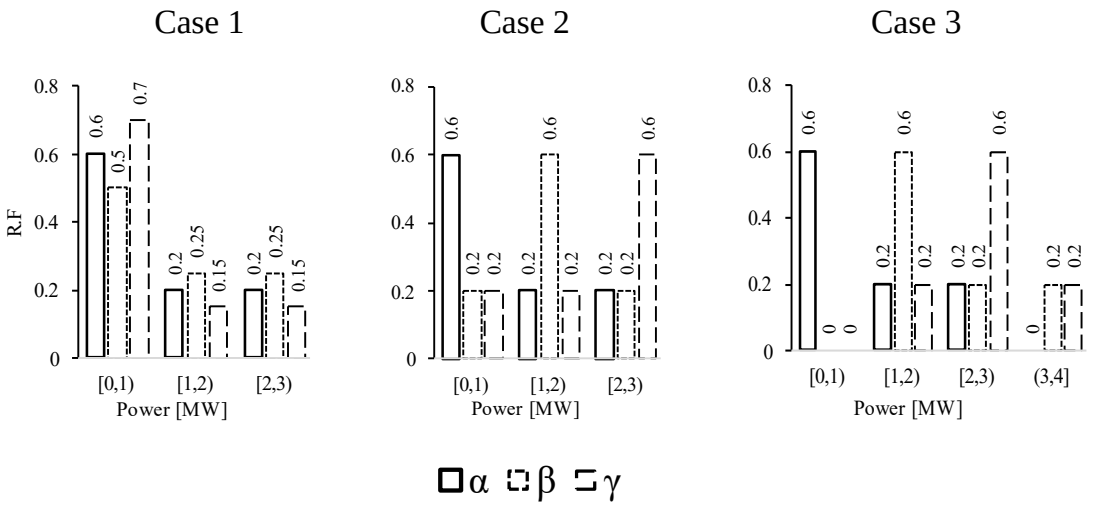

Figure 6.5) Three illustrative cases, each containing three distributions, used for demonstrating the effectiveness of proposed error measures.

Table 6.1) Obtained distances using tailored and proposed losses regarding Figure 6.5

	Case 1			Case 2			Case 3		
	$\overleftrightarrow{\alpha\beta}$	$\overleftrightarrow{\beta\gamma}$	$\overleftrightarrow{\alpha\gamma}$	$\overleftrightarrow{\alpha\beta}$	$\overleftrightarrow{\beta\gamma}$	$\overleftrightarrow{\alpha\gamma}$	$\overleftrightarrow{\alpha\beta}$	$\overleftrightarrow{\beta\gamma}$	$\overleftrightarrow{\alpha\gamma}$
Par*	0.46	0.94	0.49	2.68	2.42	5.1	6.73	2.8	5.42
CE	1.40	1.63	1.404	2.00	2.00	2.00	32.5	2.0	32.5
FKL	0.029	0.13	0.033	0.63	0.63	0.63	31.13	0.63	31.13
RKL	0.029	0.12	0.031	0.63	0.63	0.63	11.12	0.63	11.12
JSD	0.007	0.03	0.008	0.15	0.15	0.15	0.48	0.15	0.48
WD	**0.15**	**0.3**	**0.15**	**0.4**	**0.4**	**0.8**	**1.0**	**0.4**	**1.4**

*: Par stands for the distance based on parametric Weibull distribution

based measures. In this case, it is expected that $\overleftrightarrow{\beta\gamma} < \overleftrightarrow{\alpha\beta} < \overleftrightarrow{\alpha\gamma}$. The parametric error measure Par while satisfying $\overleftrightarrow{\beta\gamma} < \overleftrightarrow{\alpha\beta}$ and $\overleftrightarrow{\alpha\gamma}$, due to fitting errors, counterintuitively, returns a lower value for $\overleftrightarrow{\alpha\gamma}$ compared with $\overleftrightarrow{\alpha\beta}$. The next four entropy-based measures only satisfy that $\overleftrightarrow{\beta\gamma} < \overleftrightarrow{\alpha\beta}$ and $\overleftrightarrow{\alpha\gamma}$. However, they return the same value for $\overleftrightarrow{\alpha\beta}$ and $\overleftrightarrow{\alpha\gamma}$, despite

their recognizable dissimilarity. This is due to the insensitivity of the entropy-based measures with respect to the variations of distributions on different supports. Nevertheless, WD, by leveraging the information captured in the geometry of support, returns a sensible value regarding all three distances, i.e., $0.4<1<1.4$.

Therefore, considering the outcomes of the presented intuitive example, it can be concluded that the proposed WD-based metric is more effective than all other measures and is able to determine a reliable distance in all cases considered.

6.5.2 Day-Ahead Wind Power Temporal Distribution Forecasting

This section investigates the performance of the devised DWPF model, described in Section 6.2, and trained by various proposed losses (see Section 6.3). Also the performance of the DWPF model is compared with the ACWGAN model (which is presented in Chapter 5). For this purpose, 6000 hours of real wind power data (with second-wise temporal granularity) for a 5 MW wind turbine, obtained from [47], are used to predict the temporal distribution of wind power in DWPF. The dataset is split into the ratio of 0.6:0.2:0.2 (train: validation: test sets). The input features used in the proposed model include wind power distributions of 6 previous hours (with 5 equidistant intervals on the support), mean temperature of one previous hour, and timestamps along with predictions of temperature and the hourly mean wind speed for the target period. The DWPF output target is hourly wind power distribution (with 30 equidistance intervals on the support), for 36-hour ahead. The architecture of the models (developed in pytorch [110]) consists of dense layers, batch normalization, dropout, ReLU, and SoftMax units [102], [103]. All hyperparameters of the models along with the

optimizer's parameters are tuned by 50 trial runs using the tree-structured Parzen estimator, from Optuna package [111]. Accordingly, the DWPF model trained with WD-based loss uses two dense hidden layers with 234 and 122 neurons, along with two dropout units with rates of 0.156 and 0.152, and Adam optimizer with an initial learning rate of 0.009.

The forecasted temporal distribution for one hour using the naive model, ACWGAN model, as well as tailored losses (Par, CE, FKL, RKL, JSD) and proposed WD-based loss is shown in the green graph in Figure 6.6. The target distribution for the corresponding hour is shown in blue graph. Notably, the naive model assumes that the day-ahead temporal distribution of wind power for each hour is the same as that of the same hour in the previous day. It can be seen that the naive model achieves the worst performance among the models. The ACWGAN model yields significantly superior results compared to the naive model and slightly outperforms the parametric model. Also, the results obtained with the nonparametric losses are better than those obtained with the parametric loss. This is due to the misrepresentation of the wind variability by a structured distribution as well as its fitting errors. Furthermore, the models trained with CE and FKL losses are performing better than those trained with RKL and JSD. The reason is that RKL has zero-enforcing behavior, leading to lower coverage of the support, which is important for wind power values. Also, the poorer result of JSD is due to the insensitivity of its gradient for non-overlapping distributions. Finally, the DWPF model trained with the proposed WD-based loss demonstrates the best results in Figure 6.6, thanks to its effective gradient flow for training the model.

Table 6.2 quantitively reports the performance of each model (indicated in the rows of the Table) against various metrics (indicated in the columns of the Table) for the predicted distributions in Figure 6.6. It can be seen that while the obtained results by the WD-based loss for all metrics

(indicated in the last row of Table 6.2) are smaller than or very close to the results of other models, its result for the WD metric, i.e., 0.02, is significantly better than the WD metric results of all other models. Note that the WD-metric is a more reliable error measure for distributions as already demonstrated in Section 6.5.1.

Table 6.3 reports the performance of all models using the entire test set, which includes one month of day-ahead forecast with a 36-hour horizon. This Table has the same row/column description as Table 6.2. Considering the WD metric, it can be seen that the naïve, ACWGAN and parametric models with the WD of, respectively, 1.60, 0.41 and 0.47 have the poorest performance among all models of Table 6.3.

For the reasons explained above, models trained with FKL and CE losses perform better than those trained with RKL and JSD losses. The WD metric for CE and FKL losses is, respectively, 0.18 and 0.17, while it is higher for RKL and JSD losses (0.27 and 0.21). Notably, the proposed A4model with the WD-based loss obtains the best result for the WD-metric (0.14) among all models of Table 6.3. In addition, the results of the WD-based model for other metrics are still better or very close to the results of other models.

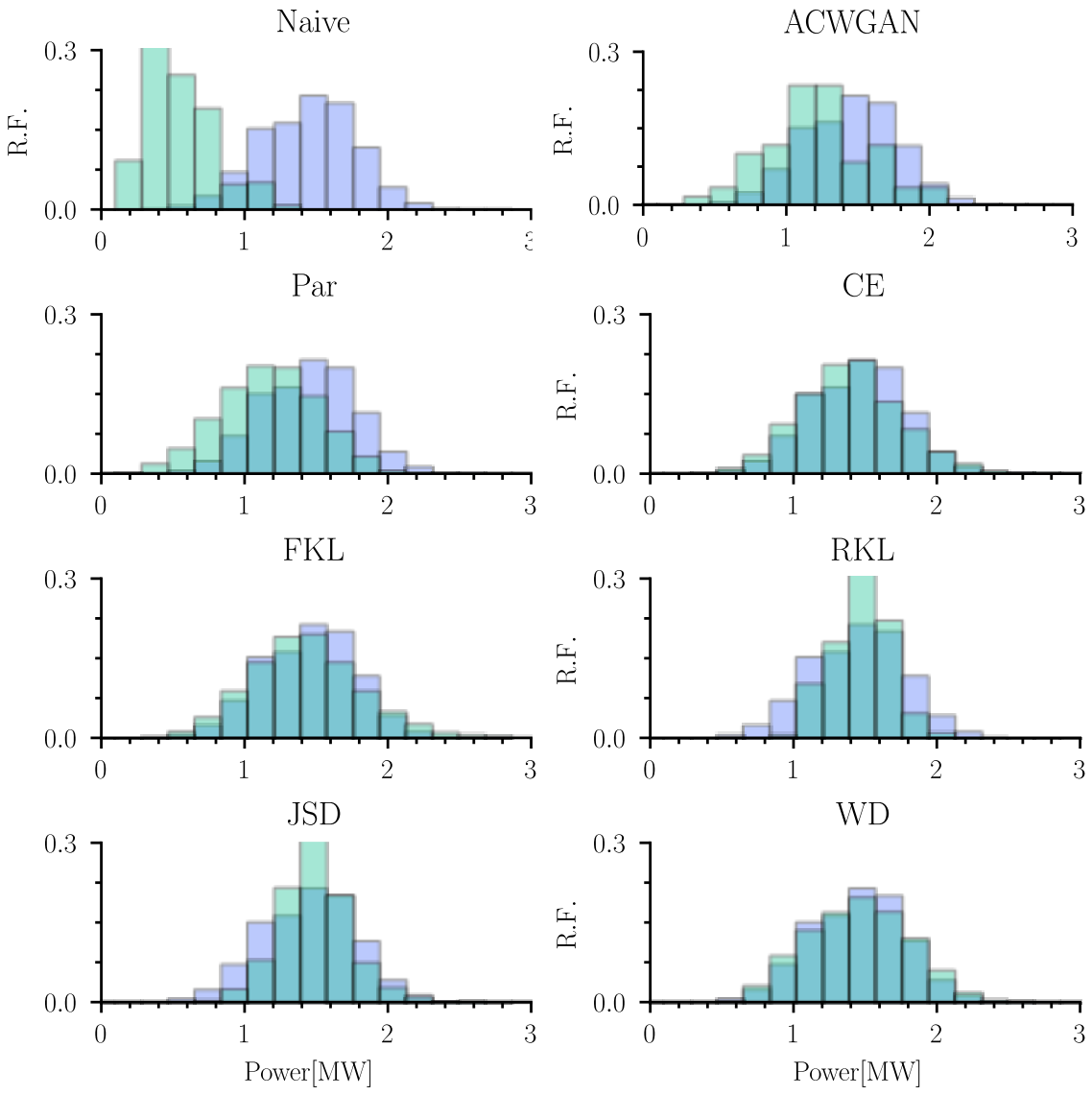

Figure 6.6) Forecasted temporal distributions (in green), for one hour, using a naive approach, ACWGAN model, and Parametric, CE, FKL, RKL, JSD and WD losses. The target distribution is shown in blue.

Table 6.2) The obtained error metrics, regarding Figure 6.6, for training the presented DWPF model using proposed losses

Loss\Metric	CE	FKL	RKL	JSD	WD
Naive	21.64	19.64	8.57	0.76	**0.90**
ACWGAN	3.66	1.66	1.34	0.11	**0.23**
Par	3.29	1.28	1.51	0.10	**0.27**
CE	2.94	0.94	1.01	0.02	**0.06**
FKL	2.96	0.96	1.20	0.02	**0.07**
RKL	3.56	1.56	0.99	0.09	**0.13**
JSD	3.09	1.09	0.93	0.05	**0.09**
WD	**2.91**	**0.91**	**0.95**	**0.01**	**0.02**

Table 6.3) The obtained error metrics of DWPF for one month using proposed losses

Loss\Metric	CE	KLF	RKL	JSD	WD
Naive	19.54	18.07	17.81	0.68	**1.60**
ACWGAN	7.83	7.31	6.49	0.37	**0.41**
Par	7.56	6.16	9.29	0.45	**0.47**
CE	2.50	1.04	2.54	0.10	**0.18**
FKL	2.49	1.02	2.46	0.10	**0.17**
RKL	5.30	3.83	1.64	0.45	**0.27**
JSD	3.06	1.60	1.41	0.14	**0.21**
WD	**2.53**	**1.07**	**1.56**	**0.08**	**0.14**

6.5.3 Added Value of The Proposed Losses in a WPP Decision-Making Framework

In this section, the WPP trading framework for day-ahead energy and reserve bidding, presented in 6.4, is employed to compare the added value of the proposed WD-based loss with the added values of the tailored losses and a naive model. The WPP uses the forecasted wind power temporal distributions from t=13 to 36, obtained in Section 6.5.2, as input to the bidding framework to maximize the total day-ahead profit $\mathcal{R}$ using (6.13a). The models presented in this chapter are also evaluated against the data-driven decision framework that includes ACWGAN (as discussed in chapter 5). Table 6.4 summarizes the profit deviations, calculated via (6.14), which are attained using the predictions obtained by a naive model, ACWGAN data-driven model (for short ACWGAN) and proposed losses for the DWPF problem. The reported results in Table 6.4 belong to the prediction of a single hour. The market rates for $\lambda_t^{\mathrm{Eo}}, \lambda_t^{\mathrm{E}\uparrow}, \lambda_t^{\mathrm{E}\downarrow}$, λ_t^{Ro} and $\lambda_t^{\mathrm{R}\downarrow}$, are, respectively, 85, 75, 80, 90, and 120 €/MW(h). These rates are obtained from the electricity market in France using ENTSO-E Transparency Platform [48]. Table 6.4 indicates that the ACWGAN outperforms the naive and parametric models. Meanwhile, compared to other models, they all have a poor performance. The total profit deviation $\Delta\mathcal{R}$ in naive, ACWGAN and parametric models is, respectively, € 75.49, € 19.71, and € 23.76, which are significantly higher than those of other approaches. The results of FKL are better than those of other entropy-based losses. Finally, Table 6.4 shows that the optimal profits obtained by the WD loss are the best ones with the minimum deviations with respect to the profits obtained by the perfect information. From Table 6.4 it is seen that the profit deviations of the WD loss model ($\Delta\mathcal{R}^{R}$, $\Delta\mathcal{R}^{E}$ and $\Delta\mathcal{R}$) are significantly lower than the profit deviations of all other models.

A comprehensive profit deviation analysis, using (6.14), is then performed for one month of day-ahead energy and reserve trading by the forecasted wind power distributions. The forecasts are obtained by a naive model, ACWGAN model and our developed DWPF problem which encompasses the several proposed losses. The results of this extensive analysis are shown in Table 6.5. Also, the real market rates are obtained from ENTSO-E Transparency Platform [48]. It can be seen that the naive model, ACWGAN and parametric losses return significantly higher profit deviations compared with non-parametric losses. CE and FKL perform better than RKL and JSD with lower profit deviations in Table V. Remarkedly, the model trained by the proposed WD-based loss obtains the best results with the lowest profit deviations in Table 6.5.

Table 6.4) The deviations (€) in optimal profits of the energy and reserve markets as well as in the total profit for one hour.

	Naive	ACWGAN	Par	CE	FKL	RKL	JSD	**WD**
$\Delta\pi^R$	65.3	31.55	32.11	14.9	15.18	17.16	16.52	**0.53**
$\Delta\pi^E$	10.19	11.48	8.35	11.00	14.01	14.13	12.53	**1.00**
$\Delta\pi$	75.49	19.71	23.76	3.90	1.16	3.03	3.99	**0.47**

Table 6.5) The deviations (€) in optimal profits of the energy and reserve markets as well as in the total profit for one month.

	Naive	ACWGAN	Par	CE	FKL	RKL	JSD	**WD**
$\Delta\pi^R$	50993.74	10872.57	11342.63	3570.65	2571.32	4773.85	2873.60	**1576.18**
$\Delta\pi^E$	27048.72	6598.14	7068.25	1849.05	1803.59	3768.78	2778.35	**1601.41**
$\Delta\pi$	68663.62	13873.69	14037.07	4001.94	2428.37	6977.16	4874.08	**1666.30**

The WD-based model obtains significantly lower $\Delta\mathcal{R}^R$, $\Delta\mathcal{R}^E$ and $\Delta\mathcal{R}$ than all other models in Table 6.5. These results show that using such a dedicated WD-based loss model can significantly improve WPP's bidding decisions in an energy and reserve market environment.

6.6 Discussion and Conclusion

This chapter formulates DWPF in a new fashion that provides complementary information around intra-period wind variability by forecasting wind temporal distribution with high resolution. Several classical loss functions are tailored to this problem to provide candidate solutions. In addition, a new loss function based on Wasserstein Distance (WD) is proposed to account for the limitations of parametric and entropy losses. The proposed WD-based loss is effectively designed to allow continuous gradient learning of the model. The results on forecast performance, first, show that the tailored entropy-based losses perform better than the parametric, ACWGAN and naive models. Furthermore, the WD-based loss, which takes into account the cross-correlation between distribution intervals, demonstrates the most accurate prediction results, among all losses, for wind temporal distribution. Additionally, the predictions obtained by the proposed models, as well as naive and ACWGAN models, are fed into a wind power bidding problem to evaluate their performance in the market context. It is found that, by leveraging the WD-based DWPF model, compared to other models, wind power producer is exposed to significantly lower deviations from the profit obtained by perfect information.

6.7 Related Publication

S.A. Hosseini, J.-F. Toubeau, N. Amjady, F. Vallée, "Day-Ahead Wind Power Temporal Distribution Forecasting With High Resolution "*IEEE Trans. Power Syst.*,(*In Revision*), 2023.

Chapter 7. Discussion and Conclusion

In this chapter, Section 7.1 restates the motivations, challenges, and objectives addressed in this thesis. Then, the research findings are summarized in Section 7.2. Reflections and considerations related to other elements of the study, such as the integration of battery storage systems and intra-park dynamic effects, are discussed in Section 7.3. The final conclusion of the work is drawn in Section 7.4. Prospects for future work are outlined in Section 7.5.

7.1 Overview

Wind power with a global capacity of 743 GW (expected to rise more than tenfold by 2050 under 1.5 °C scenario [2]), is considered as the mainstream option to address today's serious concerns about global warming, over-depletion of fossil fuels, and energy crisis [112]. Despite the social and environmental values of WP, its intermittent nature is currently seen as a threat to the reliability and security of power systems. To circumvent this threat, the system operator, e.g., Transmission System Operator (TSO) in Europe, currently, relies on ancillary services (also called reserve power or flexibility solution) provided by conventional generation units, e.g., fuel-based, to continuously compensate for the WP intermittency. While this practice is moderately feasible for power systems with low WP share, in a future scenario where WP share becomes more significant or even exceeds conventional generation share, such an approach becomes inappropriate. This is because balancing the intermittency caused

by a high WP share requires an abundant volume of reserve power from conventional sources, which are physically limited in size and number. Besides that, this practice is inconsistent with climate goals and also entails high costs for end-users.

7.1.1 Motivation

Current wind turbine control schemes technically qualify WP Producers (WPPs) to provide frequency containment reserve (FCR) by rapidly regulating the output power [113], thus recovering the system from undue frequency distortions. Therefore, it is desirable that WPPs, besides delivering energy, also contribute to the safe operation of the grid. Thus, a larger WP share can be integrated without the need to install additional fossil fuel power plants for system balancing. The provision of these services by WPP not only supports grid security but also has a positive social impact due to its low marginal cost.

7.1.2 Challenges

Such a sustainable approach toward a net-zero and resilient power system faces major challenges from the perspective of WPPs and TSOs.

Firstly, WPPs require an accurate portrayal of the variability and intermittency of WP for day-ahead energy and reserve scheduling. This WP portrayal requires a wind power forecasting model with a high temporal resolution, e.g., minute-wise to second-wise, over the day-ahead horizon (e.g., 24 hours). However, due to the curse of dimensionality, decreasing the forecast timescale to one minute or second within the day-ahead horizon drastically reduces the model performance.

Secondly, the current reserve procurement mechanisms used by TSOs assume that the offered reserve volumes are almost always available as classically these services are provided by conventional units with low uncertainty. This setting hinders the effective participation of WPPs in reserve procurement due to the inevitable link between WP uncertainty and WP bid volume.

Thirdly, WPPs are responsible for real-time deviations in both energy and reserve market floors. These deviations are settled at different timescales. Therefore, a sophisticated bidding strategy that accounts for uncertainties at multiple timescales is required.

7.1.3 Objectives

The objectives of this thesis that are addressed in response to the challenges, outlined in Section 7.1.2, are as follows:

1- Capturing wind fluctuations and uncertainty at very-short timescales (minute to second) within the day-ahead horizon.

2**-** Incorporating a confidence-based metric regarding the reliability of the offered services into the day-ahead market in the WPP bidding framework.

3- Optimizing WPP's energy and reserve scheduling in the day-ahead market considering wind uncertainty at different resolutions, aligned with the time intervals of the financial compensation mechanisms.

7.2 Summary of Findings

In the beginning, Chapter 3 evaluates the negative impact of simplifying the availability of wind capacity by ignoring its real-time fluctuations. It is shown that the wind power producer's revenue significantly deviates from its expected value by ignoring fast wind fluctuations. More importantly, the

transmission system operator is not informed about the confidence level of the contracted reserve bid. Thus, in a long run, it may discourage the transmission system operator to rely on wind power producers as reliable reserve providers.

A new bidding framework for WPP has then been developed, in Chapter 4, to address this problem. This framework takes into account hourly wind uncertainty and integrates a risk constraint for reserve power availability into the bidding strategy. This allows WPP to maximize its profit while also adhering to market policies on the reliability of capacity services. The proposed framework demonstrates the potential benefits of increased profits for WPP while accommodating a wide range of confidence levels set by the TSO for low to medium levels of turbulence intensity. However as wind uncertainty is inadequately represented (through hourly timescales), in a high turbulence condition, the ex-post revenue and reserve confidence level highly deviate from expected values.

In Chapter 5, a deep-learning scenario generation model is developed to address the challenge of modeling wind uncertainty with high resolution. The model utilizes a novel auxiliary classifier in a Wasserstein-based Generative Adversarial Network to generate wind scenarios with minute-level resolution. The results demonstrate that the proposed method generates wind scenarios that are superior to state-of-the-art methods, as measured by similarity and statistical metrics. Additionally, a dedicated decision that considers wind uncertainties with different temporal resolutions, also enriched by a probabilistic constraint on real-time reserve availability, is developed. The model leverages the benefits of the proposed scenario generation model and multi-resolution trading formulation to obtain the optimal share of energy and reserve power. Analysis shows the combination of the proposed scenario generation method and the devised

bidding model outperforms previous methods, even those with probabilistic constraints regarding reserve availability, in terms of reserve unavailability risk and profit deviation. Our analysis reveals that the combination of the proposed scenario generation method and bidding model outperforms previous methods, including those with probabilistic constraints on reserve availability as presented in Chapter 4. Nevertheless, it should be noted that although scenario generation methods offer potential outcomes, they have limitations such as difficulty in capturing time dependence structures.

In Chapter 6, a new approach to formulating day-ahead wind power forecasting is presented that provides complementary information regarding intra-period wind variability by forecasting the temporal distribution of wind power with second-wise resolution. Also, the time dependence structures of time steps are captured within this method. To address the limitations of traditional methods, several classical loss functions are tailored to the problem and a novel loss function based on Wasserstein distance is proposed. The results indicate that tailored entropy-based losses perform better than parametric and naive models, with the WD-based loss demonstrating the most accurate predictions for wind temporal distribution among all loss functions. Then a fluctuation-aware bidding framework, considering uncertainty at different resolutions, is developed that directly takes the generated temporal distributions as input. The numerical results show that the combination of the proposed temporal distribution forecast model and bidding framework significantly leads to lower deviations from the profit compared to other models such as the one presented in chapter 5 or the ones using tailored losses.

7.3 Critical Reflections and Considerations

The objective of this study was to provide a framework for wind power scheduling framework that takes into account wind fluctuations and their

impact on reserve service reliability and producer profitability. Despite the valuable insights provided by the developed models and results, it is important to acknowledge and reflect on the limitations of the study's design and methodology. This section serves as a foundation for future work section (Section 7.5) by critically discussing the limitations and suggesting improvements.

- **Spatial correlation:**

The forecasting and scenario generation models developed in this work focus primarily on the temporal correlation of wind speed. This approach is effective for single and small wind farms, where wind conditions are homogeneous within the farm. However, for wind power producers with multiple and dispersed wind assets, considering temporal correlation alone may not provide an accurate prediction of wind speed. In this case, it is important to also include spatial dependencies in wind speed prediction and consider the influence of wind conditions in the surrounding area. This provides a more comprehensive understanding of wind conditions and enables WPP to make informed decisions about available wind energy.

- **Intra-park aerodynamic interaction**

The aerodynamic interaction between airflow and wind turbines, the so-called wake effect, is not addressed in this study. This approach is practical when dealing with a single wind turbine or situations with large distances between turbines, since the effects of the wake may be negligible under such conditions. Nevertheless, in large wind farms, this phenomenon plays a major role in the accurate assessment of WP and the response delay of downstream wind turbines [114].

- **Influential Assumptions on Price**

The analysis conducted in this thesis is influenced by two underlying assumptions that affect our modeling approach.

1) Negative price

It is important to clarify that negative prices in the electricity market are not necessarily due to increased use of renewable energy sources. Rather, they are due to the presence of inflexible generation plants (that cannot readily adjust their output) and the fixed incomes, e.g., wind certificates, received by wind parks (that counterbalance negative prices). In contrast, wind farms can now adjust their output in a timely manner. Therefore, this study assumes that as the use of flexible resources increases, the occurrence of negative prices becomes less likely in the future. Consequently, the proposed bidding strategy does not consider the impact of negative prices. However, in power systems with an excess of inflexible generation or frequent transmission congestion, negative prices may occur more often and affect the profitability of a portfolio.

2) Price-taker/maker

In addition, the WPP under study is assumed to be of small size. This implies that the WPP does not have significant market power and cannot influence prices. Therefore, the bidding strategy developed for WPP, in this thesis, uses a price-taker model. However, if a WPP has market dominance, a price-maker model may be a more appropriate modeling option. This is because, unlike a price-taker model, this model can better represent the dynamics of the market and the behavior of the participants.

- **Multi-technology portfolio**

This study develops a bidding model for a single technology portfolio, i.e., WPP, that carefully accounts for the effects of intra-period wind

variability. Accordingly, WPP is, by itself, able to hedge against the penalties arising from real-time wind power deviations. However, when feasible, a portfolio may consider a hybrid system that incorporates additional technologies, such as a battery storage system (BESS) into a wind power system. This approach offers some advantages, including the ability to achieve a better return on investment through market arbitrage and hedging against wind uncertainties, as well as improving the overall reliability of the system.

Nevertheless, combining technologies like BESS with wind power can lead to considerable changes in TSO operations and financial performance of energy portfolios, demanding thorough analysis during the planning phase.

A critical factor to consider is the upfront cost of integrating other technologies into wind energy systems, which can be relatively high. In addition, these technologies require sophisticated control systems to function optimally. The additional maintenance costs must be carefully considered. The degradation costs of some technologies, such as BESS, can also be significant, especially since the charging and discharging profile is highly volatile and changes rapidly. This is due to the volatility of wind energy and the stochasticity of system reserve requirements.

Moreover, the disposal and recycling of certain technologies can be a difficult and costly process. In Australia, for example, tons of photovoltaic panels have reached their end-of-life cycle. Accordingly, Breakthrough Victoria has recently invested $10 million and invited researchers to take on the challenge of solar waste management.

It's important to note that all of these considerations, whether implicitly or explicitly are associated with costs, which can have a significant impact

on the levelized cost of energy. Therefore, the decision to integrate BESS or other technologies into the WP portfolio must be made after careful consideration of the pros and cons and evaluation of the economic feasibility and risk assessment of such a project.

7.4 Final Conclusion

Recent regulatory and technological advances in the electric power industry have opened new opportunities for Wind Power Producers (WPPs) to provide energy and balancing services, such as Frequency Containment Reserve, thus enabling them to capitalize on the flexibility of the system and enhanced market profit. However, maintaining the reliability of the offered reserve, which is critical to ensure system stability, is a major challenge for WPPs due to the high volatility of wind energy. This thesis has developed and gradually improved the necessary models for WPPs to account for wind fluctuations in energy and reserve power scheduling. The proposed models first capture the day-ahead wind fluctuations and then use them in multi-resolution bidding models enriched with probabilistic constraints to ensure reserve availability.

Regarding the wind fluctuations assessments, a scenario generation model and a forecast model, both with a day-ahead horizon, are developed. The scenario generation model is a GAN-based model that is improved by adding a new agent as an auxiliary classifier over the common competing generator and critic players. The auxiliary classifier takes a priori information about the range of wind fluctuations as input to generate minute-wise wind power scenarios for each hour of the day-ahead horizon. The quality of the generated scenarios by this model is higher than in other models. However, the time dependence between successive hours is not accounted for, and the minute resolution is still rather high to accurately account for the continuous availability of wind energy. To address these

limitations, a day-ahead forecasting model is proposed that directly accounts for the time dependence of successive periods, in the training process, and captures the second-wise wind variability within the day-ahead horizon. The proposed model uses a novel approach by forecasting the temporal distribution of wind for each hour of the day-ahead horizon. In addition, an effective loss function based on Wasserstein distance was developed to train the model. The results show that the proposed model significantly outperforms its counterparts.

Regarding the decision framework, this study proposes a single-resolution and a multi-resolution model for optimal wind power scheduling. To enhance the reliability of wind power scheduling, the proposed decision frameworks employ a probabilistic constraint to ensure the confidence level of reserve availability. The single-resolution model employs hourly wind uncertainty within a stochastic bidding framework to account for real-time deviations and determine the reliability of the offered power. This model, which includes the reserve power confidence level, shows better performance compared to the model that excludes it, as measured by reserve reliability and real-time penalties imposed on the WPP. However, the performance of the model deteriorates in the presence of strong wind fluctuations. To address this issue, a multi-resolution model was developed to account for the deviations in reserve power and the confidence level of the offered services by leveraging the produced scenarios with high temporal resolution. The results show that the proposed data-driven WPP decision framework significantly improves both profit loss and reserve reliability under all wind fluctuation levels compared to the single-resolution model.

Overall, portfolios that rely solely on wind energy can mitigate wind energy volatility by using a dedicated scheduling framework that accounts

for fluctuations in wind power. Therefore, these portfolios can be considered as reliable providers of reserve capacity.

7.5 Future Work

This section introduces new opportunities for future research based on the discussion provided in Section 7.3.

One potential avenue for future research lies in the exploration of the use of deep learning techniques to better understand and account for the spatiotemporal correlation of wind power among producers with multiple and widely scattered wind assets. With an increasing need for informed decision-making in this field, recent years have witnessed a growing interest in the application of deep neural networks, as a possible solution, to model the complex relationships between wind patterns over both space and time. In addition, advances in deep-learning techniques can be used to develop computationally efficient surrogate models that can replace time-consuming high-fidelity Computational Fluid Dynamic (CFD) simulations. In this way, intra-farm aerodynamic interactions can be considered in the day-ahead wind power scheduling. An additional avenue for future research is to assess the feasibility of implementing the decisions obtained in day-ahead during the operation stage. To achieve this, we can rely on the control methods developed for the reserve and energy allocation in wind farms, proposed by other researchers in the BEOWIND project [114]. This research could evaluate the performance of the proposed data-driven bidding approach in real-world settings, while considering complex aerodynamic interactions among turbines, including wake effects, and other technical constraints.

Regarding the atypical scenario of negative electricity prices, it is suggested to modify the auction frameworks to account for this rare event.

To effectively address negative pricing, the auction framework should include a calculation of the net pay and revenue of the portfolio during the scheduling process. It is worth noting that with current advances in wind power control technology, wind portfolios are able to mitigate negative price impacts by participating in balancing markets and adjusting their power output. Another promising avenue for future research would be to extend the proposed model to account for the presence of large wind power producers that act as price-makers. The price-maker assumption can be modeled using a variety of techniques. One widely employed approach is game theory, which captures the strategic interaction between wind power producers and other market participants.

Furthermore, although integrating wind power technologies with other systems, such as large-scale battery storage, has some limitations (as discussed in Section 7.3), it can potentially offer higher flexibility and return by leveraging market arbitrage and hedging against weather-related uncertainties. In this regard, the proposed high-resolution forecasting and advanced decision framework for energy and reserve market participation can be adapted to accommodate multi-technology portfolios. By broadening its applicability and enhancing its potential to optimize market participation strategies, this approach could contribute to a more comprehensive evaluation of the added value of using a multi-technology framework that includes wind assets. Consequently, this expanded analysis may lead to improvements in cost-efficiency, sustainability, and reliability of the overall power system.

Finally, another promising research direction could involve investigating effective policy interventions and systemic changes in energy planning and decision-making that prioritize long-term sustainability, social equity, and environmental concerns. This research area could explore novel regulatory

frameworks, incentives, and pricing mechanisms that encourage resource efficiency and clean technologies such as wind power while simultaneously addressing the limitations of conventional short-term growth-driven models.

List of Publications related to Thesis

The publications listed below present the research contributions of this dissertation.

Journal Papers

S.A. Hosseini, J.-F. Toubeau, Z. De Grève, Y. Wang, N. Amjady and F. Vallée, "Data-Driven Multi-Resolution Probabilistic Energy and Reserve Bidding of Wind Power," **in *IEEE Transactions on Power Systems***, vol. 38, no. 1, pp. 85-99, Jan. 2023.

S.A. Hosseini, J.-F. Toubeau, Z. de Grève, and F. Vallée, "An advanced day-ahead bidding strategy for wind power producers considering confidence level on the real-time reserve provision," **in *Applied Energy***, vol. 280, Dec. 2020.

S.A. Hosseini, J.-F. Toubeau, N. Amjady, and F. Vallée, "Day-Ahead Wind Power Temporal Distribution Forecasting With High Resolution," **in *IEEE Transactions on Power Systems* (In Revision)**, 2023.

Conference Papers

S.A. Hosseini, J.-F. Toubeau, N. Singh, J. De Kooning, N. Kayedpour, G. Crevecoeur, Z. De Grève, F. Vallée, L. Vandevelde, "Impact of fast wind fluctuations on the profit of a wind power producer jointly trading

in energy and reserve markets," in **The 9th Renewable Power Generation Conference** (RPG Dublin 2021), Dublin, Ireland, 2021, pp. 240–245.

N. Singh**, S.A. Hosseini**, J.-F. Toubeau, J. De Kooning, N. Kayedpour, G. Crevecoeur, Z. De Grève, F. Vallée, L. Vandevelde,, "Prediction-based Wind Turbine Operation for Active Participation in the Day-Ahead and Reserve Markets, "***IEEE Power Energy Society General Meeting***, 2022, pp. 1-5.

Seminars/Posters

S.A Hosseini, J.-F Toubeau, F. Vallée "On the Impact of Oversimplified Power Curves in the Optimal Bidding Strategy of Wind Power Producer Taking Part in A Joint Energy & Reserve Market". Poster session presented at BERA PhD Day on Wind Energy, Ghent, Belgium, 2020.

S.A Hosseini, J.-F Toubeau, F. Vallée "Advance Generative Model for Scenario Generation of Wind Power Distributions With Hight Granularity", **18th EAWE** Seminar on Wind Energy, Bruges, Belgium, 2022

References

[1] Z. Tang, Y. Yang, and F. Blaabjerg, "Power electronics: The enabling technology for renewable energy integration," *CSEE Journal of Power and Energy Systems*, vol. 8, no. 1, pp. 39–52, 2022, doi: 10.17775/CSEEJPES.2021.02850.

[2] I. Renewable Energy Agency, *World Energy Transitions Outlook 2022: 1.5°C Pathway*. 2022. [Online]. Available: www.irena.org

[3] L. Hirth, "Electricity market design - Section 2," *Neon Energy*, 2022. https://neon.energy/en/seminars/ (accessed Mar. 06, 2023).

[4] IRENA, "Renewable Power Generation Costs in 2018," Abu Dhabi, 2019.

[5] F. Gökgöz and M. T. Güvercin, "Energy security and renewable energy efficiency in EU," *Renewable and Sustainable Energy Reviews*, vol. 96, pp. 226–239, 2018, doi: 10.1016/j.rser.2018.07.046.

[6] S. V. Valentine, "Emerging symbiosis: Renewable energy and energy security," *Renewable and Sustainable Energy Reviews*, vol. 15, no. 9, pp. 4572–4578, 2011, doi: 10.1016/j.rser.2011.07.095.

[7] D. Schlissel , A. Smith, and R. Wilson, "Coal-Fired Power Plant Construction Costs," Synapse Energy Economics Inc., Jul. 2008.

[8] IRENA, "Future of wind: Deployment, investment, technology, grid integration and socio-economic aspects (A Global Energy Transformation paper)," Abu Dhabi, 2019.

[9] International Renewable Energy Agency (IRENA), "Technologies - Capacity and Generation," IRENA. [Online]. Available: https://www.irena.org/Data/View-data-by-topic/Capacity-and-Generation/Technologies [Accessed: March 10, 2023].

[10] IAEW, "Definition of new/changing requirements for Market designs," 2020.

[11] C. W. Potter and M. Negnevitsky, "Very short-term wind forecasting for Tasmanian power generation," *IEEE Transactions on Power Systems*, vol. 21, no. 2, pp. 965–972, 2006, doi: 10.1109/TPWRS.2006.873421.

[12] L. Exizidis, J. Kazempour, A. Papakonstantinou, P. Pinson, Z. de Grève, and F. Vallée, "Incentive-Compatibility in a Two-Stage Stochastic Electricity Market With High Wind Power Penetration," *IEEE Transactions on Power Systems*, vol. 34, no. 4, pp. 2846–2858, 2019, doi: 10.1109/TPWRS.2019.2901249.

[13] J. Bottieau, L. Hubert, Z. de Grève, F. Vallée, and J.-F. Toubeau, "Very-Short-Term Probabilistic Forecasting for a Risk-Aware Participation in the Single Price Imbalance Settlement," *IEEE Transactions on Power Systems*, vol. 35, no. 2, pp. 1218–1230, 2020, doi: 10.1109/TPWRS.2019.2940756.

[14] A. Giannitrapani, S. Paoletti, A. Vicino, and D. Zarrilli, "Bidding Wind Energy Exploiting Wind Speed Forecasts," *IEEE Transactions on Power Systems*, vol. 31, no. 4, pp. 2647–2656, 2016, doi: 10.1109/TPWRS.2015.2477942.

[15] Y. Jeong, K. Johnson, and P. Fleming, "Comparison and testing of power reserve control strategies for grid-connected wind turbines," *Wind Energy*, vol. 17, no. 3, pp. 343–358, 2014, doi: 10.1002/we.1578.

[16] Y. Wang, H. Bayem, M. Giralt-Devant, V. Silva, X. Guillaud, and B. Francois, "Methods for Assessing Available Wind Primary Power

Reserve," *IEEE Trans Sustain Energy*, vol. 6, no. 1, pp. 272–280, 2015, doi: 10.1109/TSTE.2014.2369235.

[17] K. van den Bergh and E. Delarue, "Energy and reserve markets: interdependency in electricity systems with a high share of renewables," *Electric Power Systems Research*, vol. 189, p. 106537, 2020, doi: 10.1016/j.epsr.2020.106537.

[18] J.-F. Toubeau, J. Bottieau, Z. de Grève, F. Vallée, and K. Bruninx, "Data-Driven Scheduling of Energy Storage in Day-Ahead Energy and Reserve Markets With Probabilistic Guarantees on Real-Time Delivery," *IEEE Transactions on Power Systems*, vol. 36, no. 4, pp. 2815–2828, 2021, doi: 10.1109/TPWRS.2020.3046710.

[19] S. A. Hosseini, J. F. Toubeau, Z. de Grève, and F. Vallée, "An advanced day-ahead bidding strategy for wind power producers considering confidence level on the real-time reserve provision," *Appl Energy*, vol. 280, Dec. 2020, doi: 10.1016/j.apenergy.2020.115973.

[20] M. A. Hossain, R. K. Chakrabortty, S. Elsawah, and M. J. Ryan, "Very short-term forecasting of wind power generation using hybrid deep learning model," *J Clean Prod*, vol. 296, p. 126564, 2021, doi:10.1016/j.jclepro.2021.126564.

[21] H. B. Gooi, D. P. Mendes, K. R. W. Bell, and D. S. Kirschen, "Optimal scheduling of spinning reserve," *IEEE Transactions on Power Systems*, vol. 14, no. 4, pp. 1485–1492, 1999, doi: 10.1109/59.801936.

[22] F. Bouffard and F. D. Galiana, "An electricity market with a probabilistic spinning reserve criterion," *IEEE Transactions on Power Systems*, vol. 19, no. 1, pp. 300–307, 2004, doi: 10.1109/TPWRS.2003.818587.

[23] S. A. Pourmousavi Kani and M. M. Ardehali, "Very short-term wind speed prediction: A new artificial neural network–Markov chain model,"

Energy Convers Manag, vol. 52, no. 1, pp. 738–745, 2011, doi:10.1016/j.enconman.2010.07.053.

[24] R. Meyer, "Vertical Economies and the Costs of Separating Electricity Supply—A Review of Theoretical and Empirical Literature," *The Energy Journal*, vol. 33, no. 4, pp. 161–185, 2012, [Online]. Available: http://www.jstor.org/stable/23268109

[25] T. Taluo, L. Ristić, and M. Jovanović, "Dynamic Modeling and Control of BDFRG under Unbalanced Grid Conditions," *Energies (Basel)*, vol. 14, no. 14, 2021, doi: 10.3390/en14144297.

[26] J. Lin and F. H. Magnago, *Electricity Markets: Theories and Applications: Theories and Applications*, First., vol. 1. Hoboken: Wiley-IEEE Press, 2017.

[27] L. Meeus, *The Evolution of Electricity Markets in Europe*. Edward Elgar Publishing, , 2020.

[28] Nord Pool Group, "EUPHEMIA Public Description: Price Coupling Algorithm," Nord Pool Group, Bruxelles, Belgium, 2019.

[29] Elia, "BRP Contract: Coordination agreement between Elia System Operator and the Balance Responsible Party," Elia, Jan. 2020. [Online], Belgium, 2020.

[30] B. Canizes, J. Soares, P. Faria, and Z. Vale, "Mixed integer non-linear programming and Artificial Neural Network based approach to ancillary services dispatch in competitive electricity markets," *Appl Energy*, vol. 108, pp. 261–270, 2013, doi:10.1016/j.apenergy.2013.03.031.

[31] S. R. Dabbagh and M. K. Sheikh-El-Eslami, "Risk Assessment of Virtual Power Plants Offering in Energy and Reserve Markets," *IEEE Transactions on Power Systems*, vol. 31, no. 5, pp. 3572–3582, 2016, doi: 10.1109/TPWRS.2015.2493182.

[32] A. A. de la Nieta, J. Contreras, and J. I. Muñoz, "Optimal coordinated wind-hydro bidding strategies in day-ahead markets," *IEEE Transactions on Power Systems*, vol. 28, no. 2, pp. 798–809, 2013, doi: 10.1109/TPWRS.2012.2225852.

[33] K. Afshar, F. S. Ghiasvand, and N. Bigdeli, "Optimal bidding strategy of wind power producers in pay-as-bid power markets," *Renew Energy*, vol. 127, pp. 575–586, 2018, doi: 10.1016/j.renene.2018.05.015.

[34] L. Chinmoy, S. Iniyan, and R. Goic, "Modeling wind power investments, policies and social benefits for deregulated electricity market – A review," *Appl Energy*, vol. 242, pp. 364–377, 2019, doi:10.1016/j.apenergy.2019.03.088.

[35] M. Vilim and A. Botterud, "Wind power bidding in electricity markets with high wind penetration," *Appl Energy*, vol. 118, pp. 141–155, 2014, doi:10.1016/j.apenergy.2013.11.055.

[36] G. N. Bathurst, J. Weatherill, and G. Strbac, "Trading wind generation in short term energy markets," *IEEE Transactions on Power Systems*, vol. 17, no. 3, pp. 782–789, 2002, doi: 10.1109/TPWRS.2002.800950.

[37] J. M. Morales, A. J. Conejo, and J. Pérez-Ruiz, "Short-Term Trading for a Wind Power Producer," *IEEE Transactions on Power Systems*, vol. 25, no. 1, pp. 554–564, 2010, doi: 10.1109/TPWRS.2009.2036810.

[38] D. Lee, H. Shin, and R. Baldick, "Bivariate Probabilistic Wind Power and Real-Time Price Forecasting and Their Applications to Wind Power Bidding Strategy Development," *IEEE Transactions on Power Systems*, vol. 33, no. 6, pp. 6087–6097, 2018, doi: 10.1109/TPWRS.2018.2830785.

[39] Z. Zhang and Z. Chen, "Optimal wind energy bidding strategies in real-time electricity market with multi-energy sources," *IET Renewable Power*

Generation, vol. 13, no. 13, pp. 2383–2390, Oct. 2019, doi: 10.1049/iet-rpg.2019.0058.

[40] R. Ghaffari and B. Venkatesh, "Network constrained model for options based reserve procurement by wind generators using binomial tree," *Renew Energy*, vol. 80, pp. 348–358, 2015, doi:10.1016/j.renene.2015.02.008.

[41] M. Rahimiyan, J. M. Morales, and A. J. Conejo, "Evaluating alternative offering strategies for wind producers in a pool," *Appl Energy*, vol. 88, no. 12, pp. 4918–4926, 2011, doi:10.1016/j.apenergy.2011.06.038.

[42] J. Liang, S. Grijalva, and R. G. Harley, "Increased Wind Revenue and System Security by Trading Wind Power in Energy and Regulation Reserve Markets," *IEEE Trans Sustain Energy*, vol. 2, no. 3, pp. 340–347, 2011, doi: 10.1109/TSTE.2011.2111468.

[43] T. Soares, P. Pinson, T.V. Jensen, and H. Morais, "Optimal offering strategies for wind power in energy and primary reserve markets," IEEE Trans Sustain Energy, vol. 7, no. 3, pp. 1036–1045, 2016, doi: 10.1109/TSTE.2016.2516767.

[44] T. Soares, T. v. Jensen, N. Mazzi, P. Pinson, and H. Morais, "Optimal offering and allocation policies for wind power in energy and reserve markets," *Wind Energy*, vol. 20, no. 11, pp. 1851–1870, Nov. 2017, doi: 10.1002/we.2125.

[45] Elia, "Data Download," *https://www.elia.be/en/grid-data/data-download-page*, 2020.

[46] E. Cheynet, "Wind field simulation (the user-friendly version)," *https://zenodo.org/record/3817905#.Y5IFLHbMJD8*, 2020.

[47] P. Domagalski and L. R. Sætran, "Frøya wind data (1Hz)." Zenodo, Sep. 2019. doi: 10.5281/zenodo.3403362.

[48] L. Hirth, J. Mühlenpfordt, and M. Bulkeley, "The ENTSO-E Transparency Platform–A review of Europe's most ambitious electricity data platform," *Appl Energy*, vol. 225, pp. 1054–1067, 2018.

[49] I. Dunning, J. Huchette, and M. Lubin, "JuMP: A Modeling Language for Mathematical Optimization," Aug. 2015, doi: 10.1137/15M1020575.

[50] A. J. Conejo, M. Carrión, and J. M. Morales, Decision Making Under Uncertainty in Electricity Markets, ser. International Series in Operations Research & Management Science. New York, NY: Springer, 2010, doi: 10.1007/978-1-4419-7421-1.

[51] L. T. Anstine, R. E. Burke, J. E. Casey, R. Holgate, R. S. John, and H. G. Stewart, "Application of Probability Methods to the Determination of Spinning Reserve Requirements for the Pennsylvania-New Jersey-Maryland Interconnection," *IEEE Transactions on Power Apparatus and Systems*, vol. 82, no. 68, pp. 726–735, 1963, doi: 10.1109/TPAS.1963.291390.

[52] O. Abedinia, M. Zareinejad, M. H. Doranehgard, G. Fathi, and N. Ghadimi, "Optimal offering and bidding strategies of renewable energy based large consumer using a novel hybrid robust-stochastic approach," *J Clean Prod*, vol. 215, pp. 878–889, 2019, doi: 10.1016/j.jclepro.2019.01.085.

[53] H. Khodaei, M. Hajiali, A. Darvishan, M. Sepehr, and N. Ghadimi, "Fuzzy-based heat and power hub models for cost-emission operation of an industrial consumer using compromise programming," *Appl Therm Eng*, vol. 137, pp. 395–405, 2018, doi:10.1016/j.applthermaleng.2018.04.008.

[54] S. A. Hosseini, N. Amjady, M. Shafie-khah, and J. P. S. Catalão, "A new multi-objective solution approach to solve transmission congestion

management problem of energy markets," *Appl Energy*, vol. 165, pp. 462–471, 2016, doi:10.1016/j.apenergy.2015.12.101.

[55] H. Khaloie *et al.*, "Coordinated wind-thermal-energy storage offering strategy in energy and spinning reserve markets using a multi-stage model," *Appl Energy*, vol. 259, p. 114168, 2020, doi: 10.1016/j.apenergy.2019.114168.

[56] G. Mavrotas, "Effective implementation of the ε-constraint method in Multi-Objective Mathematical Programming problems," *Appl Math Comput*, vol. 213, no. 2, pp. 455–465, 2009, doi: 10.1016/j.amc.2009.03.037.

[57] J.-F. Toubeau, Z. D. Grève, P. Goderniaux, F. Vallée, and K. Bruninx, "Chance-Constrained Scheduling of Underground Pumped Hydro Energy Storage in Presence of Model Uncertainties," *IEEE Trans Sustain Energy*, vol. 11, no. 3, pp. 1516–1527, 2020, doi: 10.1109/TSTE.2019.2929687.

[58] J. Luedtke, S. Ahmed, and G. L. Nemhauser, "An integer programming approach for linear programs with probabilistic constraints," *Math Program*, vol. 122, no. 2, pp. 247–272, Apr. 2010, doi: 10.1007/s10107-008-0247-4.

[59] A. Ruszczyński, "Probabilistic programming with discrete distributions and precedence constrained knapsack polyhedra," *Mathematical Programming, Series B*, vol. 93, no. 2, pp. 195–215, Dec. 2002, doi: 10.1007/s10107-002-0337-7.

[60] S. A. Hosseini *et al.*, "Impact of fast wind fluctuations on the profit of a wind power producer jointly trading in energy and reserve markets," in *The 9th Renewable Power Generation Conference (RPG Dublin Online 2021)*, 2021, pp. 240–245. doi: 10.1049/icp.2021.1386.

[61] Y. Chen, Y. Wang, D. Kirschen, and B. Zhang, "Model-Free Renewable Scenario Generation Using Generative Adversarial Networks," *IEEE*

Transactions on Power Systems, vol. 33, no. 3, pp. 3265–3275, 2018, doi: 10.1109/TPWRS.2018.2794541.

[62] X. Yang, H. He, J. Li, and Y. Zhang, "Toward Optimal Risk-Averse Configuration for HESS With CGANs-Based PV Scenario Generation," *IEEE Trans Syst Man Cybern Syst*, vol. 51, no. 3, pp. 1779–1793, 2021, doi: 10.1109/TSMC.2019.2905776.

[63] Y. Chen, P. Li, and B. Zhang, "Bayesian Renewables Scenario Generation via Deep Generative Networks," Feb. 2018, [Online]. Available: http://arxiv.org/abs/1802.00868

[64] Y. Xie, C. Li, M. Li, F. Liu, and M. Taukenova, "An overview of deterministic and probabilistic forecasting methods of wind energy", doi: 10.1016/j.isci.

[65] X. Yang, H. He, J. Li, and Y. Zhang, "Toward Optimal Risk-Averse Configuration for HESS With CGANs-Based PV Scenario Generation," *IEEE Trans Syst Man Cybern Syst*, vol. 51, no. 3, pp. 1779–1793, 2021, doi: 10.1109/TSMC.2019.2905776.

[66] A. Leon and K. Chough, *Analysis of mixed data: Methods and Applications*, First edition. Chapman and Hall/CRC, 2013.

[67] Z. Liang, X. Su, and K. Feng, "Drought propagation and construction of a comprehensive drought index based on the Soil and Water Assessment Tool (SWAT) and empirical Kendall distribution function : a case study for the Jinta River basin in northwestern China," *Natural Hazards and Earth System Sciences*, vol. 21, no. 4, pp. 1323–1335, 2021, doi: 10.5194/nhess-21-1323-2021.

[68] C. Jiang, Y. Mao, Y. Chai, M. Yu, and S. Tao, "Scenario Generation for Wind Power Using Improved Generative Adversarial Networks," *IEEE*

Access, vol. 6, pp. 62193–62203, 2018, doi: 10.1109/ACCESS.2018.2875936.

[69] Y. Wang, G. Hug, Z. Liu, and N. Zhang, "Modeling load forecast uncertainty using generative adversarial networks," *Electric Power Systems Research*, vol. 189, p. 106732, 2020, doi: 10.1016/j.epsr.2020.106732.

[70] C. Zhao, C. Chen, Z. He, and Z. Wu, "Application of auxiliary classifier wasserstein generative adversarial networks in wireless signal classification of illegal unmanned aerial vehicles," *Applied Sciences*, vol. 8, no. 12, Dec. 2018, doi: 10.3390/app8122664.

[71] C. Zhao, C. Chen, Z. Cai, M. Shi, X. Du, and M. Guizani, "Classification of Small UAVs Based on Auxiliary Classifier Wasserstein GANs," in *2018 IEEE Global Communications Conference (GLOBECOM)*, 2018, pp. 206–212. doi: 10.1109/GLOCOM.2018.8647973.

[72] J. Wang, M. Shahidehpour, and Z. Li, "Security-Constrained Unit Commitment With Volatile Wind Power Generation," *IEEE Transactions on Power Systems*, vol. 23, no. 3, pp. 1319–1327, 2008, doi: 10.1109/TPWRS.2008.926719.

[73] P. Pinson, H. Madsen, H. A. Nielsen, G. Papaefthymiou, and B. Klöckl, "From probabilistic forecasts to statistical scenarios of short-term wind power production," *Wind Energy*, vol. 12, no. 1, pp. 51–62, 2009, doi: 10.1002/we.284.

[74] S. Albatran, S. Harasis, M. Ialomoush, Y. Alsmadi, and M. Awawdeh, "Realistic Optimal Power Flow of a Wind-Connected Power System With Enhanced Wind Speed Model," *IEEE Access*, vol. 8, pp. 176973–176985, 2020, doi: 10.1109/ACCESS.2020.3027065.

[75] S. Rahmani and N. Amjady, “A new optimal power flow approach for wind energy integrated power systems,” *Energy*, vol. 134, pp. 349–359, 2017, doi:10.1016/j.energy.2017.06.046.

[76] D. and G. S. Padala Manisha and Das, “Effect of Input Noise Dimension in GANs,” in *Neural Information Processing*, M. and A. M. A. and W. K. W. and H. A. N. Mantoro Teddy and Lee, Ed., Cham: Springer International Publishing, 2021, pp. 558–569.

[77] M. Arjovsky, S. Chintala, and L. Bottou, “Wasserstein GAN,” Jan. 2017, [Online]. Available: http://arxiv.org/abs/1701.07875

[78] B. Adlam, C. Weill, and A. Kapoor, “Investigating Under and Overfitting in Wasserstein Generative Adversarial Networks,” Oct. 2019, [Online]. Available: http://arxiv.org/abs/1910.14137

[79] I. Gulrajani, F. Ahmed, M. Arjovsky, V. Dumoulin, and A. Courville, “Improved Training of Wasserstein GANs,” Mar. 2017, [Online]. Available: http://arxiv.org/abs/1704.00028

[80] Y. Zhang and Q. Yang, “A Survey on Multi-Task Learning,” *IEEE Trans Knowl Data Eng*, vol. 34, no. 12, pp. 5586–5609, 2022, doi: 10.1109/TKDE.2021.3070203.

[81] S. Shokrzadeh, M. Jafari Jozani, and E. Bibeau, “Wind turbine power curve modeling using advanced parametric and nonparametric methods,” *IEEE Trans Sustain Energy*, vol. 5, no. 4, pp. 1262–1269, Oct. 2014, doi: 10.1109/TSTE.2014.2345059.

[82] M. Abadi et al., "TensorFlow: Large-Scale Machine Learning on Heterogeneous Systems," 2015.

[83] Energinet, “TSO Electricity,” *https://www.energidataservice.dk/organizations/tso-electricity*, 2021.

[84] M. N. Fekri, A. M. Ghosh, and K. Grolinger, "Generating Energy Data for Machine Learning with Recurrent Generative Adversarial Networks," *Energies*, vol. 13, no. 1, 2020, doi: 10.3390/en13010130.

[85] F. Ye, F. Zhu, Y. Fu, and B. Shen, "ECG Generation With Sequence Generative Adversarial Nets Optimized by Policy Gradient," *IEEE Access*, vol. 7, pp. 159369–159378, 2019, doi: 10.1109/ACCESS.2019.2950383.

[86] O. Abedinia, M. Lotfi, M. Bagheri, B. Sobhani, M. Shafie-Khah, and J. P. S. Catalao, "Improved EMD-Based Complex Prediction Model for Wind Power Forecasting," *IEEE Trans Sustain Energy*, vol. 11, no. 4, pp. 2790–2802, 2020, doi: 10.1109/TSTE.2020.2976038.

[87] J. Yan, H. Zhang, Y. Liu, S. Han, L. Li, and Z. Lu, "Forecasting the High Penetration of Wind Power on Multiple Scales Using Multi-to-Multi Mapping," *IEEE Transactions on Power Systems*, vol. 33, no. 3, pp. 3276–3284, 2018, doi: 10.1109/TPWRS.2017.2787667.

[88] Y. Sun, Z. Li, X. Yu, B. Li, and M. Yang, "Research on Ultra-Short-Term Wind Power Prediction Considering Source Relevance," *IEEE Access*, vol. 8, pp. 147703–147710, 2020, doi: 10.1109/ACCESS.2020.3012306.

[89] Y. Zhang and J. Dong, "Least Squares-based Optimal Reconciliation Method for Hierarchical Forecasts of Wind Power Generation," IEEE Transactions on Power Systems, 2018, doi:10.1109/TPWRS.2018.2868175.

[90] J. Liang and W. Tang, "Ultra-Short-Term Spatiotemporal Forecasting of Renewable Resources: An Attention Temporal Convolutional Network-Based Approach," in *IEEE Transactions on Smart Grid*, vol. 13, no. 5, pp. 3798-3812, Sept. 2022, doi: 10.1109/TSG.2022.3175451.

[91] R. J. Bessa, V. Miranda, A. Botterud, J. Wang, and E. M. Constantinescu, "Time adaptive conditional kernel density estimation for

wind power forecasting," *IEEE Trans Sustain Energy*, vol. 3, no. 4, pp. 660–669, 2012, doi: 10.1109/TSTE.2012.2200302.

[92] Z. Zheng, L. Wang, L. Yang, and Z. Zhang, "Generative Probabilistic Wind Speed Forecasting: A Variational Recurrent Autoencoder Based Method," *IEEE Transactions on Power Systems*, vol. 37, no. 2, pp. 1386–1398, 2022, doi: 10.1109/TPWRS.2021.3105101.

[93] J. Dowell and P. Pinson, "Very-Short-Term Probabilistic Wind Power Forecasts by Sparse Vector Autoregression," *IEEE Trans Smart Grid*, vol. 7, no. 2, pp. 763–770, 2016, doi: 10.1109/TSG.2015.2424078.

[94] J. S. Roungkvist and P. Enevoldsen, "Timescale classification in wind forecasting: A review of the state-of-the-art," *J Forecast*, vol. 39, no. 5, pp. 757–768, Aug. 2020, doi: 10.1002/for.2657.

[95] K. P. Murphy, *Machine learning : a probabilistic perspective*. MIT Press, 2012.

[96] S. A. Hosseini, J. F. Toubeau, Z. de Grève, Y. Wang, N. Amjady, and F. Vallée, "Data-Driven Multi-Resolution Probabilistic Energy and Reserve Bidding of Wind Power," *IEEE Transactions on Power Systems*, 2022, doi: 10.1109/TPWRS.2022.3155865.

[97] V. Prema, M. S. Bhaskar, D. Almakhles, N. Gowtham, and K. U. Rao, "Critical Review of Data, Models and Performance Metrics for Wind and Solar Power Forecast," *IEEE Access*, vol. 10, pp. 667–688, 2022. doi: 10.1109/ACCESS.2021.3137419.

[98] J. Wu, "Information Theory and Decision Tree", Nanjing University, 2017.

[99] C. P. Burgess *et al.*, "Understanding disentangling in β-VAE," Apr. 2018, [Online]. Available: http://arxiv.org/abs/1804.03599

[100] T. Brijs, C. de Jonghe, B. F. Hobbs, and R. Belmans, “Interactions between the design of short-term electricity markets in the CWE region and power system flexibility,” *Appl Energy*, vol. 195, pp. 36–51, 2017, doi: 10.1016/j.apenergy.2017.03.026.

[101] L. B. Shi, Z. X. Weng, L. Z. Yao, and Y. X. Ni, “An analytical solution for wind farm power output,” *IEEE Transactions on Power Systems*, vol. 29, no. 6, pp. 3122–3123, Nov. 2014, doi: 10.1109/TPWRS.2014.2315498.

[102] A. F. Agarap, “Deep Learning using Rectified Linear Units (ReLU),” Mar. 2018, [Online]. Available: http://arxiv.org/abs/1803.08375

[103] B. Gao and L. Pavel, “On the Properties of the Softmax Function with Application in Game Theory and Reinforcement Learning,” 2017. [Online]. Available: https://www.researchgate.net/publication/315834599

[104] M. Catalano, A. Lijoi, and I. Prünster, “Measuring dependence in the Wasserstein distance for Bayesian nonparametric models,” *Ann Stat*, vol. 49, no. 5, pp. 2916–2947, Oct. 2021, doi: 10.1214/21-AOS2065.

[105] O. Bousquet, S. Gelly, I. Tolstikhin, C.-J. Simon-Gabriel, and B. Schoelkopf, “From optimal transport to generative modeling: the VEGAN cookbook,” May 2017, [Online]. Available: http://arxiv.org/abs/1705.07642

[106] S. Kolouri, G. K. Rohde and H. Hoffmann, "Sliced Wasserstein Distance for Learning Gaussian Mixture Models," 2018 IEEE/CVF Conference on Computer Vision and Pattern Recognition, Salt Lake City, UT, USA, 2018, pp. 3427-3436, doi: 10.1109/CVPR.2018.00361.

[107] S. T. Rachev and L. Rüschendorf, Mass Transportation Problems: Applications, ser. Probability and Its Applications. New York, NY: Springer, 1998, doi: 10.1007/b98894.

[108] S. Kolouri, P. E. Pope, C. E. Martin, and G. K. Rohde, “Sliced-Wasserstein Autoencoder: An Embarrassingly Simple Generative Model,” Apr. 2018, [Online]. Available: http://arxiv.org/abs/1804.01947

[109] S. Prillo and J. M. Eisenschlos, “SoftSort: A Continuous Relaxation for the argsort Operator,” Jun. 2020, [Online]. Available: http://arxiv.org/abs/2006.16038

[110] A. Paszke et al., "PyTorch: An Imperative Style, High-Performance Deep Learning Library," arXiv preprint arXiv:1912.01703, 2019. [Online]. Available: https://arxiv.org/abs/1912.01703

[111] J. Bergstra, R. Bardenet, Y. Bengio, and B. Kégl, “Algorithms for Hyper-Parameter Optimization.” Curran Associates Inc., NY, United States, 2011.

[112] Z. Guo, W. Wei, L. Chen, Z. Dong, and S. Mei, “Parametric Distribution Optimal Power Flow With Variable Renewable Generation,” *IEEE Transactions on Power Systems*, May 2021, doi: 10.1109/TPWRS.2021.3110528.

[113] M. Debouza and A. Al-Durra, “Grid Ancillary Services From Doubly Fed Induction Generator-Based Wind Energy Conversion System: A Review,” *IEEE Access*, vol. 7, pp. 7067–7081, 2019, doi: 10.1109/ACCESS.2018.2890168.

[114] N. Kayedpour, N. Singh, J. D. M. De Kooning, L. Vandevelde, and G. Crevecoeur, “An optimal wind farm control strategy for grid frequency support using particle swarm optimization,” in *11th International Conference on Renewable Power Generation - Meeting net zero carbon (RPG 2022)*, 2022, pp. 80–84. doi: 10.1049/icp.2022.1675.

Abstract:

In the rapidly evolving electricity market, wind energy portfolios are increasingly incentivized to actively participate in both the energy and reserve markets, driven by policy changes and advancements in wind farm control technology. This thesis empowers wind energy portfolios with the required decision framework to effectively engage in day-ahead energy and reserve markets. The first aspect of our framework is the day-ahead prediction of wind fluctuations at extremely short timescales, such as minutes or seconds, for optimal reserve scheduling, while also considering wind variability at rather longer timescales, e.g., hourly, for optimal energy scheduling. The second aspect of the framework involves developing a dedicated decision model that leverages the obtained information on wind uncertainty at both resolutions, to optimize the allocation of wind energy in day-ahead energy and reserve markets. Crucially, the decision framework also addresses the reliability of offered reserve services, ensuring system operators can confidently rely on them. Our results show that the proposed data-driven decision framework significantly improves both the profit and reserve reliability of wind energy portfolios.

Seyyed Ahmad Hosseini pursued his Ph.D. program in 2020 in the Power Systems and Markets Research Group at the University of Mons, Belgium, while working there as a research assistant. In the first quarter of 2023, he further expanded his academic experience by participating as a visiting scholar at Federation University Australia. His primary research interests encompass machine learning, incorporation of wind power into electricity markets, and decision-making processes in uncertain conditions.